ISSN 1028-8546

Azərbaycan Milli Elmlər Akademiyası
Fizika-Riyaziyyat və Texnika Elmləri Bölməsi
Fizika İnstitutu

4

Fizika

Cild
VII
2001

Bakı ✵ Elm

BINARITY OF NOVAE

M.B. BABAYEV

Shamakhy Astrophysical Observatory named after N. Tusi, National Academy of Sciences
373243, Shemakha, Pirgulu, Azerbaijan

The continuous and complex investigations showed that Nova Delphins 1967=HR Del has two types of changeable minima on the orbital light curve with different periods – (P_1≈0.14 days and P_2≈0.19 days) and amplitudes Δm_1≈0^m.70 and Δm_2≈0^m.90). It is a triple star as the repeated Nova T CrB (1866, 1946).

Establishment of the binary nature of Novae plays the fundamental role in interpretation of this phenomenon. Duplicity of stars is a key in understanding of the mechanism and reason of flare of Nova and is basic for the whole modern picture of the phenomenon.

At observing of former Nova DQ Her in 1956, Walker [1] for the first time has found regularly repeating deep decreases of the brightness of this star with period 4h39min - the eclipses. In 1963 he has also discovered that Auriga Nova is the eclipsing binary star with the period 4h59min.

P. Kraft [2] has discovered the binary nature of Nova Agl 1918 from periodic changes of the radial velocity of this star. In 1980 it was reported that the brightness of this star varied with the same period (3h19min), which was established by Kraft [3]. It was revealed that the light curve was eclipsing (the duration of eclipse was 33 min, and the deepness – 0.36). The same author [4] from spectral data has detected binarity of Nova Per 1901. Its orbital period was determined ambiguously; according to Kraft [4] it was 1.904 days, but Paczynski [4] has found the value of 0.685 days.

In the last years it was discovered binarity of HR Del 1967 (period is 4h35min) VD Pav (4h18min), 1500 Cyg (about 3.5hours). Vaikoff and Vekhinger [4] confirmed with the help of spectral observations, that for the slow Novae RR Pic the exact value of the orbital period is 3h29min. Many observations of Nova confirm the presence of periodic changes of their brightness as in binaries.

Similarity of periods of typical Nova is not casual, it specifies similarity of the structure of binary systems where Novae outburst. The discovery of binarity has allowed for the first time to obtain directly an estimation of masses of Nova. In 1964 R. Kraft has obtained masses of components of the binary system of Novae based on the analysis of light curves and radial velocity curves. Finally, he has shown that Novae were low mass stars with masses from 0.2 to 0.6 mass of the Sun, but the mass of repeated Nova T CrB is considerable larger - 3.7 masses of the Sun.

Now, it is commonly believed that all Novae are close binary systems. The binary star consists of a blue hot star, being white dwarf, and cold componenta of Red dwarf. The blue component in result of burst gives Nova. It is surrounded by the disk formed in result of gas stream from the red component. The matter gradually falls on to the surface of the white dwarf. This process refers to as accretion, and the disk itself is called the accretion disc. Observations of binary Novae, carried out in last years, have confirmed the existence of disks around white dwarfs. The disk manifests itself well in those systems, where eclipses are observed.

The periodic fluctuations of brightness were found by Kohoutek and Pauls [5] and M. Babaev [6] for slow Nova HR Del 1967 (fig.1). Recently the binarity was revealed with the help of the spectrophotometrical method. In 1979 Hutchings [7] has found that the Nova HR Del is the binary and the period of variability of this system was -0.17098 days (=4h06min). After this we carried out photographic observations during 12-14.06.1978, 27-29.08.1979, 16-18.09.1980 and 30-31.07.1981 on the 350 mm AST - 452 telescope at Shemakha Astrophysical Observatory (ShAO) of the Azerbaijan Academy of Sciences and 70 images of HR Del have been received.

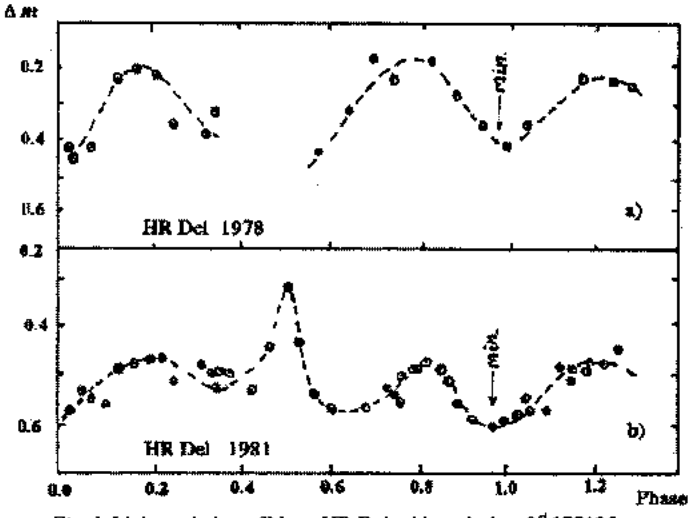

Fig. 1. Light variation of Nova HR Del with period P=0^d.177125
a) 1978; b) 1981

Nova HR Del was observed by us photographically with the aim to investigate the changes of the brightness and to determine the orbital period. Therefore for revealing of the binarity of Nova HR Del in 1978, 16 images with 6 minutes expositions was taken again for one night and 36 pictures in 1981 also for one night with an exposition 6 minutes (fig.1). In this figure the change of photographic magnitude of the star with the phase is shown, which was calculated with elements which we determined [8].

$$MinI = J.D.2443674^d.242750 + 0^d.177125E$$

The period determined by us is in the good accordance with the data received in 1978 and 1981 and with the value of the period obtained by Hutchings [7]. The amplitude of variation of the brightness of HR Del in the first minimum is 0^m.15÷0^m.20. So, for the period of HR Del we have adopted the value P=0.1771250±0.0007 days. The shape of the light change shows, that in addition to the founded period there is the period of 0.13 days with variable amplitude.

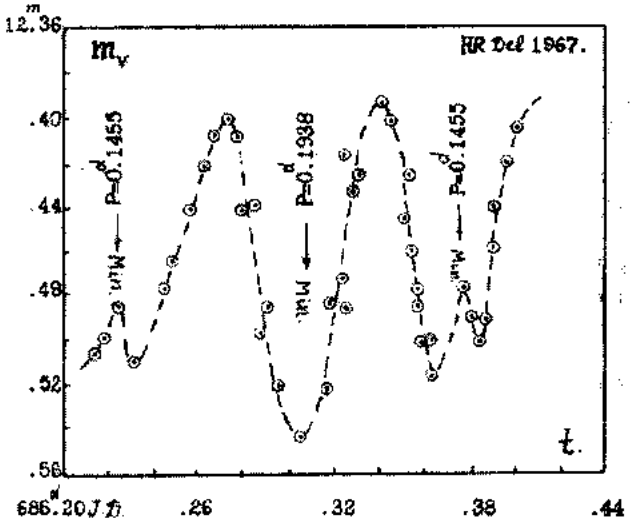

Fig.2. Light curve of HR Del in 1986

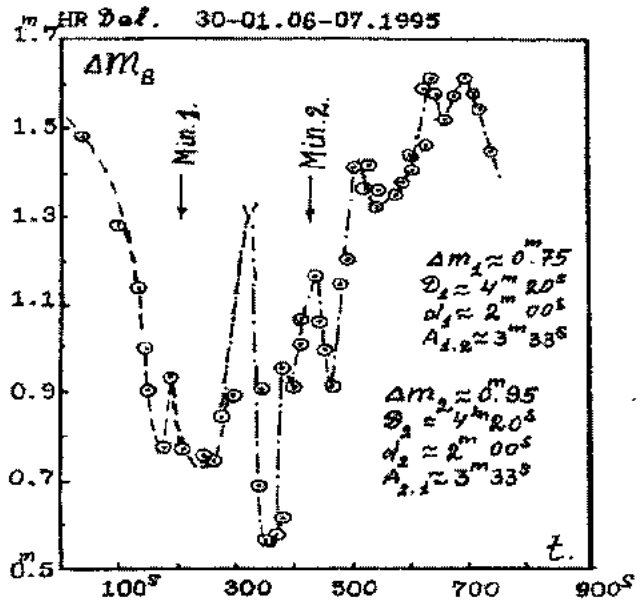

Fig.3. Light curve of HR Del in 1995.

During 13 nights from August 12 to September 13, 1986 at fist with the telescope AZT-8, and then from August 13 to August 14, 1987 with the 2 m telescope ShAO with the help of the photometer AFM-6 by the method of photon counting, we carried out photo-electrical observations of HR Del for specification of the orbital period, for which different authors give different values. In spite of this, by using these observational materials we revealed that Nova HR Del has two types of brightness changes, which are due to the binarity of the Nova. The periods are variable with mean values of ~ 0.1455 and 0.1938 days (fig. 2) [8].

As can be seen from fig. 2 except the minimum 0.17÷0.21 days – P=0.1938 days (according to different authors) connected, apparently, with the binarity of HR Del, there are also minima with periods 0.13÷0.14 days (~P=0.1455 days) [8]. Thus, it was found that Nova Del 1967 is the cataclysmic variable star with some peculiarities, one of them is the double minima. Therefore we observed the Nova Del 1967 from 30.01., 06.07.1995 to 26-27.07.1995 with the aim of determination of the orbital period and detection ultra-short changes of brightness by the photoelectrical method.

The observations were carried out on the telescope CEIS - 600 at ShAO with the help of the photometer AFM-6 by the methods of photon counting as it was done earlier. Photometric observations were carried out mainly with the filter "B" in system UBVR for increase the accuracy.

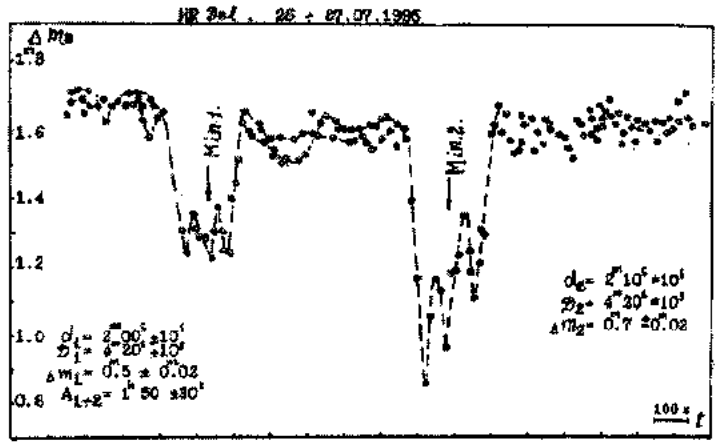

Fig.4. Light curve of HR Del in 1995

The processing of this material showed, that Nova Del 1967 has double minima with different periods and amplitudes which alternate each other (fig. 3 and 4). As it can be seen in these figures, the observational material obtained in different nights again demonstrate that this Nova has periodic changes in brightness with two minima not similar to any other type of Novae. The comparison of these two figures shows that these minima have approachements and removals as in the triple system. Such character of changes gives us an opportunity to say, that in this system either two stars were burst or the star which was burst has been broken up into two parts. Probably the further continuous and detailed observations will confirm this phenomenon if it is the real one and it will be unique for Novae.

The author expresses thanks to Dr. S.K. Zeinalov for useful discussions and Dr G.A.Ismailov for critical remarks.

[1] *M.F. Walker*. Ap. J. 1956, v. 123, p. 68.
[2] *R.P. Kraft*. Ap. J. 1958, v. 127, p. 625.
[3] *R.P. Kraft*. Vzrivnie peremennie kak dvoinie zvezdy. Mir, .Moskow-1965, 94p. (in Russian).
[4] *V.P. Arkhipova*. Kosmonavtika, Astronomia, 1984,10, 64 p. (in Russian).
[5] *L. Kohoutek, P. Pauls*. As Ap, 1980, v. 92, №1, p. 200.
[6] *M.B. Babaev*. ShAO, 1983, №71, p. 16.
[7] *J.B. Hutchings*. Ap. J, 1979, v. 232, p. 176.
[8] *M.B. Babaev*. ShAO, 1983, №71, p. 16.
[9] *M.B. Babaev, M.S. Gadzhiev*. Perem. Zvezdi., 1994, v.23, №5, p. 305.
[10] *M.B. Babaev, M.S. Gadzhiev*. Astronomoch.Tzirkulyar., 1990, №1546, p. 17.

BINARITY OF NOVAE

M.B. Babayev

YENİLƏRİN QOŞALILIĞI

Uzunmüddətli, ardıcıl və hərtərəfli müşahidələrin tədqiqi göstərdi ki, Yeni Delfin 1967-HR Del ulduzunun orbital işıqlılıq əyrisində müxtəlif periodlu – ($\sim 0^d,14 \div \sim 0^d,19$) və amplitudalı – ($\sim 0^m,70 \div \sim 0^m,90$) iki minimumu vardır.

М.Б. Бабаев

ДВОЙСТВЕННОСТЬ НОВЫХ

Продолжительные и комплексные исследования показали, что у Новой Дельфина 1967=HR Del имеется два типа изменчивого минимума на орбитальной кривой блеска с разными периодами – ($P_1 \approx 0^d.14$ и $P_2 \approx 0^d.19$) и амплитудами – ($\Delta m_1 \approx 0^m.7$ и $\Delta m_2 \approx 0^m.9$). Она является тройной звездой как повторная Новая звезда T CrB (1886, 1946)

Received: 03.03.01

INFLUENCE OF THE ADDITIONAL ELECTRICAL FIELD ON I-V CHARACTERISTIC OF REAL SCHOTTKY DIODES

R.K. MAMEDOV
Baku State University
Baku 370148, street. Z.Khalilov 23

The real Schottky diodes are usually exposed to an additional electrical field arising in near contact region of the semiconductor, because of an emission non-uniformity of the interface. It is established, that under influence of the additional electrical field, the non-ideality factor of the forward branch of their volt-ampere characteristic increases, its reverse branch is not saturated and strong raise occurs of the reverse current at low voltages, i.e. a premature breakdown of the transition takes place.

INTRODUCTION

In spite of intensive research of physical characteristics of real Schottky diodes (RSD), the analysis of influence of an additional electrical field on current transportation property has not received the due reflection in the literature. Such additional electrical field arises because of an emissive inhomogeneity of the interface and exists in the near contact region of the semiconductor almost of all kinds RSD. Research of influence of an additional electrical field on a voltage-current characteristic of RSD causes doubtless interest because of the high scientific and practical significance of RSD.

MAIN THEORETICAL THESES

A potential barrier height of RSD, having even an ideal homogeneous interface, because of limitation of the contact area, does not remain identical on all contact surface. Really, on an interface of real Schottky diodes, made on the basis of a close contact of the metal (with the work of exit Φ_M) and the semiconductor (with the work of exit Φ_S), a potential barrier arises with the height Φ_B, equal to the contact potential difference between contact surfaces of the metal and the semiconductor (i.e., $\Phi_B=\Phi_M-\Phi_S$). The contact surface of RSD is limited by free surfaces of the metal and the semiconductor. As a result a contact potential differences of values $(\Phi_M-\Phi_B)$ and $(\Phi_S-\Phi_B)$ arises [1-3] between a contact surfaces with Φ_B and free metal surfaces with Φ_M and the semiconductor surface with Φ_S. The electrical field of the potential Φ_B is main and it concentrates in all the near contact region of the semiconductor. At the same time, the additional electrical field of contact potential differences $(\Phi_M-\Phi_B)$ and $(\Phi_S-\Phi_B)$ concentrates in the peripheral contact region of the semiconductor RSD. As the work of exit of a metal and semiconductor is about 4-5eV [1,4] and a potential barrier height of RSD is of the order of 1eV [5], then the strength of an additional electrical field becomes commensurate with the strength of the main electrical field in the near contact region of the semiconductor. Therefore, a potential barrier on the peripheral contact surface and on inner contact surfaces of RSD has different heights.

However, RSD owing to a series of such causes as a polycrystalline structure of the metal, unevenness of solid-state interaction, congestion of stranger atoms and molecules etc., which in practice are always inherent to an inhomogeneous interface and their potential barrier has a different height along a contact surface [6,7,8]. Then RSD is represented as combination of the two parallel separate microcontacts with different local barrier heights. Such notion of RSD at first seems nonconvincing. Indeed, because of a inhomogeneity of the interface, the difference of potential barrier heights of microcontacts can reach up to 1eV, and the potential barrier of RSD has the same height. Therefore, the real contacts metal and semiconductor, consisting of two parallel separate microcontacts with different local barrier heights, would not have normal rectifying properties. Actually, RSD are produced without the special difficulty with satisfactory qualities and they are widely used in different electronic devices. However, some important problems of physics of RSD still remain open [5]. This contradiction is eliminated at account of the fact, that on the interface of RSD microcontacts with different local barrier heights and linear dimensions of the order of sizes of the crystalline grains of the metal, are in the direct electrical contact and interacting between themselves create an additional electrical field in the near contact region of the semiconductor. As a result, the barrier height along the contact surface smoothes and RSD is characterized by an average height of the potential barrier.

Independently of a degree of complexity of a contact area configuration and distribution of microcontacts with different local potential barrier heights along a contact surface, RSD is represented as combination of two interacting sites with different local barrier heights. The potential barrier heights of the first and second sites becomes, accordingly, lower and higher than the average potential barrier height on all contact surface of RSD. The dependence of the potential barrier height of the first site of RSD on the voltage is determined by the anomalous Schottky effect, and the second site of RSD by the normal Schottky effect.

Let's designate the average potential barrier height of the first site of RSD through Φ_{B1}, and its increment under influence of the second site through $\Delta\Phi_{O1}$, and the average potential barrier height of the second site of RSD through Φ_{B1} and its decrease under influence of the first site through $\Delta\Phi_{O2}$.

At application of an external voltage to RSD, according to anomalous Schottky effect, the dependence of the increment of the potential barrier height of the first site $\Delta\Phi_{B1}$ on the voltage U in the first approximation is expressed by the formula:

$$\Delta\Phi_{B1}=\Delta\Phi_{O1}\pm\beta qU \qquad (1)$$

where the dimensionless factor $\beta < 1$.

The dependence of a decrease of the barrier height $\Delta\Phi_{B2}$ on the voltage U for the second site of RSD, according to normal Schottky effect, is determined by the known formula:

$$\Delta\Phi_{B2} = q\left[\left(q^3 N_D/8\pi^2\varepsilon_s^3\right)\left(U_D - U - kT/q\right)\right]^{1/4}. \quad (2)$$

Here all notations are generally accepted [4]

At the application of the forward voltage to RSD with the contact area S, made of a n-type semiconductor, in a near contact region of semiconductor interfaces an external field and an additional field are parallel for the first site and are antiparallel for the second site. Barrier heights of both sites of RSD decrease on the value qU with growth of the voltage for electrons proceeding from the semiconductor to the metal. If contact areas of the first and second site of RSD are equal, accordingly, to g_1S and g_2S (where $g_1+g_2=1$), then according to the thermionic emission theory [5], the forward branch of the volt-ampere characteristic of RSD is expressed by the formula:

$$I_F = g_1 I_{F1} + g_2 I_{F2} = SAT^2\left\{g_1 \exp\left[-\left(\Phi_{B1} + \Delta\Phi_{01} + \beta qU\right)/kT\right] + g_2 \exp\left[-\left(\Phi_{B2} - \Delta\Phi_{B2}\right)/kT\right]\right\}\left[\exp\left(qU/kT\right) - 1\right] \approx$$
$$\approx S_{EF} AT^2 \exp\left(-\Phi_{BE}/kT\right)\exp\left(qU/n_F kT\right) \quad (3)$$

where index 1 and 2 demonstrate corresponding parameters for the first and second site of RSD.

At the application of a reverse voltage to RSD, in the near contact region of the semiconductor interfaces an external field and an additional field are antiparallel for the first site and parallel for the second site. When the additional electrical field penetrates into the semiconductor on the depth l, larger than the width of a depletion layer of the semiconductor d, then redistribution of free carriers of charges occurs outside of d. Exactly this redistribution of free charges carriers causes the formation of the part $\Delta\Phi_{B1}'$ of the increment $\Delta\Phi_{B1}$ of the first site. With growth of the voltage $U=U_C$ up to the definite critical value U_{CR} (where $qU_C < \Delta\Phi_{B1}'$ and $qU_{CR} = \Delta\Phi_{B1}'$), the value Φ_{B1}' is partially compensated. At $0 < U_C \le U_{CR}$ the reverse current does not flow through the first site of RSD and $\Delta\Phi_{B1}$ decreases on the value βqU, and $\Delta\Phi_{B2}$ increases. Such current transportation property was observed experimentally both at research of a contact surface of RSD with the help of a scanning electron microscope [9,10], and at research of a reverse branch of volt-ampere characteristic of RSD [11].

According to the thermionic emission theory, the reverse branch of volt-ampere characteristic of RSD at the account of a bove mentioned facts is described by the formula:

$$I_R = g_1 I_{R1} + g_2 I_{R2} = SAT^2\left\{g_1 \exp\left[-\left(\Phi_{B1} + \Delta\Phi_{01} - \beta qU\right)/kT\right] \cdot \left[\exp\left(-q\left(U - U_C\right)/kT\right) - 1\right] + \right.$$
$$\left. + g_2 \exp\left[-\left(\Phi_{B2} - \Delta\Phi_{B2}\right)/kT\right] \cdot \left[\exp\left(qU/kT\right) - 1\right]\right\} \approx S_{EF} AT^2 \exp\left(-\Phi_{BE}/kT\right)\exp\left(qU/n_R kT\right) \quad (4)$$

where $U_C=0$ at the forward direction and $U_C=U\le U_{CR}$ at the reverse direction.

When the additional electrical field penetrates into the semiconductor on the depth $l<d$, then the critical voltage will be $U_{CR}=0$ ($U_C=0$) and both the forward and the reverse currents begin to flow through the first site of RSD at once with growth of the voltage (beginning from zero).

RESULTS OF CALCULATION

For a quantitative estimation of influence of the additional electrical field on volt-ampere characteristic of RSD, their forward and reverse branches were constructed according to formulas (1) - (4). Thus following reasonable values of electrophysical parameters of RSD were used:

$\Phi_{B1}+\Delta\Phi_{01}=0.60eV$; $\Phi_{B2}-\Delta\Phi_{02}=0.65eV$; $\beta=0.02$; $U_D=0.5V$; $U_{CR}=2V$; $A=120Acm^{-2}K^{-2}$; $T=300K$; $kT=0.026eV$; $N_D=5.5\cdot10^{15}cm^{-3}$; $\varepsilon s=10.6\cdot10^{-13}K1.V^{-1}cm^{-1}$; $U_{BR}=100V$; $S=10^{-4}cm^2$; $g_2=1-g_1$; $g_1=1$; 0.5; 10^{-1}; 10^{-2}; 10^{-3}; 10^{-4}; 10^{-8}; 0; $U_F=0-0.3V$; $U_R=0-100V$.

In fig. 1 forward volt-ampere characteristics of RSD are shown at different values g_1 and g_2, calculated on the formulas (3) taking into account formulas (1) and (2). It is seen, that the current of the general contact at $g_1=1$ and $g_2=0$ consists only of the current of the first site of RSD with the effective barrier height Φ_{B9}=0.60eV and non-ideality factor n_F=1.02, and at $g_1=0$ and $g_2=1$ consists only of the current of the second site of RSD with Φ_{B9}=0.65eV and n_F=1.01. At decrease of g_1 from 1 up to 10^{-2}, the contribution of the current of the first site of RSD to the current of the general contact decreases. Therefore the effective barrier height of the general contact of RSD increases up to the value 0.65eV and the non-ideality factor decreases up to the value n_F=1.01.

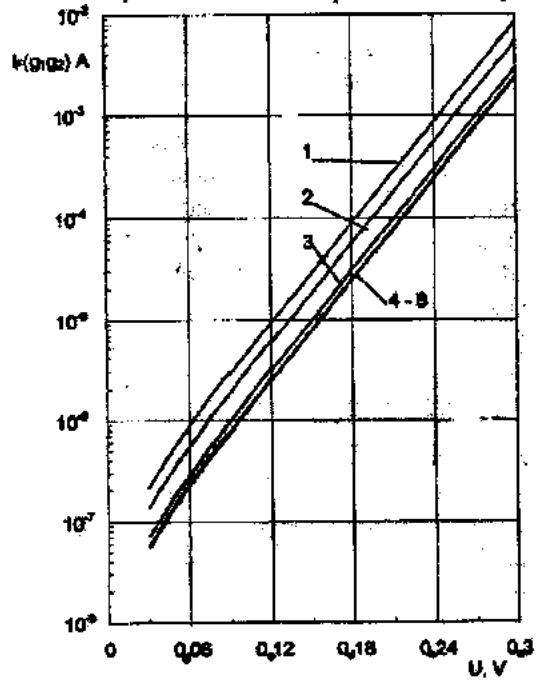

Fig. 1. Forward I-V characteristics of real Schottky diodes at

$g_2=1-g_1$, where g_1: 1) - 1; 2) – 0.5; 3) -10^{-1}; 4) -10^{-2}; 5) -10^{-3}; 6) -10^{-4}; 7) -10^{-8}; 8) - 0.

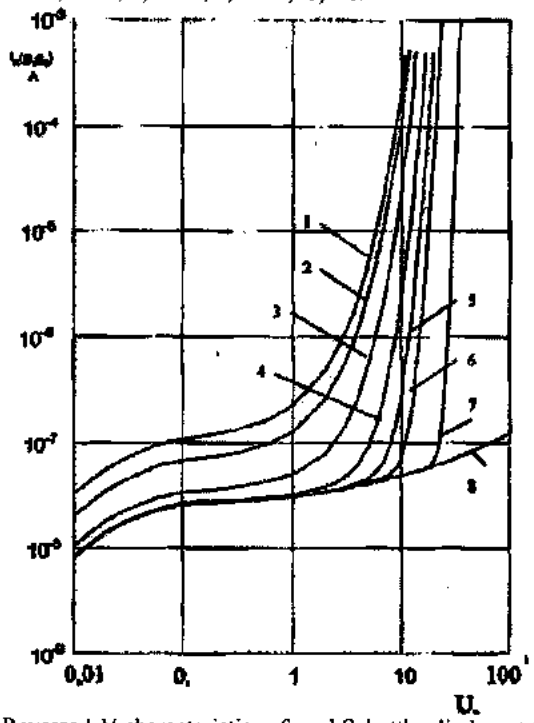

Fig.2. Reverse I-V characteristics of real Schottky diodes at $U_C=0$ and $g_2=1-g_1$, where g_1: 1) - 1; 2) – 0.5; 3) -10^{-1}; 4) -10^{-2}; 5) -10^{-3}; 6) -10^{-4}; 7) -10^{-8}; 8) - 0.

At further decrease of g_1, i.e. at $0\le g_1<10^{-2}$, the contribution of the current of the first site to the current of the general contact of RSD is not essential. It is necessary to mark, that at $\beta=0.1$ the factor n_F increases and becomes equals 1.11.

In fig.2 reverse branches of the volt-ampere characteristic of RSD are constructed on the formula (4) at $U_C=0$ and different values g_1 and g_2. At $g_1=1$ and $g_2=0$ the current of the general contact consists only of the current of the first site of RSD with the effective barrier height $\Phi_{BE}=0.60$eV and area $S_{EF}=S$. The dependence of the reverse current on the voltage at $U\ge0.1$V has the exponential nature and is determined by the formula:

$$I_R=S_{EF}AT^2\exp(-\Phi_{BE}/kT)\exp(qU/n_RkT) \quad (5)$$

Here the dimensionless factor n_R becomes equal to $n_R=n_F/(n_F-1)=51$. At the voltage $U=10$V the barrier height of RSD decreases on $\beta qU=0.2$eV and the reverse current raises on four order of magnitude. At $g_1=0$ and $g_2=1$ the current of the general contact consists only of the current of the second site of RSD with the effective barrier height $\Phi_{BE}=0.65$eV and its dependence on the voltage expresses by the formula:

$$I_R = S_{EF}AT^2\exp\left(-\Phi_{BE}/kT\right)\exp\left\{q\left[\left(q^3N_D/8\pi^2\varepsilon_s^3\right)\left(U_D+U-kT/q\right)\right]^{1/4}/kT\right\} \quad (6)$$

It is seen from the figure that at $g_2=1$ the current I_R increases nonconsiderably with growth of the voltage.

At $g_1<1$, $g_2>0$ reverse branches of the volt-ampere characteristic of RSD express by the sum $I_R=g_1I_{R1}+g_2I_{R2}$. At $g_1\ge0.01$ volt-ampere characteristics of the general contact are completely determined by the current of the first site of RSD. With decrease of g_1, i.e. at $g_1<0.01$, the weak growth of the back current of the general contact takes place at initial values of the voltage. Even at $g_1=10^{-8}$ it is watched only up to $U=25$V.

In fig.3 the reverse branches of the volt-ampere characteristics of RSD are constructed on the formula (4) at $U_C\neq0$ and different values g_1 and g_2. At $g_1=1$ and $g_2=0$ with increase of the voltage $U=U_C$ up to the value $U=U_{CR}=2$V, the reverse current does not flow through RSD. At $U>2$V the current starts to flow through contact which increases exponentially with the voltage growth according to the formula:

$$I_R = S_{EF}AT^2\exp\left[-\left(\Phi_{BE}-\beta qU\right)/kT\right]\cdot \left[\exp\left(q\left(U-U_C\right)/kT\right)-1\right] \quad (7)$$

At $g_1=0$ and $g_2=1$, the volt-ampere characteristic expresses by the formula (6). At $g_1<1$ and $g_2>0$ currents of the general contact consist of the sum of currents of two sites of RSD.

As it is seen from fig. 2 and fig. 3, the sharp growth of the reverse current of RSD reminds the process of the electric breakdown of the transition, whose theoretical value is 100V. A breakdown voltage of RSD is usually determined as the voltage, at which the reverse current starts strongly to increase. Whereas it is seen from fig. 2, that at $g_1=10^{-2}$ the increase of the reverse current becomes noticeable at $I_R=0.001$ A and the reverse voltage has the value $U=6$V much smaller, than the breakdown voltage 100V. Notwithstanding that, at $g_1<10^{-2}$ the current of the first site of RSD has not an effect in the current of the general contact in the forward direction, it becomes essential in backwards.

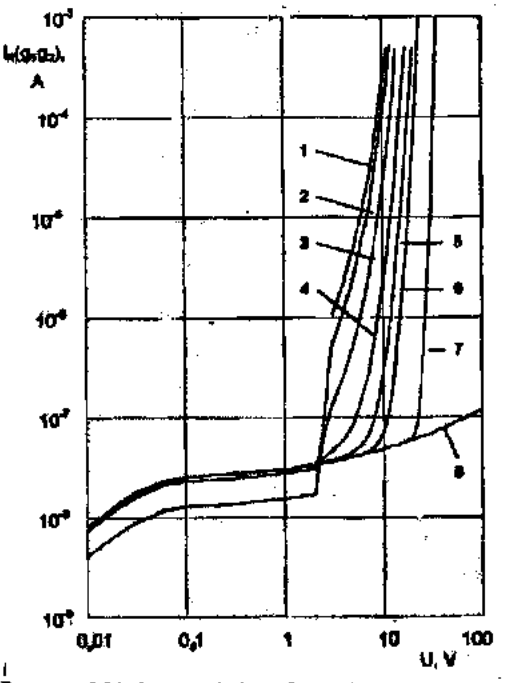

Fig.3. Reverse I-V characteristics of real Schottky diodes at $U_C\neq0$ and $g_2=1-g_1$, where g_1: 1) - 1; 2) – 0.5; 3) -10^{-1};

4) -10^{-2}; 5) -10^{-3}; 6) -10^{-4}; 7) -10^{-8}; 8) - 0.

Thus at g_1=10^{-5} the early breakdown is watched at U=12V, and at g_1=10^{-8} the voltage of the premature is only U=25V. Only at g_1=0 and g_2=1 a breakdown of the RSD takes place at the voltage U=100V.

CONCLUTIONS

In summary it is possible to say, that under influence of the additional electrical field the non-ideality factor of the forward branch of their volt-ampere characteristics of RSD increases, its reverse branch is not saturated and at low voltages the strong growth of the reverse current occurs, i.e. there is a premature breakdown of RSD.

[1] *L.N. Dobretsov, M.V. Gomaiunova.* Emmision electronics, M., Science, 1966,564p. (in Russian).

[2] *R.K. Mamedov.* Izv. AN. Az. SSR, seriya fiz.mat., 1984, №5, p.73, (in Russian).

[3] *R.K.Mamedov.* Proceeding of the 4-th Baku International Congress on Energy, Ecology, Economy. Baku, 1997, p.205.

[4] *V.S. Fomenco.* Emmision properties of materials, Kiev, Naucova Dumka 1981,338 p.

[5] *S.M. Zee.* Physics of semiconductor devices, M., "Energy", 1973, 650 p.

[6] *S.G. Askerov.* Letter to TFJ, 1977, v.3, №18, p. 968.

[7] *A.N. Korol, B.E. Strecha.* In J. Semiconducting engineering and microelectronics, 1974, №18, p. 39.

[8] *V.A. Jonson, R.N. Smith, H.J. Yecrian.* J.Appl. Phys., 1950, v.21, p.283.

[9] *G.J. Russel, M.J. Robertson, J. Woods.* Phys. Statys Solidi, 1980, (a) 57, № 1, p.253.

[10] *R.B. Marcus, S.E. Haszko, S.P. Murarka, J.C. Irvin.* J., Electrochem. Soc.: Solid-State science and technology, 1974, v.121, № 5, p.692

[11] *R.K. Mamedov , M.A. Nabiev.* Phys.Sol.St., 1986, v.20, № 2, p.332.

R.Q. Məmmədov

REAL ŞOTTKİ DİODLARININ VAX-na ƏLAVƏ ELEKTRİK SAHƏSİNİN TƏSİRİ

Real Şottki diodları, adətən, yarımkeçiricinin kontaktaltı hissəsində kontakt səthinin emissiya qeyri-bircinsliyi hesabına yaranan əlavə elektrik sahəsinin təsirinə məruz qalır. Aşkar edilmişdir ki, əlavə elektrik sahəsinin təsiri ilə VAX-ın qeyri-idеallıq əmsalı artır, əks istiqamətdə cərəyanın doyma halı baş vermir və gərginliyin kiçik qiymətlərində əks cərəyan sürətlə artır, yəni keçiddə vaxtından əvvəl elektrik deşilməsi baş verir.

Р.К. Мамедов

ВЛИЯНИЕ ДОПОЛНИТЕЛЬНОГО ЭЛЕКТРИЧЕСКОГО ПОЛЯ НА ВАХ РЕАЛЬНЫХ ДИОДОВ ШОТТКИ

Реальные диоды Шоттки обычно подвергаются воздействию дополнительного электрического поля, возникающего в приконтактной области полупроводника из-за эмиссионной неоднородности границы раздела. Установлено, что под влиянием дополнительного электрического поля коэффициент неидеальности прямой ветви их ВАХ увеличивается, ее обратная ветвь не насыщается и при низких напряжениях происходит сильное возрастание обратного тока, т.е. происходит преждевременный пробой перехода.

Received: 23.05.01

CONCENTRATION PHASE TRANSITION IN Ag_2Te WITH AN EXCESS OF Ag

F.F. ALIEV
Institute of Physics of Azerbaijan National Academy of Sciences
370143, H. Javid av., 33, Baku

The concentration phase transition (CPT) was observed in samples Ag_2Te with the excess of Ag>0,01 at.% at investigation of the concentration and temperature dependences of electric and thermoelectric properties. It is supposed, that the appearance of CPT is connected with the formation of the new sublattice of Ag in Ag_2Te beginning from the excess ~0,01 at.%. It is shown that the first sublattice of Ag_I atoms creates the two-electrons donor and the second-(Ag_2) one-electron donor. The last fact is caused by the position of the Fermi level lower or inside of the impurity state.

Electric and thermoelectric properties of Ag_2Te have been investigated with the excess of Ag up to ~0.25 at %. Concentration phase transition (CPT) is observed in crystals with excess of Ag 0.1÷12 at %. Transition is connected with the appearance of new sublattice Ag in Ag_2Te.

Ag_2Te is classified among narrow-band semiconductors with high electron mobility, small lattice thermal conduction and having the structural phase transition in the temperature range 390÷450K [1-3]. Therefore investigation of concentration and temperature dependences of kinetic parameters is important for revealing of application field in electron technology.

Investigations are carried out on a series of Ag_2Te samples: the stoichiometric composition with the excess of Te (up to 1.0 at %) and Ag (up to 0.25 at %). As it is known [2], the excess of Te up to 1.0 at % does not cause a falling of the second phase, any changes in crystal structure are not observed and causes the formation of p-Ag_2Te [3]; and it is established, that the hole concentration is proportional to Te content [1]. Excess of Ag in homogeneity region leads to the formation of n-Ag_2Te.

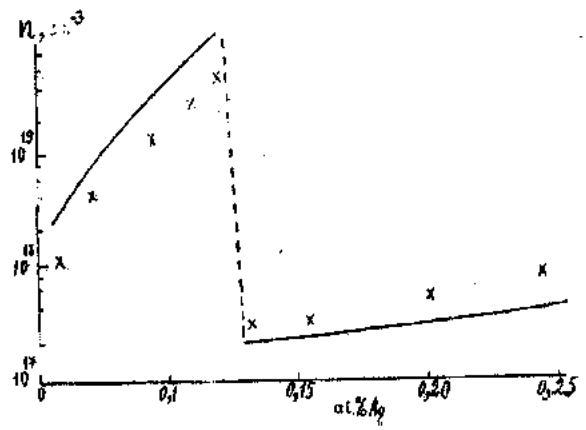

Fig.1 Electron concentration dependence on the excess of *Ag*. Solid line is calculated.

At investigation of kinetic effects in n-Ag_2Te it is found that the excess of Ag up to ~0.10 at % leads to the rise of the electron concentration (n) up to n~$5.0\cdot10^{19}$cm^{-3} and the excess of Ag up to ~ 0.12 at % decreases n sharply about by a factor of 10^2 (fig.1), i.e. CPT takes place. This fact has not been described in literature.

With this aim concentration and temperature dependences of the Hall coefficient R, electroconductivity σ and thermoelectromotive force α_0 have been investigated for revealing of CPT mechanism in n-Ag_2Te.

Samples have been obtained by the common technology with the excess of Ag up to 0.25 at %. Refined silver with 99.99% purity and Te of TA-1 model after two fold distillation in vacuum were used for Ag_2Te synthesis. Samples were cut out to the shape of the parallelepiped with sizes 2x3x10 mm^3. Obtained experimental data of temperature dependences $R(T)$, $\sigma(T)$ and $\alpha_0(T)$ for two samples of n- Ag_2Te with the excess of Ag 0.10 and 0.12 at % are presented on fig.2.

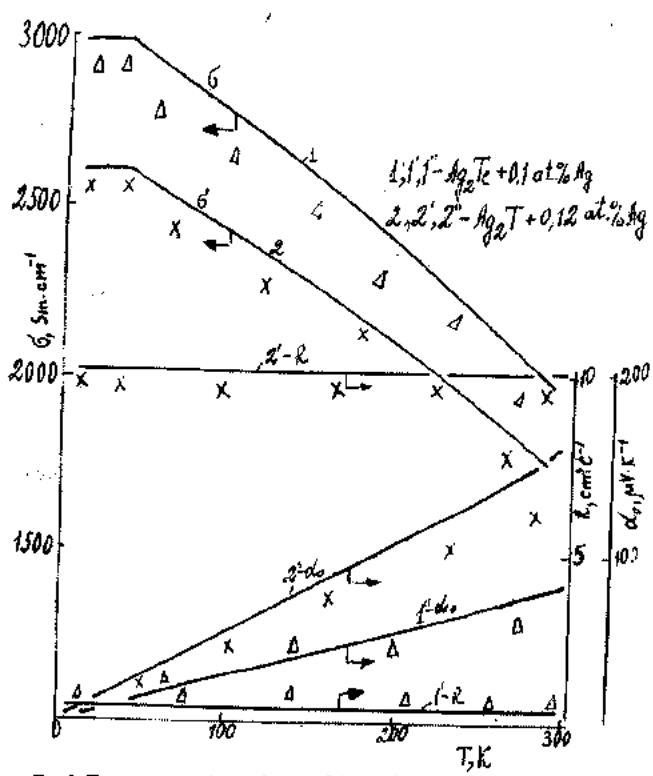

Fig.2. Temperature dependence of the Hall coefficient R (at H=12kE) electroconductivity σ and thermoelectromotive force α_0. Solid lines are calculated.

It is seen that for both samples the behavior of $R(T)$, $\sigma(T)$ and $\alpha_0(T)$ is characteristic for semiconductors with one kind of charge carriers in the degenerate state and Cane's law of dispersion [4]. In spite of essential distinction of their concentrations, qualitative distinctions are not observed in them. Authors [5] suggested that in Ag chalkogenides Ag can be two-electron donor giving two electrons into the conduction

band ($Ag^+ \rightarrow Ag^{3+}+2e^-$). Then the forming two-electron state is located either at the expense of strong interaction with the lattice or strong interaction with vacancies and other defects. Our experimental data on samples with Ag content up to 0.10at.% (fig.1) confirm hypothesis of authors [5]. Starting with the excess of Ag 0.12 at.%, the electron concentration rises proportionally to Ag content, i.e. in this case the excess of Ag plays a role of one-electron donors.

In paper [6] it is noted, that there are two structurally different types of Ag atoms in Ag_2Te. Ag_I atom is surrounded by four Te atoms on distances 2.87; 2.91; 3.04 and 2.99Å; Ag_2 atom has five nearest neighbours on the distances 3.04; 3.01; 2.95; 2.90 and 2.85Å. In both positions the cell has 4 (Ag_2Te) and all atoms occupy the disposition of 4 order. Thus Ag atoms form 2 sublattices of Ag atoms in the structure. CPT takes place at the transition from the first position (Ag_I) to the second one (Ag_2).

Ag_2Te relates to the class of compensated semiconductors [7,8]. Thus Te atoms create acceptor levels disposed on the distance $(0.03\text{-}7\cdot10^{-5}T\cdot K^{-1})$eV from the conduction bottom [4], and Ag atoms in the forbidden band create local energy donor levels [9].

In literature an activation energy value of donors E_d is absent. Experimental determination of E_d at the small value of band gap $E_g=(0{,}03\text{-}7\cdot10^{-5}T\cdot K^{-1})$eV and the high value of the donor concentration N_d is very difficult. In this situation the following method is suggested [4]. At any degree of the electron gas degeneration with a nonstandard band thermal, EME forces are expressed according to [10].

$$\alpha_0 = -\frac{K_0}{e}\left[\frac{I^1_{r+1.2}(\mu^*,\beta)}{I^0_{r+1.2}(\mu,\beta)} - \mu^*\right] \qquad (1)$$

where $\mu^*=\mu/K_0T$ is the reduced chemical potential, μ and $I^m_{n,k}$ are the Fermi level and two – parametric Fermi integral, $\beta=K_0T/E_g$ is the parameter specifying a non-parabolic of the band. From (1) μE_d values have been determined at T=15 K. If μ, N_d and m_n [4] magnitudes (m_n is the effective electron mass on the Fermi level) are known, you can define E_d according to [10]:

$$E_d = K_0T/n\left[\frac{2\pi^{3/2}\hbar N_d}{(2m_nK_0T)^{3/2}}\right] - 2\mu \qquad (2)$$

Magnitudes E_{d_0} have been calculated (at T=0K) taking into account the dependence $E_g(T)$ [4]: $E_{d_0}\approx$2meV (at $N_d=(1.1\div50)\cdot10^{18}sm^{-3}$) and $E_{d_0}\approx$5meV (at $N_d=(1.1\div6.25)\cdot10^{17}sm^{-3}$) (counting from the bottom of the conduction band) (fig.3).

If you take into consideration that weak compensation goes in the concentration interval $N_d=(1.1\div5.0)\cdot10^{18}sm^{-3}$, and high compensation goes in the interval $N_d=(1.1\div6.25)\cdot10^{17}sm^{-3}$, then the state density in both cases are expressed, respectively [11]:

$$\rho(\varepsilon)=\frac{N_d}{y\sqrt{\pi}}\exp\left(-\varepsilon^2/y^2\right) \text{ and } \rho(\varepsilon)=\frac{3E_d^3}{2\varepsilon^4}N_d, \qquad (3)$$

where $y=0{,}26E_d'(N_a/N_d)^{1/4}$, $E_d'=\left(\frac{4\pi}{3}N_d\right)^{1/3}\frac{e^2}{\chi}$ [11], N_a is the acceptor impurity concentration, χ is the dielectric constant of the crystal. Chemical potential in the first case is calculated from (2), and in the second case is calculated according to [11]:

$$\mu = -\frac{E_d'}{2^{1/3}(1-N_a/N_d)} \qquad (4)$$

If the value μ is known, then the concentration can be presented as

$$n = \int_{-E_d'}^{\mu}\upsilon(\varepsilon)d\varepsilon \qquad (5)$$

and temperature dependence of thermoelectromotive forces as (1), R and σ as

$$R = \frac{1}{en},\ \sigma = enU_n(T). \qquad (6)$$

Temperature dependence of the electron mobility $U_n(T)$ at any degree of electron gas degeneration for a non-standard band has been determined earlier.

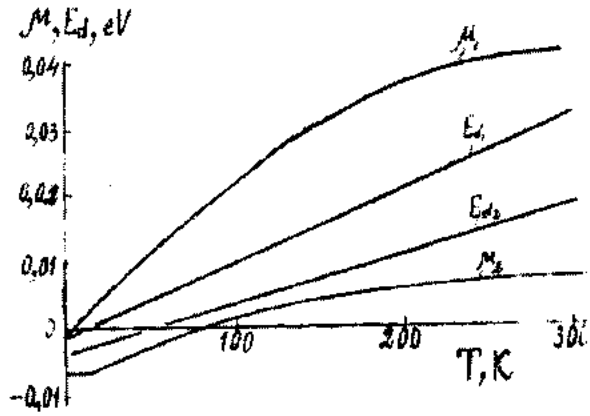

Fig.3. Temperature dependences of the chemical potential (μ) and activation energy of donors (E_d) $\cdot\mu_1E$ and μ_2E are calculated in Ag_2Te with the excess of Ag 0.10 and 0.12 at %, respectivety.

Calculated data are presented on fig.1,2. As it is seen, calculated curves n to CPT are below. The reason is due to the error of the application field of the formula (3). Agreement of calculated and experimental curves R, σ and α_0 confirms the assumption, that N_dAg_2Te is weakly and highly compensated semiconductor in corresponding above mentioned intervals. It offers the scope for understanding of the origin of CPT in Ag_2Te. New sublattice Ag (position Ag_2) is formed in the cell Ag_2Te starting with the excess of Ag 0.12 at %. In this case the crystal is highly compensated at the expense of interaction with vacancies and other defects. Then the electron concentration, localized in donors $n=N_d-N_a$, is much less than the donor concentration. Thus at all temperatures all electrons can be arranged in donors, whose energy levels are significantly reduced by the potential of neighbour

charged impurities. As a result, μ is below than the level of the isolated impurity (fig.3). The less electron concentration of n the deeper μ is arranged.

If we do not take into consideration Hauss fluctuations [11] it can be suggested that another positively charge donor can appeare in the vicinity of some donors on the distance $r<<N_d^{-1/3}$, where μ is above the impurity state. At $r>>\alpha$ (α - is the effective Bohr radius) the correction of E to the energy level in the first donor is defined only by the Coulomb potential of the second donor, i.e. $E=-e^2/\varkappa r$. In this case it is suggested that the second donor is empty. Band energy of the second electron in the couple of donors is close to $R\ E_d^1$. Therefore at the high compensation, when μ is below the donor impurity level and is into the impurity state (fig.3), only one electron can correspond to the couple of close donors.

[1] *S.A. Aliev, F.F. Aliev, S.G. Abdinov, Z.S. Gasanov, D.M. Ragimov.* Izv. VUZ , Fizika 6, 1990, p.41.

[2] *S.A. Aliev, F.F. Aliev, G.P. Pashaev.* Izv. Acad. of Sci. Ser. «Neorg. Materials», 1993, vol.29, №8, p. 1073.

[3] *S.A. Aliev, F.F. Aliev, Z.S. Gasanov.* FTT, 1998, 40, 9, p. 1693.

[4] *F.F. Aliev.* Fizika, 2000, c. 6, №1, p. 53-56.

[5] *I.A. Drapkin, B.J. Meidzhes.* FTP, 1987, 21, 9, p.1715.

[6] *A.I. Fruch.* Kristalogr, 1959, Bd 112, s.44.

[7] *V.I. Vinetskyi, G.A. Kholodar.* «Statistical interaction of electrons and defects in semiconductors». Kiev , «Naukova Dumka», 1969, p. 186. (in Russian)

[8] *S.A. Aliev, F.F. Aliev.* Izv. Acad. Of Sci. Ser. «Neorg. Materials». 1988, 24, 2, 341.

[9] *V.V. Gorbachov, I.M. Putilin.* Izv. Acad. Of Sci. Ser. «Neorg. Materials», 1988, 24. 2. 341.

[10] *B.M. Askerov.* «Kinetic effects in semiconductors», L., «Nauka», 1970, p.303 (in Russian).

[11] *B.I. Shklovskii, A.L. Efros.* «Electron properties of doped semiconductors». M. «Nauka», 1979, p.416 (in Russian).

F.F. Əliyev

Ag_2Te KRİSTALININ Ag ARTIQLIĞINDA KONSENTRASİYA FAZA KEÇİDİ

Ag_2Te kristalında 0.25 at.% Ag artıqlığı ilə olan nümunələrin elektrik və termoelektrik xassələri tədqiq olunmuşdur. Ag artıqlığının 0.1÷0.12at.%-də konsentrasiya faza keçidi (KFK) aşkar olunmuşdur. Keçid yeni alt qəfəsin Ag artıqlığının hesabına yaranması ilə əlaqələnmişdir.

Ф.Ф. АЛИЕВ

КОНЦЕНТРАЦИОННЫЙ ФАЗОВЫЙ ПЕРЕХОД В Ag_2Te С ИЗБЫТКОМ Ag

При исследовании концентрационных и температурных зависимостей электрических и термоэлектрических свойств Ag_2Te обнаружен концентрационный фазовый переход (КФП) в образцах с избытком Ag>0.01at.%. Предполагается, что появление КФП связано с образованием новой подрешетки Ag в Ag_2Te начиная с избытка ~ 0.01 at.%. Показано, что первая подрешетка атома Ag_i создает двухэлектронный донор, а вторая – (Ag_2) - одноэлектронный донор. Последнее связано с нахождением уровня Ферми ниже или внутри примесного состояния.

Received: 04.06.01

GRAPH –THEORETIC ANALYSIS METHOD OF NON-LINEAR KINETICS OF BIOCHEMICAL REACTIONS

Sh.K. BAYRAMOV
Azerbaijan Medical University
370022, Bakikhanov str. 23, Baku, Azerbaijan

Using the double barrel graph theory, the algorithmic method for determination of characteristic polynomial coefficients of system nonlinear kinetics equation of biochemical reactions is offered. Several characteristic polynomial coefficients are expressed by stoichiometric coefficients of reagents in the biochemical reaction system and their analytical expressions are obtained.

Key words: nonlinear enzyme kinetic, double barrel graph theory.

INTRODUCTION

At last time, theoretical methods for solution of kinetic problems based on linear graph theory, are widely used in biokinetic studies [1-8]. Linear graphs are used at analysis of the steady- and pre-steady-state (transient phase) of enzyme reactions with a single enzyme form participating in each elementary reaction. In linear mechanisms, the enzyme forms do not interact with each other at any stage. Moreover, each stage of the enzyme reaction in the transient phase according to assumption is a pseudo-first-order reaction because a change of the substrate concentration is negligible during the formation of intermediate enzyme forms.

In living cells, concentrations of many enzymes are often of the same magnitude, as concentrations of the metabolites, i.e. compounds participating in the elementary stages at similar concentrations are equivalent components of elementary reactions in many cases. Such systems are nonlinear. Development of more simple and convenient methods for research of stability of stationary states in nonlinear kinetic systems has not lost the importance. An attraction of the theory of double barrel graphs [9] (bigraphs) allows essentially to simplify the research scheme of stationary state stability.

BASIC DEFINITIONS AND THEORETICAL TREATMENTS

Two types of tops are used in representation of double barrel graph theory, where substances (reagents) are tops of the type A, and reactions are tops of the type B. Tops of different types are connected with oriented branches. The branch going from the substance, participating in the reaction, and other branch going from the reaction to the substance, which is produced as a result of this reaction, form a "positive" pathway. Graphically it is represented as $A_i \rightarrow B_k \rightarrow A_j$, where A is the top - substance, B_k is the top - reaction. Two branches going from two substances, participating in the same reaction, make a "negative" pathway, $A_i \rightarrow B_k \leftarrow A_j$. The closed sequence of ways forms the "cycle". Parity of a cycle is determined by the parity of a number of negative pathways in it. Unity of non-crossed on tops A cycles and branches, going from the substance to the reaction, is called as a "subgraph". The number of tops A in "subgraph" is called to as his "order". The m – order "fragment" is m reactions chosen from the scheme, considered in relation to chosen m substances. Other substances not participating in chosen reactions, do not enter in the "fragment" and are considered as constants. "Fragment" of the scheme refers to "critical" if the sum of coefficients of all his "subgraphs", containing odd number of "even" cycles, is more than the sum of coefficients of all other subgraphs. Subgraphs with odd number of even cycles give the negative contribution to the coefficients of a characteristic polynomial and are the reason of instability.

Stability of the stationary state is investigated by linearization of nonlinear kinetic equations near stationary points. Eigenvalues governing the behavior of the system near these steady states are solutions of the characteristic equation $|\lambda I - J|=0$, where λ is an eigenvalue, I is the unit matrix, J is the Jacobian. Stability is provided, if the Jacobian matrix for system of kinetic equations with elements:

$$J_{ij} = \sum_{k=1}^{m} \gamma_{ij} \partial \upsilon_k / \partial u_j$$

has eigenvalues with negative real parts. Here, m is the number of reaction stages, $\gamma_{ik}=\beta_{ik}-\alpha_{ik}$, β_{ik} and α_{ik} are the stoichiometric coefficients (numbers of molecules of the compound U_i generated and going into the k-th reaction, respectively), u_i is the concentration of the i-th compound, υ_k is the rate of the k-th reaction. If even though one of coefficients α_i of the characteristic polynomial Jacobian matrix of the reaction system

$$P = \lambda^n + a_1\lambda^{n-1} + a_2\lambda^{n-2} + \ldots + a_m \qquad (1)$$

(where m corresponds to the rank of the γ_{ik} matrix of the reaction system) changes its sign from plus to minus, when the reagent concentrations are changed, then the steady state of the system becomes unstable. According to Ivanova [10], if the lower coefficient (α_m) is negative and there are not steady-state points on the border of the polyhedron of invariance, determined by the material balance equations in the phase space, then there should be several steady-state points within the polyhedron (multiple steady states).

If $\alpha_m>0$ at any concentration, then there is a single steady state point (if boundary conditions are fulfilled). In this case, if another coefficient $\alpha_{m-k}<0$ $(k<m)$, the single steady state point can be unstable. A stable limitary cycle, i.e. self-oscillations, occurs in the vicinity of this single unstable steady-state point.

Thus, the analysis of existence of critical regimes is related with coefficients of the characteristic polynomial (1). The stage of determination of characteristic polynomial

coefficients is the most toilful stage in the analysis of nonlinear systems. In this work, we offer an algebraic algorithmic method for determination of these coefficients by using of bigraphs.

For this aim let's rewrite elements of the Jacobian matrix in the form:

$$J_{ij}=\sum_{k=1}^{m}(\beta_{ik}-\alpha_{ik})\partial\upsilon_k/\partial u_j=\sum_{k=1}^{m}\left((\beta_{ik}\partial\upsilon_k/\partial u_j-\alpha_{ik}\partial\upsilon_k/\partial u_j)_{i\neq j}+(\gamma_{ik}\partial\upsilon_k/\partial u_j)_{i=j}\right)=$$

$$=\sum_{k=1}^{m}(P_{ji}^k+N_{ji}^k+H_i^k)$$

where,

$$P_{ji}^k=\beta_{ik}\frac{\partial\upsilon_k}{\partial u_j},\quad N_{ji}^k=-\alpha_{ik}\frac{\partial\upsilon_k}{\partial u_j},\quad H_i^k=\gamma_{ik}\frac{\partial\upsilon_k}{\partial u_i}. \tag{2}$$

From the point of view of the double barrel graph theory, these quantities have a real topological sense: P_{ji}^k is the positive pathway from A_j-top to A_i-top through B_k-top, i.e. the pathway corresponds to the generation of compound i in the reaction k; N_{ji}^k is the negative pathway from A_j- top to A_i-top through B_k-top, i.e. the pathway corresponds to interaction of compounds j and i in the reaction k; H_i^k is the half-pathway (or segment) of compound i involved in the reaction k. Here it is necessary to note that in non-autocatalytic reactions $\beta_{ij}=0$ at $\alpha_{ij}\neq 0$ and therefore in this case we obtain the value for half-pathway as in [11]:

$$H_i^k=-\alpha_{ik}\frac{\partial\upsilon_k}{\partial u_i}$$

This expression is true only for non-autocatalytic reactions.

If the reaction proceeds according to the mass action law, i.e., if

$$\upsilon_k=K_k u_1^{\alpha_{1k}}\ldots u_n^{\alpha_{nk}}$$

where K_k is the rate constant of k-th reaction stage, then expressions for pathways and half-pathways are simplified:

$$P_{ij}^k=\alpha_{ik}\beta_{jk}\frac{\upsilon_k}{u_i};\ N_{ij}^k=-\alpha_{ik}\alpha_{jk}\frac{\upsilon_k}{u_i};\ H_i^k=\alpha_{ik}\gamma_{ik}\frac{\upsilon_k}{u_i} \tag{3}$$

(υ_k is the rate of the stage k, u_i is the concentration of the i– th compound).

Let's write the sum of elements of the i-th column of the Jacobian matrix. This sum will be called by the nodal polynomial for the i–th A-top of a bigraph. The nodal polynomial is equal to the sum of all pathways (positive and negative) and half-pathways originating from the given i - th A-top:

$$M_i=\sum_{j=1}^{n}\sum_{k=1}^{m}\left(P_{ij}^k+N_{ij}^k+H_i^k\right) \tag{4}$$

For the determination of coefficients α_i of the characteristic polynomial (1), using the conception of the nodal polynomial, we offer following rules of determination:

- α_1 is the sum of all half-pathways originating from all nodes with the negative sign, i.e., α_1 is determined as the sum of contributions of all possible first-order "subgraphs":

$$\alpha_1=-\sum_{i=1}^{n}\sum_{k=1}^{m}H_i^k \tag{5}$$

- α_2 is the sum of all twin products of all nodal polynomials, i.e., α_2 is determined as the sum of contributions of all possible two-order "subgraphs":

$$\alpha_2=\sum_{i=1}^{n}\sum_{j=1}^{n}M_iM_j\quad(i\neq j) \tag{6}$$

- α_3 is the sum of all triple products of all nodal polynomials, i.e., α_3 is determined as the sum of contributions of all possible three-order "subgraphs":

$$\alpha_3=\sum_{i=1}^{n}\sum_{j=1}^{n}\sum_{k=1}^{n}M_iM_jM_k\,(i\neq j,\ i\neq k,\ j\neq k),\ etc. \tag{7}$$

Some of members obtaining in these products are equal to zero. These members are determined by following rules of "member reduction":

- a product where the index of one B–top presents more than once is equal to zero;
- products where pathways do not form cycles (determined by lower indices of the pathways) also are equal to zero (cyclic products are included into the sum with the opposite sign);

- members corresponding to the product of the pathway and the half-pathway are equal to zero.

EXPRESSION OF POLYNOMIAL COEFFICIENTS VIA STOICHIOMETRIC COEFFICIENTS OF REAGENTS

The above-stated rules allow us to express coefficients α_i of the characteristic polynomial (1) through stoichiometric coefficients of reagents. Really, taking into account (3) and (4) in (5), we obtaine for α_1:

$$\alpha_1 = \sum_{i=1}^{n}\sum_{k=1}^{m} \alpha_{ik}\gamma_{ik}\ \frac{\overline{\upsilon}_k}{\overline{U}_i} \tag{8}$$

Other coefficients are expressed through stoichiometric coefficients with point of view of reduction rules. In the present work, results of calculations for characteristic polynomial coefficients α_2 ,α_3 and α_4 are presented:

$$\alpha_2 = \sum_{i=1}^{n}\sum_{j>i}^{n} \alpha_{ik_1}\alpha_{jk_2}(\gamma_{ik_1}\gamma_{jk_2} - \gamma_{ik_2}\gamma_{jk_1})\ \frac{\overline{U}_{k_1}}{\overline{U}_i}\ \frac{\overline{U}_{k_2}}{\overline{U}_j}\ k_1 \neq k_2,\ k_1 = 1, 2 \ldots m,\ k_2 = 1, 2 \ldots m \tag{9}$$

$$\alpha_3 = \sum_{i=1}^{n}\sum_{j>i}^{n}\left\{\sum_{l>j}^{n} b_{31}b_{32} - \sum_{l\neq i,j}^{n} b_{31}(b_{33} + b_{34})\right\}\frac{\overline{\upsilon}_{k_1}}{\overline{U}_i}\ \frac{\overline{\upsilon}_{k_2}}{\overline{U}_j}\ \frac{\overline{\upsilon}_{k_3}}{\overline{U}_l} \tag{10}$$

where

$$b_{31} = \alpha_{lk_1}\alpha_{jk_2}\alpha_{lk_3},$$
$$b_{32} = \gamma_{ik_1}\gamma_{jk_2}\gamma_{lk_3}$$
$$b_{33} = \gamma_{ik_2}\gamma_{jk_1}\gamma_{lk_3},$$
$$b_{34} = \gamma_{lk_3}\gamma_{jk_1}\gamma_{lk_2},\ k_1\neq k_2\neq k_3,\ k_1=1,2\ldots m,\ k_2=1,2\ldots m,\ k_3=1,2\ldots m.$$

For the coefficient α_4 we obtaine:

$$\alpha_4 = \sum_{i=1}^{n}\sum_{j>i}^{n}\left\{\sum_{l>j}^{n}\sum_{h>l}^{n} b_{41}b_{42} - \sum_{l>i}^{n}\left(\sum_{h>l}^{n} b_{41}b_{33}\gamma_{hk_4} + \sum_{h\neq i,j,l}^{n} b_{41}b_{34}\gamma_{hk_4} + \sum_{h>i}^{n} b_{41}(b_{43}-b_{44})\right)\right\}\frac{\overline{U}_{k_1}\overline{U}_{k_2}\overline{U}_{k_3}\overline{U}_{k_4}}{\overline{U}_i\overline{U}_j\overline{U}_l\overline{U}_h}$$

here,

$$b_{41} = b_{31}\alpha_{hk_4}$$
$$b_{42} = b_{31}\alpha_{hk_4},$$
$$b_{43} = \gamma_{ik_4}\gamma_{jk_1}\gamma_{lk_2}\gamma_{hk_3},$$
$$b_{44} = \gamma_{ik_2}\gamma_{jk_1}\gamma_{lk_4}\gamma_{hk_3},$$
$$k_1\neq k_2\neq k_3\neq k_4\ ,\ k_1=1,2\ldots m,$$
$$k_2=1,2\ldots m\ ,\ k_3=1,\ 2\ldots m,\ \ k_4=1,2\ldots m.$$

In this formulas $\overline{\upsilon}_k$, and $\overline{U}_i$ are the stationary rate of k_i-th reaction and the stationary concentration of i-th reaction component, respectively.

At necessity it is possible to obtain corresponding expressions also for other coefficients. For this purpose it is necessary to express nodal polynomials through stoichiometric coefficients and to reject members which are equal to zero on the appropriate items of the reduction rules. It is necessary to note that the negative members in the obtained expressions of characteristic polynomial coefficients express contributions of destabilizing interactions in the reaction system. Contributions from cyclic fragments in the structure of the reaction graph are such. If the sum of negative members is more than the sum of positive members then the appropriate interaction causes destabilization of a stationary state and it can be the reason of existence of multi steady state and/or self-oscillation regimes in reaction system.

In some relatively simple cases, the obtained expressions of polynomial coefficients allow to predict kinetic behavior of a system without necessary calculations. For example, let us consider the problem of existence of self-oscillation regimes in three – component nonautocatalitic biochemical systems. From the formula (8) it follows, that for all nonautocatalitic reactions $\alpha_1>0$. The sign of the second coefficient is determined from (10) and it is obvious, that for ordinary biochemical reactions, where at each elementary stage no more than two various components participate, $\alpha_2>0$. This reason leads to the following conclusion: Self-oscillations are impossible in three-component nonautocatalitic, biochemical systems in range of the first-order approximation of stability.

As an example of illustration of the offered approach we shall consider the following system of reactions. It is the scheme of the well-known substrate inhibition reaction.

$$E + S \rightarrow ES \qquad (r1)$$
$$E\ S \rightarrow E + P \qquad (r2)$$
$$ES + S \rightarrow ESS \qquad (r3)$$
$$ESS \rightarrow ES + S \qquad (r4)$$

In this system there are 4 interacting substances (*A*-tops) and 4 reactions (*B*-tops). In the representation of the double barrel graph the considered system is represented as:

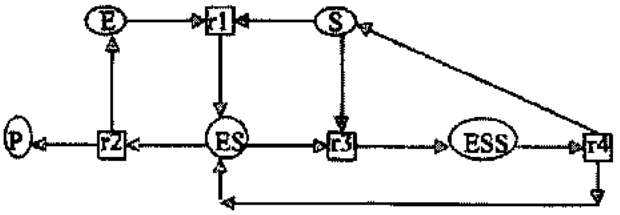

In this figure, letters in circles (*A*-tops) mean reagents, and figures in squares (*B*-tops) - the reactions. The arrow going from i-th A-top to j-th B-top means the entry of the i-th reagent in j-th reaction. The arrow going from j-th B-top to i-th *A*-top means formation of i-th reagent at the j-th reaction.

For the research of nonlinear kinetics of the given reaction system we shall write matrixes of stoichiometric coefficients, β_{ij}, α_{ij} and γ_{ij} ($i=1 \dots 4$, number of interacting reagents, and $j=1 \dots 4$, number of reactions):

$$\beta_{ij} - \alpha_{ij} = \gamma_{ij}$$

$$\begin{array}{c|cccc} S & 0 & 0 & 0 & 1 \\ E & 0 & 1 & 0 & 0 \\ ES & 1 & 0 & 0 & 1 \\ ESS & 0 & 0 & 1 & 0 \end{array} - \begin{array}{|cccc} 1 & 0 & 1 & 0 \\ 1 & 0 & 0 & 0 \\ 0 & 1 & 1 & 0 \\ 0 & 0 & 0 & 1 \end{array} = \begin{array}{|cccc} -1 & 0 & -1 & 1 \\ -1 & 1 & 0 & 0 \\ 1 & -1 & -1 & 1 \\ 0 & 0 & 1 & -1 \end{array}$$

It is easy to show that the rank of γ_{ij} matrix is equal to 3.

It means, that in the system there is one balance equation, and only 3 from 4 variable of concentrations of reagents are independent. It is obvious, because the total enzyme concentration must conserve:

$$E+ES+ESS=E_o=Const. \qquad (11)$$

Therefore the characteristic polynomial of the system will be in the third order:

$$P = \lambda^3 + \alpha_1\lambda^2 + \alpha_2\lambda + \alpha_3$$

On the other hand, it is easy to show, that on border of a polyhedron of the invariance, determined by the equation (11), there are no stationary points, i.e. there is no a stationary point, where concentrations of some reagents are equal to zero. Therefore if $\alpha_3>0$ then the stationary point of the system is unique. However if $\alpha_3<0$ and other coefficients are positive, then in the system multiple stationary points are presented, i.e. poly-stability takes place. If $\alpha_3>0$ and at least one of other coefficients (α_1 or α_2) are negative, then sustained oscillations arise around this stationary point. Let coordinates of a stationary point will be $(\overline{u_1}, \overline{u_2}, \overline{u_3}, \overline{u_4})$.

We shall proceed now to definition of coefficients α_i. They are determined from the 4x4 dimensional determinant of the Jacobian matrix. Really, we are interested only in signs of these coefficients and arising in these coefficients negative components cause interest with the point of view of a possibility of critical phenomena in the kinetics of given system. According to formulas (8-10) we obtaine:

$$\alpha_1 = \frac{\overline{\upsilon}_1 + \overline{\upsilon}_3}{\overline{u}_1} + \frac{\overline{\upsilon}_1}{\overline{u}_2} + \frac{\overline{\upsilon}_2 + \overline{\upsilon}_3}{\overline{u}_3} + \frac{\overline{\upsilon}_4}{\overline{u}_4} > 0$$

$$\alpha_1 = \frac{\overline{\upsilon}_1\overline{\upsilon}_3}{\overline{u}_1\overline{u}_2} + \frac{\overline{\upsilon}_1\overline{\upsilon}_4}{\overline{u}_1\overline{u}_4} + \frac{\overline{\upsilon}_1\overline{\upsilon}_2}{\overline{u}_2\overline{u}_3} + \frac{\overline{\upsilon}_1\overline{\upsilon}_4}{\overline{u}_2\overline{u}_4} + \frac{\overline{\upsilon}_2\overline{\upsilon}_4}{\overline{u}_3\overline{u}_4} + \frac{1}{\overline{u}_1\overline{u}_3} > \left(2\overline{\upsilon}_1\overline{\upsilon}_3 + \overline{\upsilon}_1\overline{\upsilon}_2 + \overline{\upsilon}_2\overline{\upsilon}_3\right) > 0$$

$$\alpha_3 = \frac{\overline{\upsilon}_1\overline{\upsilon}_2}{\overline{u}_1\overline{u}_3} \cdot \left(\frac{\overline{\upsilon}_4}{\overline{u}_4} - \frac{\overline{\upsilon}_3}{\overline{u}_2}\right)$$

We see that, coefficients α_1 and α_2 are positive at any positive values of concentration of reagents. It means, that sustained oscillations in the considered system are impossible. However, there is an opportunity for existence of the multi-stability. It is possible, if $\overline{u}_2 < \overline{u}_4$, since in the stationary state $\overline{\upsilon}_3 < \overline{\upsilon}_4$ and therefore, $\alpha_3 < 0$. This conclusion can seem unusual, because in many models the multi-stability and self-oscillations coexist and are realized by change of kinetic parameters. This example shows that there are systems admitting multi-stationarity and not admitting self-oscillations. In this example our purpose is to show the certain advantage of the offered method of the analysis of nonlinear kinetics of biochemical reactions. Therefore we do not stop on the analysis of a condition of multi-steady states in the considered system. However we would like to note, that this obtained condition of multi-stability not always hits to an eye at research by other methods.

CONCLUSION

The obtained expressions of polynomial coefficients can seem as complicated at first glance. However, they are, much more simple in comparison with other methods [10,12] and they are easily programmed on electronic means of calculation.

Moreover, the offered method for the determination of characteristic polynomial coefficients has the important advantage: this method allows to distinguish the fragments, which are the critic fragments. In other words, above-stated facts allow to see, that interaction of what reagents in what stages of a reaction are destabilizing factor for the stable

stationary state. It is very important for the understanding of the molecular basis and mechanisms of non-ordinary behavior of biochemical reaction systems.

[1] *M.V. Volkenstein, B.N. Goldstein.* An application of graph theory to complex reactions. Dokl. AN. SSSR, 1966, 170, p.963-965.
[2] *B.N. Goldstein, M.V. Volkenstein.* An investigation of complex monomolecular reaction by the method of graph. Dokl. AN. SSSR, 1968, 178, p. 386-388.
[3] *F.J.M. Horn.* Proc. Roy. Soc. London., 1973, 334, p. 299-330.
[4] *K.C. Chou, S. Forsen.* Biochem.J., 1980, 187, p. 829-835.
[5] *K.C. Chou, W.M. Liu.* J.Theor. Biol., 1981, 91 p. 285-297.
[6] *M.C.Kohn, W.J.Letzkus.* J.Theor.Biol., 1983, 100, p.293-304.
[7] *B.N. Goldstein.* J.Theor.Biol., 1983, 103, p. 247-264.
[8] *B.N. Goldstein.* Kinetic Graphs in Enzymology, 1989, Nauka, Moscow (in Russian).
[9] *A.I. Vol'pert.* Mathemat. Sbornic., 1972, 88, s. 578-288.(in Russian).
[10] *A.N. Ivanova.* Kinetika i Kataliz.,1979, 20, s. 1541-1548. (in Russian).
[11] *B.L. Clarke.* Adv. Chem. Phys.,1980, 43, p. 1-215.
[12] *Sh.K. Bayramov.* Biochemistry Moscow, 1999, 64, p.636-638.

Ş.Q. Bayramov

BİOKİMYƏVİ REAKSİYALARIN QEYRİ-XƏTTİ KİNETİKASININ QRAF-NƏZƏRİ ANALİZ METODU

İki lüləli qraf nəzəriyyəsinin tətbiqi ilə biokimyəvi reaksiyaların kinetikasının qeyri-xətti tənliklər sisteminin xarakteristik tənliyinin əmsallarının tapılması metodu verilmişdir. Bu əmsallardan bəziləri reagentlərin stexiometrik əmsalları ilə ifadə olunmuş və onların analitik ifadələri alınmışdır.

Ш.К. Байрамов

ГРАФ-ТЕОРЕТИЧЕСКИЙ МЕТОД АНАЛИЗА НЕЛИНЕЙНОЙ КИНЕТИКИ БИОХИМИЧЕСКИХ РЕАКЦИЙ

С применением теории двудольных графов предложен метод определения коэффициентов характеристического уравнения системы нелинейных кинетических уравнений биохимических реакций. Некоторые из этих коэффициентов выражены стехиометрическими коэффициентами реагентов и получены их аналитические выражения.

Received: 25.09.01

ALLOY DISORDER SCATTERING-LIMITED ELECTRON MOBILITY OF THE SEMICONDUCTOR THIN WIRES

G.B. IBRAGIMOV
Institute of Physics, Azerbaijan National Academy of Sciences
Javid av. 33, Baku, 370143

We study the effect of the alloy disorder scattering on the electron transport in a quasi one-dimensional semiconductor. It is shown that the alloy disorder gives a significant contribution to the electron scattering. It is found that the one-dimensional mobility is significantly greater than two-dimensional mobility. It is shown that the alloy disorder scattering-limited electron mobility increases with growth of the wire radius. We compare our results with different scattering mechanisms for one-dimensional system. Results are also included for the alloy composition dependence of the mobility.

1. INTRODUCTION

Recently the interest increases in the study of properties of ultrathin semiconducting wires, also called as quantum well wires with submicron dimensions. Electrons in a semiconductor quantum wire can be viewed as a quasi-one-dimensional (Q1D) electron gas [1-5]. There are Q1D structures where carriers are confined to move along the length of the wire and the motion is quantized in the transverse directions. The physical properties of low-dimensional semiconducting structures such as electronic transport characteristics differ from properties of bulk semiconductors because the translational symmetry is broken [6]. Sakaki [1] suggested to use semiconductor quantum wires as a basis for very fast transport processes. Reduction of phase space in Q1D leads to a decrease in the scattering process, therefore, the mobility of carriers has to increases in comparison with to the bulk value. These high mobilities could be utilized in high-speed device applications [1,7]. The mobility of the electrons in the Q1D electron gas is limited by various scattering processes, which have large importance at different ranges of temperature and carrier concentration. There have been calculations of electron scattering by acoustic phonon [8], impurity-limited mobility [2], phonon-limited mobility [3], the mobility of electrons scattered by impurities, by acoustic and polar optical phonons [4,9]. Alloy disorder scattering is an important scattering mechanism when the confining quantum well consists of ternary semiconductor. Alloy disorder scattering in ternary compound semiconductors and quantum well structures has been the subject of many theoretical and experimental investigations [10-20]. In its conventional theory, the constituent type A and type B atom pairs are assumed to be distributed randomly within the volume of the crystal.

The main purpose of this paper is to derive approximate analytical expressions for the momentum relaxation time associated with the electron alloy disorder interactions, and the calculation of the mobility of Q1D electron gas. The outline of this paper is as follows. In Sec.II we give the general framework of the paper. In Sec.III we present the calculation of the momentum relaxation time for the alloy disorder scattering. In Sec.IV the quantum theory of the alloy disorder-limited electron mobility of thin semiconduting wires is presented. In Sec.V some numerical results of our calculation are presented for $In_{1-x}Ga_xAs$. Finally, a brief discussion about our numerical analysis is given.

2. GENERAL FRAMEWORK

We assume that the electrons are confined to move in a cylindrical wire of radius R and are free to move along the axis of the wire, which has the length L. Within the framework of the effective-mass approximation the electron wave function in quantum wire is

$$\varphi(r) = L^{-1/2} \exp(iKz)\varphi_n(\rho), \qquad (1)$$

where $\rho=(x,y)$ and $r=(\rho,z)$ we take the wire axis as the z direction. The electron spectrum is parabolic and isotropic

$$E_{nK} = E_n + \hbar^2 K^2/2m^* \qquad (2)$$

We make the same approximation as in [2,3] i.e., we take

$$\varphi_0(\rho) = \left(\pi R^2\right)^{-1/2} Y(R-\rho) \qquad (3)$$

which means that the envelope function is constant inside a cylindrical wire of radius R and zero outside. $Y(X)$ is step function.

When the confining quantum well consists of a ternary semiconductor (like $Ga_{1-x}In_xAs$), in the virtual crystal approximation alloy disorder scattering potential has the form [17-20]:

$$H_{dis} = \delta V\left\{(1-x)\sum_{rIn} Y_{\Omega_0}(r-r_{In}) - \sum_{rICa} Y_{\Omega_0}(r-r_{Ca})\right\}, \qquad (4)$$

where $Y_{\Omega_0}(r_a - r_b) = 1/\Omega_0$ when r_a and r_b are inside the same unity cell and vanishes elsewhere, and the summations run over all the unit cells, Ω_0 is the volume of the unit cell.

The momentum relaxation time τ of electrons in a Q1D system due to the scattering potential H_{dis} is given by the relaxation rate [21]

$$\tau^{-1} = \frac{2\pi}{\hbar} \sum_{f} |< f|H_{dis}|i >|^2 (1 - \cos\theta)\, \delta(E_f - E_i) \tag{5}$$

Here, i and f represent the initial and final states and θ is the angle between the incident and scattered wave vectors of electrons along the axis of the wire. Because of the Q1D nature of the electron gas in a thin wire in the quantum limit, the scattering angle θ is limited by two values 0 and π. Thus the value $(1-\cos\theta)$ in Eq.(5) will be 2. The total wave function of the state "f" is $\varphi fT=\varphi T u_c(r_e)$, where $u_c(r_e)$, are Bloch functions corresponding to the extrema of the conduction band.

In order to evalute the matrix elements $<f|H_{dis}|i>$ in Eq.(5) we replace $r_e \rightarrow r_e + r_{In(Ga)}$ and use relations: $u_c(r_e + r_{In(Ga)}) = u_c(r_e)$ and $f_{\Omega_0} d^3 r |u_c(r)|^2 = \Omega_0$. The scattering rate induced by the alloy disorder is calculated using, the statistical average of products of two different matrix elements.

The mobility of electrons confined by Q2D quantum well and free to move along the Z axis of the thin semiconducting wire is given in the relaxation time approximation by

$$\mu = e\left[\sum_K \left(\frac{\hbar K}{m^*}\right) \tau(E_K) \frac{\partial f_0(E_K)}{\partial E_K}\right] \cdot \left(\sum f_0(E_K)\right)^{-1} \tag{6}$$

where $f_0(E_K)$ is the electron distribution function for carriers in the wire.

3. MOMENTUM SCATTERING RATE FOR ALLOY DISORDER SCATTERING

Using the wave functions given by Eq.(1) and (3), matrix elements induced by the alloy disorder become

$$<f|H_{dis}|i> = \frac{\delta V}{L} \sum_{r_p} L_0^2(\rho) e^{i\Delta K Z_p} \left[(1-x)\delta_{p,In} - x\delta_{p,Ga}\right] \tag{7}$$

where $\Delta K = K - K'$. The summation on r_p is over all the crystal unit cells and $\delta_{p,In}=1\ (=0)$ if the cell at r_p contains one In (respectively, Ga) atom.

A straightforward calculation of the square of the matrix element in (7) gives

$$|< f|H_{dis}|i>|^2 = \frac{\Omega_0 (\delta V)^2 x(1-x)}{\pi L R^2} \tag{8}$$

When (5) and (8) are combined, the momentum relaxation rate for the electron alloy disorder scattering is obtained:

$$\frac{1}{\tau} = \frac{2\Omega_0 (\delta V)^2 x(1-x) m^*}{\pi \hbar^3 R^2 K} \tag{9}$$

which combined with $E = \hbar^2 K^2 / 2m^*$ gives $\tau(E)$ explicity as a function of the energy E.

Eq. (9) shows that the scattering rate increases and the momentum relaxation time decreases as the radius of the wire decreases for scattering from the alloy disorder.

The formula similar to Eq.(9) has been obtained by Ando [19] and Bastard [18] for Q2D electron gas.

4. MOBILITY

In the general case, without approximations for using Eq. (9) in Eq.(6) the mobility can be written as

$$\mu = \frac{2e\hbar R^2 K_b T F_1(\eta)}{m^* \Omega_0 (\delta V)^2 x(1-x) n_{1D}} \tag{10}$$

Here $n_{1D} = 2\sqrt{2K_B T m^*} F_{1/2}(\eta)/\pi\hbar$ is the density of electrons per unit length of the wire, $F_n(\eta)$ is the Fermi integral of the argument $\eta = \zeta/KT$, and ζ is the chemical potential. It can be seen that in Eq.(10) the mobility increases as the wire radius increases.

For comparison we also give the result obtained for the acoustic phonon scattering limited mobility of the thin semiconducting wire [8]

$$\mu_{ac} = \frac{e\hbar}{\pi^{1/2}} (K_B T)^{1/2} \frac{p_1 u^2 A}{E_{ac}} \tag{11}$$

Here A is the cross-sectional area of the wire, p_1 is the mass density of the semiconductor, u is the sound velocity, and E_{ac} is the deformation potential. In this case, the mobility is suppressed as the cross-sectional area A of the wire decreases.

For the case of non degenerate carrier statistics, $f_0(E)$ is given by the Maxwell-Boltzmann distribution and mobility is given by

$$\mu_{n.deg.} = \frac{\pi^{1/2} e\hbar^2 R^2 (K_B T)^{1/2}}{\sqrt{2m^{*3/2}} \Omega_0 (\delta V)^2 x(1-x)} \tag{12}$$

When carriers are degenerate, at low temperature, $f_0(E)$ is given by a Fermi-Dirac distribution and mobility is $e\tau(EF)/m^*$:

$$\mu_{deg.} = \frac{\pi e\hbar^3 R^2 K_B}{2m^{*2} \Omega_0 (\delta V)^2 x(1-x)} \tag{13}$$

where the Fermi energy E_F of electrons in a degenerate 1D electron gas is $\hbar^2 K_F^2 / 2m^*$ with $K_F = \pi n_{1D}/2$.

It is noteworthy that the mobility due to the alloy disorder scattering in 3- and 2-dimensional system has the functional dependence on the temperature according to $T^{-1/2}$ [10] and T^{0} [13], respectively.

Eqs. (12)-(13) show that μ varies as T^{0} at the low temperature and as $T^{1/2}$ at the high temperature. It occurs because the density of states in a 3-, 2-, and 1-dimensional system has the functional dependence on energy according to $E^{1/2}$, E^{0} and $E^{-1/2}$ respectively.

5. NUMERICAL ANALYSIS AND DISCUSSION

As a numerical example, we consider a $Ga_xIn_{1-x}As$ quantum wire. Certain material parameters such as the effective mass m^* and lattice parameter occur in various formulas for mobility (relaxation time),. The lattice parameter has been assumed to follow Vegard's "law"

$$\alpha = \alpha_A x + \alpha_B(1 - x),$$

where α_A is the lattice parameter of the component A and α_B is the lattice parameter of the component B.

The electron effective mass m^* has been taken as

$$\frac{1}{m^*} = \frac{x}{m_A^*} + \frac{1-x}{m_B^*},$$

where m_A^* is the effective mass in the pure A component and m_B^* is the effective mass in the pure B component.

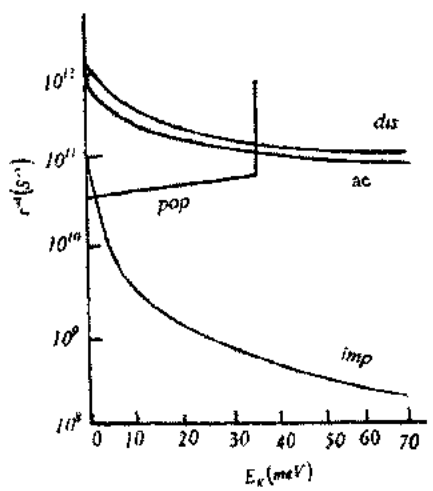

Fig.1. For a 1D $Ga_{0.8}In_{0.2}As$ system, the momentum relaxation rate is plotted as function of the electron energy E_K for alloy disorder scattering. Scattering rates for scattering from background impurity, acoustic phonon and polar optic phonon are shown for 1D GaAs system [4].

The momentum relaxation rate, τ^{-1} as a function of the longitudinal energy E_K in the $Ga_{0.8}In_{0.2}As$ is shown in fig.1. These numerical results are plotted from Eq.(9) for scattering alloy disorders. In order to compare the momentum relaxation rate for the alloy disorder scattering with momentum relaxation rate for various scattering mechanisms, values τ^{-1} for GaAs thin wire structures were found in the literature [4] and are plotted in fig.1. It is shown that for impurity, alloy disorder and acoustic phonon scattering the momentum relaxation rate diverge E_K as approaches to zero.

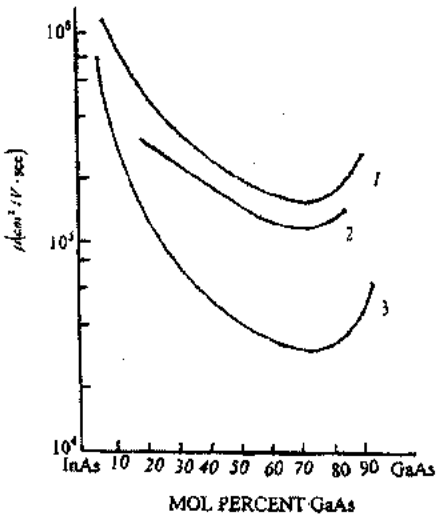

Fig.2. Dependence of the alloy disorder scattering limited electron mobility on the alloy composition for the case of $Ga_xIn_{1-x}As$ quantum wire (curve 1), quantum well structure (curve 2, [11], and 3D systems (curve 3, [10].

In fig.2 the composition dependence of the electron mobility is shown for the $In_{1-x}Ga_xAs$ quantum well wire with the radius $R=100Å$. Curves 2,3 in fig.2 show the composition dependence of the electron mobility for the $In_{1-x}Ga_xAs$ quantum well [11] and bulk $In_{1-x}Ga_xAs$ [10], respectively. In three cases bulk density of electrons is the same $n_{3D}=2\cdot10^{17}cm^{-3}$. The strength of the alloy disorder potential δV is chosen $0.53eV$.

The nature of the composite dependence of the electron mobility limited by alloy disorder scattering being $[x(1-x)m^*(x)\alpha_0(x)3]^{-2}$. Here $\alpha_0(x)$ is the lattice parameter and $m^*(x)$ is the electron effective mass at the composition x.

The minimum in mobility at about 10 per cent InAs seems are in agreement with other works [10,12]. This could be result of the influence of band structure on the scattering in the alloys.

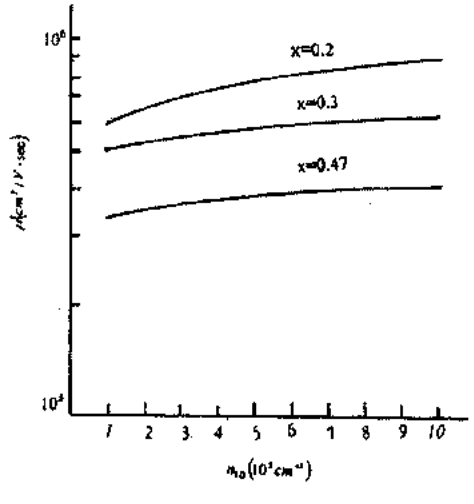

Fig.3. Variation of the mobility versus the linear density of electron for different alloy compositions.

In fig.3. the variation of electron mobility limited only by the alloy disorder scattering is shown as a function of the electron density for $Ga_{0.2}In_{0.8}As$ and $Ga_{0.47}In_{0.53}As$ cylindrical wires with the radius $R=100Å$. Thus the alloy disorder scattering is important at low concentrations especially for systems with a small Ga content x.

In conclusion, we have developed the theory for mobility assuming scattering of electrons by alloy disorder, and have found that this scattering is the dominant mechanism in ternary-based quantum wires.

[1] *H. Sakaki.* Jpn.J.Appl.Phys.1980, 19, №12, L735-1739.
[2] *J. Lee and H.N. Spector.* J.Appl. Phys. 1983, 54 (7), p.3921-3925.
[3] *G. Fishman.* Phys.Rev.B., 1987, 36 №14, p. 7448-7455.
[4] *J. Lee and M.O. Vassel.* J.Phys.C: Solid State Phys. 1984, 17, p. 2525-2535.
[5] *C.C. Wu and C.J. Lin.* J.Appl.Phys. 1988, 83 (3), p.1390-1395.
[6] *T. Ando.* J.Phys. Soc.Jap. 1982, 51, №12, p.3900-3907.
[7] *S. Briggs and J.P. Leburton.* Phys. Rev. B. 1988, 38, p.8163.
[8] *V.K. Arora.* Phys.Rev. B.23, 1981, №12, p. 5611-5612, Phys.Status Solidi B105, 1981, p. 707-713.
[9] *S. Kundu, C.K. Sakar and P.K. Basu.* J.Appl.Phys. 1990, 68(3), p.1070-1074.
[10] *L. Makowski and M. Gliksman.* J.Phys.Chem.Solid: 1973, 34, p. 487-492.
[11] *S.B. Ogale and A. Madhukar.* J.Appl.Phys.1984, 56(2), p. 368-374.
[12] *J.W. Harrison and J.R. Hauser.* J.Appl.Phys. 1976, 47, p. 292-300.
[13] *P.K. Basu and K. Bhattachayya.* Phys. Stat.Sol. (b), 1985, 128K175; *C.K. Sarkar and P.K. Basu.* Solid State Commun. 60, 1986, №6, p. 525-526.
[14] *P. Ray and P.K. Basu.* Phys.Rev. B.46, 1992, p. 9169.
[15] *M.I. Aliev, Kh.A. Khalilov, G.B. Ibragimov.* Phys. Stat. Sol.(b), 1987, 140K83.
[16] *G.B. Ibragimov.* Int. Conf. Opt. Semicond. OS2000 (Ulyanovsk), Fizika , 1999, 5, 2, 49, p.25.
[17] *J. Mycieski, G. Bastard and C. Rigaux.* Phys.Rev B16, 1975, 1977.
[18] *G. Bastard.* Appl.Phys. Letter , 1983, 43, 6 591.
[19] *T. Ando.* J.Phys. Soc.Jap., 1982, 51,№12, p.3900-3907.
[20] *S. Jaziri and R. Ferreira.* J.Appl.Phys., 1998, 84, №2, p.893-900.
[21] *B.M. Askerov.* Electron Transport Phenomena in Semiconductors (Singapore: World Scientific) 1994.

H.B. İbrahimov

KVANT NAQİLLƏRDƏ ELEKTRONLARIN ƏRİNTİNİN NİZAMSIZLIĞINDAN SƏPİLMƏSİ HALINDA YÜRÜKLÜYÜ

Kvazi birölçülü yarımkeçiricilərdə ərintinin nizamsızlığından səpilməsinin elektronların daşınmasına təsiri öyrənilmişdir. Müəyyən olunmuşdur ki, birölçülü sistemlərdə yürüklük ikiölçülü sistemlərdəki yürüklükdən çoxdur. Göstərilmişdir ki, elektronların ərintinin nizamsızlığından səpilməsi halında yürüklük kvant naqilin radiusunun artması ilə artır. Nəticələr birölçülü sistemlər üçün olan müxtəlif səpilmə mexanizmləri ilə müqayisə olunmuşdur. Yürüklüyün tərkibdən asılılığı müəyyən edilmişdir.

Г.Б. Ибрагимов

ПОДВИЖНОСТЬ ЭЛЕКТРОНОВ В КВАНТОВОЙ ПРОВОЛОКЕ, ОГРАНИЧЕННАЯ РАССЕЯНИЕМ НА СПЛАВНОМ БЕСПОРЯДКЕ

В квазиодномерном полупроводнике изучается эффект сплавного рассеяния на перенос заряда. Показано, что сплавной беспорядок дает значительный вклад в электронное рассеяние. Найдено, что одномерная подвижность намного больше, чем двумерная подвижность. Показано, что ограниченное сплавное рассеяние увеличивается с ростом радиуса проволоки. Наши результаты были сравнены с различными механизмами рассеяния для одномерных систем. Изучались также зависимости подвижности от состава сплава.

Received: 01.11.01

THE INFLUENCE OF COCON TREATMENT ON THE ELECTRIC PROPERTIES OF THE NATURAL SILK FIBROIN

R.S. ISMAILOVA
RI NAS Sector Azerbaijan
370143, H. Javid av., 31[a], Baku

The influence of thermal treatment and treatment by the liquid nitrogen of cocons, on electric properties of the natural silk fibroin has been studied. It has been established, that the polarization (ε) and tangent of angle of dielectric losses ($tg\delta$) increase with the growth of amorphous sectors, that corresponds to the sample received from cocons, treated by the liquid nitrogen. Moreover the dielectric constant, tangent of the loss angle and the electroconductivity of the fibroin, received from cocons treated by the liquid nitrogen, are on 10 % more in comparison with the fibroin, received from cocons treated by the heated air and ultrahigh frequency (UHF) field.

It has been established [1] that in the fibroin received from cocons, treated by the liquid nitrogen, the improvement of physico-mechanical properties of natural silk is observed. We connected this improvement with the increase of amorphous portion of fibrion. [2,3].

We have studied in given article the influence of cocon treatment (thermal, by the liquid nitrogen and ultrahigh-frequency field) on the polarization (ε) and tangent of angle of dielectric losses ($tg\delta$) of the natural silk fibroin. According to [4, 5] dependences of ε and $tg\delta$ on the temperature and the frequency of the electric field, authors connected with the structure of the polymer and the character of the heat motion of macromolecules.

The silk received from cocons was treated by different methods: by plunging into the liquid nitrogen during 2 minutes; by the thermal treatment at 350K during 60-90 minutes and by the UHF field (915 MHz) till 6 minutes. The samples of the silk fibroin were produced in the form of the pressed pills, on whose opposite surfaces silver layers of electrodes were sprayed. Measurements were made by means of P589 bridge in the closed volumes at temperature intervals 100-550 K.

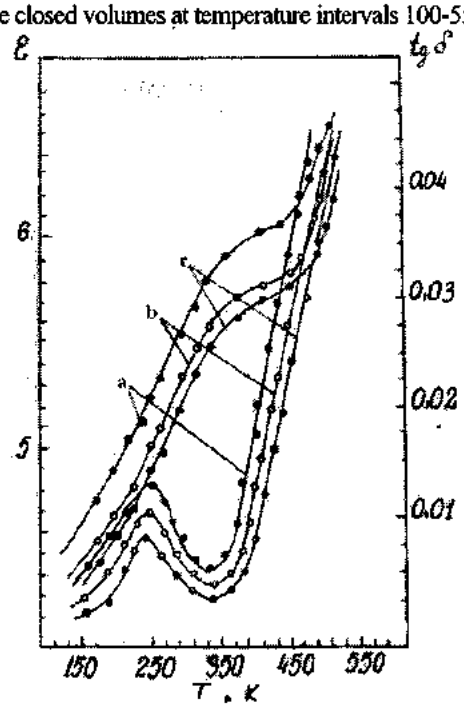

Fig.1. Temperature dependence of ε and $tg\ \delta$ of the fibroin at the frequency of the electric field 1KHz (the treatment: by the liquid nitrogen -a; by the heated air -b; by UHF field -c.

The dependences of ε and $tg\delta$ on the temperature are given on the fig.1 for the silk fibroin treated by the liquid nitrogen, heated by air and UHF field. As it is seen from the given fig.1, ε increases in steps with the increase of the temperature, and the dependences of $tg\delta$ on the temperature have maximum [6, 7], that is caused evidently by local motions of polar groups placed in the main and side chain of macromolecules, i.e. by the β - process in the silk fibroin.

The β -process at the frequency 1KHz takes place at temperatures which are lower than the vitrification temperature [4]. The transition from the glassy state to the high-elastic state takes place in temperature limits till 350K. High growth of $tg\delta$ is observed at further increase of the temperature and the second maximum is discovered before the material destruction caused by the process of dipole polarization

The last fact, apparently, is caused by the increase of leak currents, because at high temperature, thanks to the greater conductivity of the silk fibroin, dipole-segmental maximum is smoothed.

Values ε and $tg\delta$ for the fibroin received from cocons treated by the liquid nitrogen, at all temperature intervals are much more than for the fibroin, received from cocons, treated by the heated air and UHF field. Let us turn to some known considerations to explain this fact.

The silk fibroin is the partialy-crystallizing biopolymer, formed approximately from 60% of crystal and 40% of amorphous part. The crystal part mainly consists of rests of amino acids, glycin , alanin, serin and terozin. The amorphous part consists of numerous amino acid rests, containing polar groups. Moreover, intermolecular interactions in crystal region impose additional restrictions on polar group mobility. Hence it follows that the main contribution to ε and $tg\delta$ is made by amorphous parts of the silk fibroin. Consequently ε and $tg\delta$ will increase with the growth of part of amorphous sectors, that corresponds to the sample received from cocons treated by the liquid nitrogen (fig.1).

We have received the analogous conclusions by measuring of the biopolymer electroconductivity. For this we have measured the volume resistivity $\rho(T)$:

$$\rho = \frac{2\pi \cdot 1.8 \cdot 10^{10}}{\omega \cdot \varepsilon \cdot tg\delta},$$

where ρ is the volume resistivity of the dielectric (om, m), ω is the circular frequency of the electric field. For samples,

treated by different methods, the dependence $lg\rho \ (T)$ was determined at the same conditions. Obtained results are presented on the fig.2 from which follows that ρ for the fibroin, received from cocons treated by the liquid nitrogen, is considerably less than for samples, received by the heated air and UHF field. We have earlier established [1] that the electroconductivity reduces at the increase of the degree of polymer crystallinity, and the volume resistivity grows. The last fact has found the confirmation in experiments for samples received from cocons, treated by heated air and UHF field.

It is necessary to note that at the primary cocons treatment by the heated air and UHF field, the fraction of amorphous sections reduces and the quantity of submicrocracks in the fibroin will increase. The growth of submicrocracks leads to situation, when the increase of ion traps causes the decrease of mobility of latters. That is why the electroconductivity of the fibroin treated by the heated air and UHF field, reduces and the conductivity is the least at cocons treatment by the UHF field.

It has been established that the dielectric constant, tangent of the loss angle and electroconductivity of the fibroin, received from cocons treated by the liquid nitrogen, are on 10% more in comparison with the fibroin, received from cocons treated by the heated air and UHF field.

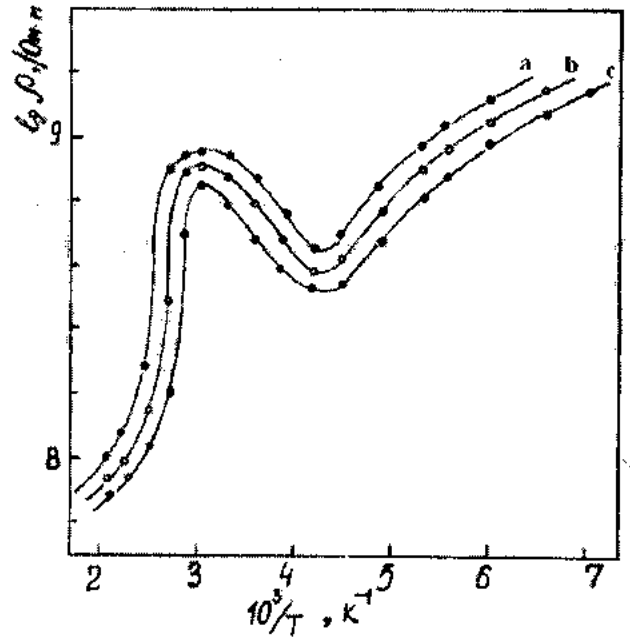

Fig.2. Temperature dependence of the fibroin specific resistance on the variable current (the treatment: by UHF field - a; by the heated air -b; by the liquid nitrogen -c).

[1] *R.S. Ismailova.* «The influence of temperature and SVS field on the physical properties of the fibroin» - Doct.Thesis, Baku, 1989, p.126.

[2] The All-Union symposium « Magnetic resonance in biology and medicine» (19-22 March, 1981): Theses of the report (AN SSSR)- M., Chernogolovka, 1981, p.302.

[3] *M.Y. Bagirov, Y.G. Shukyurov, P.S. Ismailova.* The mutual activity of UV- irradiation and selenium on the stable-deformational properties of the natural silk. «Silk», 1981, №4, pp.19-20.

[4] The electric properties of polymers. Under editing of *B.I. Sajin* L: Chemistry, 1977, p.192.

[5] *M.E. Bagirov, V.P. Malin.* The electric aging of polymer dielectrics - B., Azerneshr, 1987, p.208.

[6] *Y.M. Poplavko.* Physics of dielectrics (the lecture) (Under editing of *M.M. Nekrasov*), Kiev, Izd. UPI, 1972, p.312.

[7] *Dj. Magoshi.* The dielectric properties of the silk fibroin. Kobunsi rombunsyu, 1974, v. 31, №7,pp. 456-462,467.

R.S. İsmailova

BARAMANIN İLKİN EMALININ TƏBİİ İPƏK FİBROİNİN ELEKTRİK XASSƏLƏRİNƏ TƏSİRİ

Baramanın ilkin emalının fibroinin elektrik xassələrinə təsiri öyrənilmişdir. Müəyyən edilmişdir ki, maye azotla emal edilən baramadan alınan fibroində amorf hissələr çox olduğundan, onların polyarizasiyası (ε) və tangens bucaq əmsalı $(tg\delta)$ da artır. Bundan başqa, maye azotla emal edilmiş baramadan alınan fibroinin dielektrik nüfuzluğu, tangens bucaq əmsalı və elektrik keçiriciliyi isti hava və yüksək tezlikli sahə ilə emal edilən baramadan alınan fibroindən 10% yüksək olur.

Р.С. Исмаилова

ВЛИЯНИЕ ОБРАБОТКИ КОКОНОВ НА ЭЛЕКТРИЧЕСКИЕ СВОЙСТВА ФИБРОИНА НАТУРАЛЬНОГО ШЕЛКА

Изучено влияние термической обработки и жидким азотом коконов на электрические свойства фиброина натурального шелка. Установлено, что поляризация (ε) и тангенс угла диэлектрических потерь $(tg\delta)$ увеличиваются с ростом аморфизации участков, а это соответствует образцу, полученному из коконов, обработанных жидким азотом. Кроме того, диэлектрическая проницаемость, тангенс угла потерь и электропроводность фиброина, полученного из коконов, обработанных жидким азотом на 10% больше по сравнению с фиброином, полученным из коконов, обработанных нагретым воздухом и СВЧ полем.

Received: 25.06.01

THE MECHANICAL AND ELECTRIC DURABILITIES OF POLYMER COMPOSITIONS ON THE BASE OF POLYVINYLIDENEFLUORIDE AND PIEZOCERAMICS

S.A. ABBASOV, M.A. RAMAZANOV, Z.E. MUSTAFAEV
Institute of Physics of Azerbaijan National Academy of Sciences
370143, H. Javid av., 33, Baku

Mechanical and electric durabilities of polymer compositions on the base of polyvinylidenefluoride (PVDF) and piezoceramics of the type PCR3M and PCR8 have been studied.It was shown, that at other equal conditions the mechanical and electric durabilities of polymer compositions depend on the physical structure of piezoceramics and temperature-temporary conditions of crystallization of compositions.

At last time compositions on the base of polymers and piezoceramics are widely used in different sensors and converters devices, because they possess by piezoelectric, electric, electret and other properties [1, 2]. It is obvious, that at exploitation of such devices with elements from a polymer-piezoceramics composition, the main part plays its strength properties (the mechanical and electric durabilities).

The mechanical and electric durabilities of polymer compositions on the base of polyvinylidenefluoride (PVDF) and piezoceramics of the type PCR3M and PCR8 and the influence of temperature-temporary conditions of crystallization on these strength properties have been studied in given work.

PCR3M and PCR8 piezoceramics had zirconate-titanate-lead (ZTL) composition and, correspondingly, possessed by rhombohedral and tetragonal structure. Piezocemics were taken with sizes of particles d<50 mkm.

The powdery piezoceramics PCR3M and PCR8 were inserted in the powdery PVDF by means of the mechanical mixing of polymers with admixtures (piezoceramics).

The compositions have been received from mixtures by method of the hot pressing at the melting temperature of the polymer matrix under the pressure 15 Mpa during 15 minutes with the following cooling.

For receipt of samples with different physical structures, the process of film preparation from compositions took place in two conditions: in the first case samples, received by hot pressing, were cooled with the high rate 2000 grade/minute by means of plunging of the melt between two aluminum foils into the ice-water mixture. These samples (films) of compositions were called as «quick cooled» (QC). In the second case the melt in the press was cooled slowly up to the room temperature with the average rate 2 grade/minutes, that is was received so-called «slowly cooled» (SC) samples (films) of compositions.

Force dependences of the mechanical durability τ_σ (dependences of time passed from the moment of the sample loading till its burst on the constant mechanical stress σ) and field dependences of the electric durability τ_E (dependences of time passed from the moment of application of a high electric field to samples till its breakdown on the intensity of the field E) were registered. Dependences of τ_σ on σ and τ_E on E have been determined at the temperature 293K by methods, described in works [3, 4].

Dependences of $lg\tau_\sigma$ on σ for QC PVDF-PCR3M compositions, containing different quantities in volumetric compositions of PVDF and PCR3M, are presented on fig.1 in semilogarithmic coordinates. It is seen that in all cases $lg\tau_\sigma$ reduces in a linear fashion versus σ. It means that τ_σ reduces exponentially in the dependence on σ, when the equation is fulfiled:

$$\tau_\sigma = Ae^{-\alpha\sigma},$$

where A and α coefficients are parameters, defining the mechanical durability properties of the material; moreover A and α depend on the nature of the studied material and on the temperature of durability testing. It is seen from fig.1, that the decrease of the mechanical durability and the strength of PVDF-PCR3M composition takes place in dependence on the quantity of the inserted PCR3M admixture. According to graphics, given on fig.1, the parameter A in the exponential equation does not change, and the decrease of the mechanical strength properties of PVDF-PCR3M composition in the dependence on the content of the inserted PKR3M admixture reflects on the growth of the coefficient α.

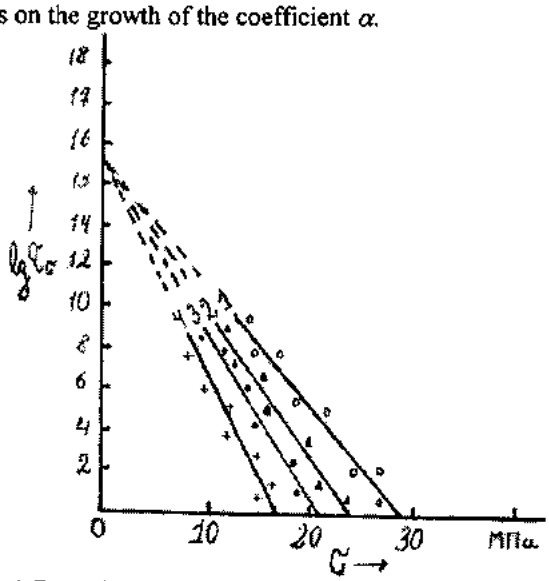

Fig. 1 Force dependences of the mechanical durability of QC samples of the PVDF-PCR3M composition in different relations of components in volumetric contents: 1 - 90÷10 ob %; 2 - 80÷20 ob %; 3 - 70÷30 ob %; 4 - 60÷40 ob %.

Force dependences of the mechanical durability in semilogarithmic coordinates of $lg\tau_\sigma$ versus σ were registered for QC PVDF-PCR8 compositions, containing different quantities in volumetric contents of PVDF and PCR8 components. Field dependences of the electric durability in semilogarithmic coordinates of $lg\tau_E$ versus E were also registered for QC PVDF-PCR3M, PVDF-PCR8 compositions, containing the different quantities in volumetric contents of components.

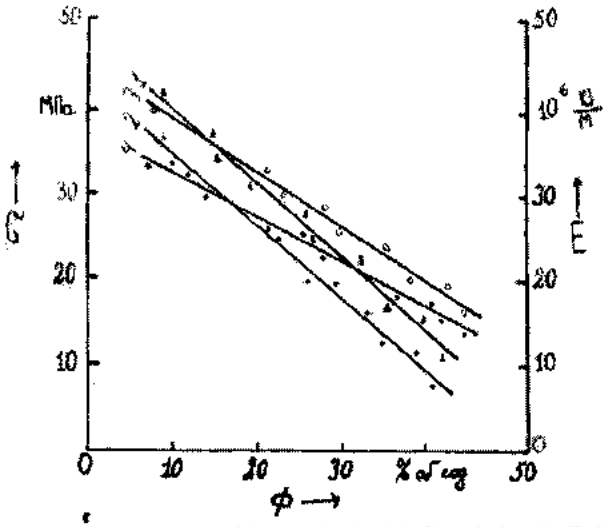

Fig. 2. Dependences of the mechanical (1,2) and electric (3,4) strengths of QC of PVDF-PCR3M and PVDF-PCR8 compositions on volumetric contents of PCR3M and PCR8 piezoceramics. 1 - PVDF-PCR3M; 2 - PVDF-PCR8; 3 - PVDF-PCR3M; 4 - PVDF-PCR8

For clarity, on the base of the force and field dependences of the mechanical and electric durabilities, correspondingly, dependences of the mechanical strength (as the mechanical strength σ the value of the explosive stress at τ_σ=1s; i.e. at $lg\tau_\sigma$=0 was taken) and the electric stability (the value of the puncture voltage at τ_E=1s., i.e. at $lg\tau_E$= 0 was taken as the electric stability E) were built for QC samples of PVDF-PCR3M and PVDF-PCR8 compositions on the quantity F of inserted PCR3M and PCR8 admixtures. Such dependences of the mechanical strength σ and the electric strength E of PVDF-PCR3M and PVDF-PCR8 compositions on the content of F admixtures of PCR3M and PCR8 piezoceramics are shown on fig.2. It is seen that the mechanical strength σ and the electric strength E of PVDF-PCR3M and PVDF-PCR8 compositions reduce at the growth of the quantity of PCR3M and PCR8 admixtures. It is also seen from fig.2 that at the same contents of PCR3M and PCR8 admixtures the mechanical strength σ and the electric strength E of the PVDF-PCR3M composition are more in comparison with σ and E of the PVDF-PCR8 composition. These experimental results are explained by the fact that the value of the rheorientation polarization and the degree of made (in the process of the polarization) domain reorientations different from 180° for PCR3M piezoceramics are more in comparison with the piezoceramics PCR8 [5]. As a result, interphase interactions in the case of PVDF-PCR3M composition are more in comparison with the interphase interactions in PVDF-PCR8 composition, that leads to the growth of the stable properties of the PVDF-PCR3M composition.

To establish the influence of the physical structure (temperature-temporary condition of the crystallization) of compositions on its mechanical durability τ_σ and the electric durability τ_E, force dependences of the mechanical durability and field dependences of the electric durability of SC and QC compositions were compared at other identical conditions.

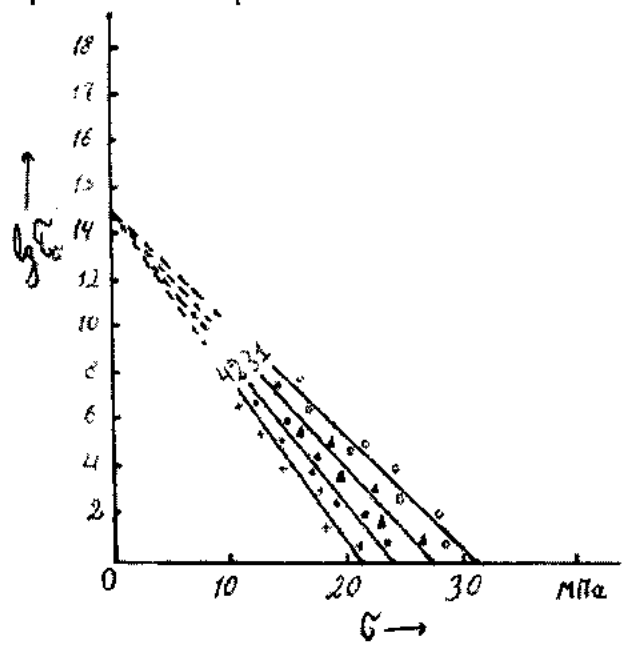

Fig.3. Force dependences of the mechanical durability of SC and QC of PVDF-PCR3M (1,2); PVDF-PCR8 (3,4) compositions in relation of components 80-20 volume %: 1,3- SC samples; 2,4- QC samples.

Force dependences of the mechanical durability of SC and QC for PVDF-PCR3M and PVDF-PCR8 compositions in the relation of components 80-20 volume % were built on fig.3. It is seen, that for both compositions the mechanical durability τ_σ of SC compositions is more in comparison with τ_σ of QC compositions at other equal conditions (at the same values of the explosive stress and temperature of measurement). The analogous results were received also in the case of force dependences of the electric durability, and exactly, the electric durability τ_E of SC compositions is more in comparison with τ_E of QC compositions. These experimental results could be connected with the thermal treatment of compositions, which takes place in the case of slow cooling. Then the amplification of the interaction occurs between phases, which is connected with the growth of the near-boundary layer and with structural changes in polymer compositions and also adhesion between the polymer matrix and piezoceramics [6-8]. It, in its turn, leads to the growth of the mechanical and electric strengths of SC PVDF-PCR3M and PVDF-PCR8 compositions.

[1] *M.A. Ramazanov, Z.G. Panakhov.* Instruments and Experimental Techniques, 1997, v. 40, №5, pp.708-709.

[2] *M.G. Shakhtakhtinskii, M.A. Kubanov, M.A. Ramazanov, A.I. Mamedov, Y.N. Gazvryan, M. A. Nuriev.* Piezoelectric microphone. A.S. 15929557.

[3] *V.R. Regel, A.I. Slutsker, E.E. Tomashevskii.* The kinetic nature of solid bodies strength. M., Science, 1974. p.560.

[4] *M.A. Bagirov, V.P. Malin, S.A. Abbasov.* The influence of the electric charges on polymer dielectrics. Baku, Elm, 1975, p.168.

[5] *E.G. Fesenko, A.Y. Dantsiger, O.N. Razumovski.* New piezoceramical materials. Izd.NII fizika at RGU 1983, p.156.

[6] *M.G. Shakhtakhtinskii, A.I. Mamedov, M.A. Ramazanov, M.M. Kuliev, M.A. Kurbanov, N.N. Aliev.* DAN Azerbaijan SSR, 1987, t. 43, ? 6, pp. 21-24

[7] *M.G. Shakhtakhtinskii, H.A. Sadigov.* The forth All-Union symposium «Actual problems of production and use of

segneto-piezo-pyroelectrics and related to them materials». Moscow, 1991, p. 24

[8] *S.A. Abbasov, M.A. Ramazanov.* Fizika, 1999, c.5, №2, pp.11-13.

S.A. Abbasov, M.Ə. Ramazanov, Z.E. Mustafayev

POLİFİNİLDENFTORİD VƏ PYEZONKERAMİKALAR ƏSASINDA ALINMIŞ POLİMER KOMPOZİSİYALARININ MEXANİKİ VƏ ELEKTRİK YAŞAMA MÜDDƏTİ

Polivinildenftorid və PKR3M, PKR8 markalı pyezonkeramikalar əsasında alınmış polimer kompozisiyalarının mexaniki və elektrik yaşama müddəti öyrənilmişdir. Göstərilmişdir ki, digər eyni şəraitlərdə polimer kompozisiyalarının mexaniki və elektrik yaşama müddətləri pyezokeramikaların fiziki quruluşundan və kompozisiyaların kristallaşmasının temperatur – zaman rejimindən asılıdır.

С.А. Абасов, М.А. Рамазанов, З.Э. Мустафаев

МЕХАНИЧЕСКАЯ И ЭЛЕКТРИЧЕСКАЯ ДОЛГОВЕЧНОСТИ ПОЛИМЕРНЫХ КОМПОЗИЦИЙ НА ОСНОВЕ ПОЛИВИНИЛДЕНФТОРИДА И ПЬЕЗОКЕРАМИКИ

Изучены механическая и электрическая долговечности полимерных композиций на основе поливинилденфторида (ПВДФ) и пьезокерамиков марки ПКР3М и ПКР8. Показано, что при прочих равных условиях механическая и электрическая долговечности полимерных композиций зависят от физической структуры пьезокерамиков и температурно-временного режима кристаллизации композиций.

Received: 22.10.01

THE ABSORPTION BAND INTENSITY OF THE IR - SPECTRUM OF THE *o* - TOLUNITRILE MOLECULE

S.D. DEMUKHAMEDOVA, Z.I. GADJIEV
Baku State University
Baku 370148, street. Z.Khalilov 23

The theoretical study of absorption bands intensities of the IR-spectrum of the *o*-tolunitrile molecule has been conducted by the method of the theoretical oscillatory spectroscopy. Theoretical values of absorption bands intensities of the IR - spectrum of the molecule have been received, the set of electrooptical parameters has been found, the analysis of the creation nature of each absorption band has been carried out and the theoretical curve of the spectral distribution of the absorption coefficient of the *o*-tolunitrile molecule has been plotted.

Vibration of polyatomic molecules are directly manifested in infrared absorption spectra of appropriate molecules. The absorption process takes place as a result of interaction of the electron and nucleus of the molecule with the electromagnetic field of the light waves. The electron shell of the molecule deforms at the nuclear vibrations. The character of these deformations depends both on the shell's structure and on the oscillation properties. Peculiarities of the structure of the electron shell of the molecule are completely manifested in intensities and polarizations of spectral lines and bands. Exploring intensities and polarizations in oscillatory spectra, we may get the information about parameters, characterizing the electron shell of the molecule. Firstly, it is dipole moments and polarizabilities of separate bonds and their derivatives on oscillatory coordinates.

On a level with the application of quantum mechanics apparatus to the task of intensities of the oscillatory absorption spectrum, giving still some divergence from the experiment because of the polyatomic molecules composition complexity, a valence-optic theory [1] is the most real base for the theoretical study of intensities in infrared absorption spectra of polyatomic molecules.

Given work is devoted to the calculation of intensities of the absorption IR-spectrum of the *o*-tolunitrile molecule by means of the program, created on the base of the valence-optic theory [2]. Calculations, according to this program, allow not only to calculate values of integral intensities of IR-absorption bands of molecules and to find electrooptic parameters, which (as force constants) reflect peculiarities of electron density distribution of molecules, but also to build theoretical IR-spectra of studied molecules, what allow directly visually to compare theoretically received spectra with their experimental IR-spectra. The frequency task has been earlier solved by us for the *o*-tolunitrile molecule. Frequencies and forms of standard vibrations of the model *o*-tolunitrile molecule have been calculated and the complete theoretical interpretation of its oscillatory spectrum has been carried out on forms of standard vibrations and the distribution of the potential energy on oscillatory coordinates [3]. The experimental IR-spectrum of the *o*-tolunitrile molecule was taken from the Saddler atlas [4].

The absorption bands intensity of IR-spectra of molecules is calculated on the base of the semiempiric theory and therefore the electrooptic parameters of molecules (dipole moments of bonds and their derivatives on oscillatory coordinates) are necessary to introduce in computer for the solution of the direct electrooptic task, when intensities and polarizations of the absorption band are calculated on the base of known electrooptic parameters. On the other hand these parameters may be calculated from experimental absorption bands of IR-spectra of molecules. It is a reverse electrooptic task, when electrooptic parameters of molecules are determined on the base of absolute intensities from the experimental spectrum. The calculated *o*-tolunitrile molecule model is shown on the fig.1.

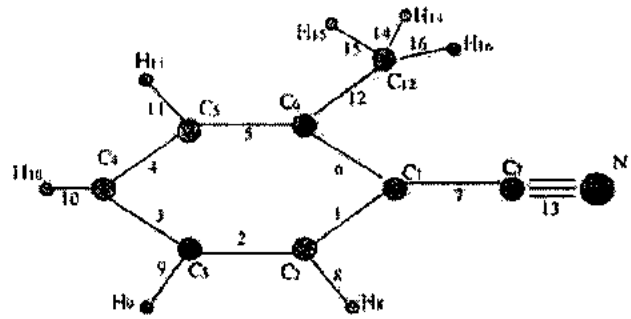

Fig.1. The calculated model and numeration of atoms and *o*-tolunitrile molecule bonds

The calculation was made by means of solution of direct and reverse electrooptic tasks for the *o*-tolunitrile molecule. The direct electrooptic task always must be solved before solving the reverse electrooptic task. If the studied molecule consists of already known fragments, then the same initial values of electrooptic parameters are given as for fragments. Initial values of electrooptic parameters for the *o*-tolunitrile molecule were taken from benzonitrile and ethane molecules. Theoretical values of intensities, calculated with these electrooptic parameters, for the model *o*-tolunitrile molecules strongly diverged from values of intensities of appropriate absorption bands of the experimental spectrum. Therefore, it is necessary to solve the reverse electrooptic task for this molecule for correction of electrooptic parameters. The parameter of calculated square difference sum and experimental intensities should be minimal at the solution of the reverse electrooptic task. Moreover, variated parameters should be in limits of the fixed interval. The interval is fixed usually on the base of additional physical considerations. The practice of solution of reverse electrooptic tasks has shown, that the choice of the change interval excludes numerous solutions of the nonlinear task.

The absolute intensity has been calculated by us for all observed absorption bands of the experimental spectrum of the *o*-tolunitrile molecule (see table 3) before solving of

reverse electrooptic tasks and the dependence has been analyzed of absorption bands intensities on electrooptic parameters of concrete polar bonds of the studied molecule.

Electrooptic tasks had been solved at three stages. At the first stage the electrooptic task had been solved for dipole moments of bonds of the o-tolunitrile molecule. Values of dipole moments had been variated before achievement of the best conformity of theoretical and experimental values of intensities of those absorption bands, which depend on these dipole moments. Values of dipole moments, calculated after solving of the reverse electrooptic task, are shown in the table 1, where initial values of dipole moments are pointed in brackets.

Table 1

Dipole moments of bonds of the o-tolunitrile molecule

μ_7=0.390(-0.427)	μ_8=0.844(0.816)	μ_9=0.844(0.816)	μ_{10}=0.288(0.480)
μ_{11}=0.844(0.816)	μ_{12}= -0.593(-0.13)	μ_{13}=1.602(2.020)	μ_{14}=0.101(0.305)
μ_{15}=0.101(0.305)	μ_{16}=0.101(0.315)		

At second and third stages, reverse electrooptic tasks had been solved by us for dipole moments derivatives on oscillatory coordinates, correspondingly, for non-plane and plane vibrations of the o-tolunitrile molecule and calculated values of electrooptic parameters are shown in the table 2.

Table 2.

Derivatives of dipole moments of bonds of the o-tolunitrile molecule on its oscillatory coordinates.

$\frac{\partial\mu_7}{\partial\theta_1}$ = - 0.026 (0.041)	$\frac{\partial\mu_7}{\partial\theta_7}$ = - 2.275 (-2.263)	$\frac{\partial\mu_7}{\partial\theta_{19}}$ = - 0.610 (0.557)
$\frac{\partial\mu_7}{\partial\theta_{21}}$ = 0.495 (0.451)	$\frac{\partial\mu_7}{\partial\theta_{30}}$ = - 0.041 (-0.030)	$\frac{\partial\mu_7}{\partial\theta_{43}}$ = 0.560 (0.560)
$\frac{\partial\mu_7}{\partial\theta_{44}}$ = - 0.578 (-0.451)	$\frac{\partial\mu_8}{\partial\theta_1}$ = - 0.014 (-0.019)	$\frac{\partial\mu_8}{\partial\theta_8}$ = 0.470 (0.490)
$\frac{\partial\mu_8}{\partial\theta_{20}}$ = - 0.813 (-0.203)	$\frac{\partial\mu_9}{\partial\theta_{22}}$ = 0.001 (-0.74)	$\frac{\partial\mu_{11}}{\partial\theta_{29}}$ = - 0.265 (0.246)
$\frac{\partial\mu_{12}}{\partial\theta_5}$ = 0.173 (0.392)	$\frac{\partial\mu_{12}}{\partial\theta_{12}}$ = - 0.425 (-0.477)	$\frac{\partial\mu_{12}}{\partial\theta_{18}}$ = - 0.280 (0.610)
$\frac{\partial\mu_{12}}{\partial\theta_{19}}$ = - 0.302 (-0.317)	$\frac{\partial\mu_{12}}{\partial\theta_{28}}$ = 0.551 (0.260)	$\frac{\partial\mu_{12}}{\partial\theta_{29}}$ = 0.033 (0.432)
$\frac{\partial\mu_{12}}{\partial\theta_{45}}$ = - 0.111 (-0.138)	$\frac{\partial\mu_{12}}{\partial\theta_{48}}$ = - 0.190 (-0.270)	$\frac{\partial\mu_{12}}{\partial\theta_{51}}$ = 0.352 (0.491)
$\frac{\partial\mu_{13}}{\partial\theta_7}$ = - 0.128 (-0.116)	$\frac{\partial\mu_{13}}{\partial\theta_{19}}$ = - 0.032 (0.022)	$\frac{\partial\mu_{13}}{\partial\theta_{43}}$ = - 0.203 (-0.230)
$\frac{\partial\mu_{13}}{\partial\theta_{44}}$ = - 0.571 (0.750)	$\frac{\partial\mu_{14}}{\partial\theta_{45}}$ = 0.439 (0.476)	$\frac{\partial\mu_{14}}{\partial\theta_{46}}$ = - 0.151 (0.126)

Results of the theoretical calculation of the oscillatory spectrum intensities of the o-tolunitrile molecule are shown in the table 3, where calculated values of theoretical intensities and their comparison with experimental values of intensities are shown for each observed experimental band, and also values of contributions of all electrooptic parameters, taking part in creation of all absorption bands of the IR-spectrum of the o-tolunitrile molecule, are shown.

Absorption bands of the o-tolunitrile molecule may be divided on 4 groups, taking into account the analysis of theoretically calculated values for electrooptic parameters of the o-tolunitrile molecule and dependences of absorption bands intensities of the IR-spectrum of the o-tolunitrile molecule on these parameters.

The intensity of bands of the first group depends on different combinations of dipole moments of polar bonds and on dipole moments derivatives on oscillatory coordinates of the structural element C-C=N. These absorption bands are observed in the low-frequency region of the spectrum: 430, 342, 566, 706, and 1006 cm^{-1}.

The second group of bands is absorption bands 962, 987, 1047, 1455, 2919 and 2920 cm^{-1}, whose intensity depends on dipole moments of CH bonds of benzene ring and dipole moments of CH bonds of CH_3 group. Moreover, the intensity of these absorption bands depends also on dipole moments derivatives of CH bonds, coming into the C-CH_3 group. The band at 1455 cm^{-1} is the most intensive band among these absorption bands.

The third group. Absorption bands intensity of this spectrum region depends on dipole moments of all polar CH bonds and their derivatives on angle oscillatory coordinates. Moreover intensities of some these bands depend also on dipole moments of the C-C=N group.

Table 3.

Experimental and theoretical frequencies and absorption bands intensities of the IR-spectrum of the o-tolunitrile molecule.

$V_{exper.}$	$I_{exper.}$	$I_{theor.}$	Contribution, μ	Dipole moments	Contrubution $\partial\mu_i/\partial\theta_j$	Derivatives of dip.mom. on oscil.coord.
3069	5.70	4.3			0.377	$\partial\mu_8/\partial q_8$
3063	9.79	9.5			-0.593	$\partial\mu_8/\partial q_8$
30589	1.87				0.393 0.066	$\partial\mu_8/\partial q_8$ $\partial\mu_8/\partial q_{23}$
3057	0.12	0.3			-0.08	$\partial\mu_8/\partial q_8$
2920	3.19	3.0	-0.076 0.051	μ_8, μ_9, μ_{11}, μ_{12}	-0.611 -0.610	$\partial\mu_8/\partial q_{46}$ $\partial\mu_8/\partial q_{45}$
2919	3.54	3.2	0.087 -0.059	μ_{14}, μ_{14}, μ_{16}, μ_{12}	1.221 -1.221 -0.123 0.123 0.102 -0.102	$\partial\mu_{14}/\partial q_{45}$ $\partial\mu_{14}/\partial q_{46}$ $\partial\mu_{14}/\partial q_{48}$ $\partial\mu_{14}/\partial q_{49}$ $\partial\mu_{14}/\partial q_{51}$ $\partial\mu_{14}/\partial q_{52}$
2849	1.13	1.01	0.061	μ_{14}, μ_{15}, μ_{16}	1.521 1.014 0.507 0.071	$\partial\mu_8/\partial q_8$ $\partial\mu_8/\partial q_8$ $\partial\mu_8/\partial q_8$ $\partial\mu_8/\partial q_8$
2233	10.72	9.3			0.407 0.407 -0.271 -0.271	$\partial\mu_7/\partial q_{43}$ $\partial\mu_{13}/\partial q_{43}$ $\partial\mu_{13}/\partial q_7$ $\partial\mu_7/\partial q_7$
1618	1.77	1.0		μ_{14}, μ_{15}, μ_{16} μ_7 μ_{10}	0.373 -0.311 0.281 -0.279 0.279 -0.244 -0.128 -0.115	$\partial\mu_8/\partial q_{23}$ $\partial\mu_2/\partial q_{28}$ $\partial\mu_{12}/\partial q_5$ $\partial\mu_{12}/\partial q_{18}$ $\partial\mu_{12}/\partial q_{29}$ $\partial\mu_{12}/\partial q_{19}$ $\partial\mu_{12}/\partial q_{19}$ $\partial\mu_{14}/\partial q_{49}$
1610	2.56	1.8	0.115 -0.104 0.084	μ_8, μ_9, μ_{11}, μ_{10} μ_7	-0.211 0.205 -0.189 0.154 0.143 0.110 -0.108	$\partial\mu_8/\partial q_{20}$ $\partial\mu_{11}/\partial q_{29}$ $\partial\mu_{14}/\partial q_{48}$ $\partial\mu_{14}/\partial q_{49}$ $\partial\mu_{14}/\partial q_{52}$ $\partial\mu_{12}/\partial q_5$ $\partial\mu_{14}/\partial q_{51}$
1492	8.03	3.3		μ_8, μ_9, μ_{11} μ_{10} μ_{14}, μ_{15}, μ_{16}	-0.913 -0.452 0.266 0.204 -0.186 0.166	$\partial\mu_8/\partial q_{23}$ $\partial\mu_{12}/\partial q_{28}$ $\partial\mu_9/\partial q_1$ $\partial\mu_{12}/\partial q_{48}$ $\partial\mu_{12}/\partial q_{51}$ $\partial\mu_{12}/\partial q_{52}$
1455	2.49	2.2	-0.794	μ_{14},μ_{15},μ_{16}	-1.823 1.823 -0.573 0.573	$\partial\mu_{14}/\partial q_{51}$ $\partial\mu_{14}/\partial q_{52}$ $\partial\mu_{14}/\partial q_{48}$ $\partial\mu_{14}/\partial q_{49}$
1454	6.88	5.5	0.304 0.141 0.102	μ_{14}, μ_{15}, μ_{16} μ_{10} μ_8,μ_9,μ_{11}	0.868 -0.794 -0.515 -0.311 0.238 0.198	$\partial\mu_{14}/\partial q_{51}$ $\partial\mu_{14}/\partial q_{52}$ $\partial\mu_8/\partial q_{23}$ $\partial\mu_{14}/\partial q_{49}$ $\partial\mu_{14}/\partial q_{48}$ $\partial\mu_{12}/\partial q_{48}$
1434	4.58	4.1	-0.472 0.293 -0.186	μ_{10} μ_{14}, μ_{15}, μ_{16} μ_8,μ_9,μ_{11}	1.388 -0.470 -0.411 0.251 0.158 -0.159	$\partial\mu_8/\partial q_{23}$ $\partial\mu_8/\partial q_1$ $\partial\mu_{14}/\partial q_{52}$ $\partial\mu_{14}/\partial q_{51}$ $\partial\mu_{12}/\partial q_{18}$ $\partial\mu_{12}/\partial q_{19}$

1378	4.44	3.9	-1.365 -0.158 -0.140	$\mu_{14}, \mu_{15}, \mu_{16}$ μ_{10} μ_8, μ_9, μ_{11}	-1.565 1.565 1.061 -1.048 -0.517 0.504 0.432	$\partial\mu_{12}/\partial q_{48}$ $\partial\mu_{12}/\partial q_{51}$ $\partial\mu_{14}/\partial q_{52}$ $\partial\mu_{14}/\partial q_{49}$ $\partial\mu_{14}/\partial q_{48}$ $\partial\mu_8/\partial q_{23}$ $\partial\mu_{12}/\partial q_{28}$
1300	1.01	0.8	0.126 -0.074 0.058	μ_8, μ_9, μ_{11} $\mu_{14}, \mu_{15}, \mu_{16}$ μ_7	0.224 -0.220 0.220 -0.171 -0.148	$\partial\mu_{14}/\partial q_{51}$ $\partial\mu_{12}/\partial q_{48}$ $\partial\mu_{12}/\partial q_{51}$ $\partial\mu_{14}/\partial q_{48}$ $\partial\mu_{12}/\partial q_{12}$
1283	0.75	0.9	0.292 -0.270 -0.207	$\mu_{14}, \mu_{15}, \mu_{16}$ μ_{10} μ_8, μ_9, μ_{11}	0.455 0.371 -0.371 0.313 -0.266 0.211 0.207	$\partial\mu_{12}/\partial q_{28}$ $\partial\mu_{12}/\partial q_{48}$ $\partial\mu_{12}/\partial q_{21}$ $\partial\mu_8/\partial q_{23}$ $\partial\mu_8/\partial q_1$ $\partial\mu_{14}/\partial q_{49}$ $\partial\mu_{12}/\partial q_{12}$
1251	4.465	3.8	-0.287 0.160 0.149 0.069	$\mu_{14}, \mu_{15}, \mu_{16}$ μ_8, μ_9, μ_{11} μ_{10} μ_7	-0.789 0.287 -0.234 0.234 -0.232 0.216 0.196	$\partial\mu_{18}/\partial q_{23}$ $\partial\mu_{12}/\partial q_{28}$ $\partial\mu_{12}/\partial q_{48}$ $\partial\mu_{12}/\partial q_{51}$ $\partial\mu_{14}/\partial q_{52}$ $\partial\mu_8/\partial q_1$ $\partial\mu_{12}/\partial q_{12}$
1203	1.39	0.9	0.078	$\mu_{14}, \mu_{15}, \mu_{16}$	-0.340 0.306 0.166 -0.166 -0.140 0.133	$\partial\mu_{12}/\partial q_{28}$ $\partial\mu_8/\partial q_{23}$ $\partial\mu_{12}/\partial q_{19}$ $\partial\mu_{12}/\partial q_{18}$ $\partial\mu_{12}/\partial q_5$ $\partial\mu_8/\partial q_1$
1147	0.52	0.4	-0.596 0.585 0.084	μ_8, μ_9, μ_{11} μ_{10} $\mu_{14}, \mu_{15}, \mu_{16}$	0.370 -0.343 0.097 -0.088 -0.088	$\partial\mu_{12}/\partial q_{28}$ $\partial\mu_8/\partial q_{23}$ $\partial\mu_{14}/\partial q_{49}$ $\partial\mu_{14}/\partial q_{48}$ $\partial\mu_{14}/\partial q_{52}$
1104	1.98	1.0	0.221 0.215 0.190	μ_8, μ_9, μ_{11} μ_{10} $\mu_{14}, \mu_{15}, \mu_{16}$	-0.904 -0.404 0.277 -0.201 0.182 0.175	$\partial\mu_{14}/\partial q_{51}$ $\partial\mu_{14}/\partial q_{52}$ $\partial\mu_8/\partial q_{23}$ $\partial\mu_{14}/\partial q_{49}$ $\partial\mu_{14}/\partial q_{48}$ $\partial\mu_{12}/\partial q_{48}$
1047	3.63	3.2	-0.936 0.143 -0.069	$\mu_{14}, \mu_{15}, \mu_{16}$ μ_{12} μ_8, μ_9, μ_{11}	1.117 -0.117 -0.546 0.546	$\partial\mu_{14}/\partial q_{48}$ $\partial\mu_{14}/\partial q_{49}$ $\partial\mu_{14}/\partial q_{51}$ $\partial\mu_{14}/\partial q_{52}$
1027	4.42	3.6	-0.183 0.171 -0.170	μ_8, μ_9, μ_{11} $\mu_{14}, \mu_{15}, \mu_{16}$ μ_{10}	0.372 0.360 -0.215 0.206 0.172 -0.101	$\partial\mu_8/\partial q_1$ $\partial\mu_8/\partial q_{53}$ $\partial\mu_8/\partial q_{48}$ $\partial\mu_{14}/\partial q_{49}$ $\partial\mu_{12}/\partial q_{28}$ $\partial\mu_8/\partial q_{20}$
1006	2.71	2.1	0.566 -0.565 0.056	μ_8, μ_9, μ_{11} μ_{10} $\mu_{14}, \mu_{15}, \mu_{16}$	-0.065 0.065	$\partial\mu_{14}/\partial q_{48}$ $\partial\mu_{14}/\partial q_{49}$
987	0.50	0.3	0.0638 0.083 -0.248	$\mu_{14}, \mu_{15}, \mu_{16}$ μ_{10} μ_8, μ_9, μ_{11}	-0.419 0.419 0.180 -0.180 0.075	$\partial\mu_{14}/\partial q_{49}$ $\partial\mu_{14}/\partial q_{48}$ $\partial\mu_{14}/\partial q_{52}$ $\partial\mu_{14}/\partial q_{51}$ $\partial\mu_9/\partial q_1$
962	4.39	2.3	0.717	μ_8, μ_9, μ_{11}	0.094	$\partial\mu_{14}/\partial q_{48}$

			-0.374 -0.086	μ_{10} μ_{14}, μ_{15}, μ_{16}	-0.094	$\partial\mu_{14}/\partial q_{49}$
871	0.64	0.7	-0.282	μ_{10}		
814	0.77	0.5	-0.095 -0.088 0.055	μ_{14}, μ_{15}, μ_{16} μ_{10} μ_{7}	0.209 0.126 0.119 0.098 -0.085	$\partial\mu_{8}/\partial q_{23}$ $\partial\mu_{7}/\partial q_{21}$ $\partial\mu_{12}/\partial q_{12}$ $\partial\mu_{12}/\partial q_{5}$ $\partial\mu_{8}/\partial q_{1}$
756	19.12	17.2	1.129 0.505 -0.095	μ_{8}, μ_{9}, μ_{11} μ_{10} μ_{7}	0.136 0.136	$\partial\mu_{7}/\partial q_{44}$ $\partial\mu_{13}/\partial q_{44}$
715	6.19	6.0	0.486 0.285 -0.104 0.100	μ_{8}, μ_{9}, μ_{11} μ_{10} μ_{14}, μ_{15}, μ_{16} μ_{7}	-0.133 -0.133 0.074 -0.074	$\partial\mu_{7}/\partial q_{44}$ $\partial\mu_{13}/\partial q_{44}$ $\partial\mu_{14}/\partial q_{49}$ $\partial\mu_{14}/\partial q_{29}$
706	1.62	0.9	0.151 -0.070 0.056	μ_{8}, μ_{9}, μ_{11} μ_{14}, μ_{15}, μ_{16} μ_{10}	-0.108 -0.105 -0.148 0.118 0.118 -0.111 -0.111	$\partial\mu_{12}/\partial q_{28}$ $\partial\mu_{12}/\partial q_{5}$ $\partial\mu_{7}/\partial q_{1}$ $\partial\mu_{7}/\partial q_{19}$ $\partial\mu_{13}/\partial q_{7}$ $\partial\mu_{7}/\partial q_{7}$ $\partial\mu_{7}/\partial q_{21}$
566	7.8	6.1	-0.472 -0.193 0.105 0.105	μ_{8}, μ_{9}, μ_{11} μ_{7} μ_{10} μ_{13}	0.321 0.325	$\partial\mu_{7}/\partial q_{44}$ $\partial\mu_{13}/\partial q_{44}$
535	1.45	1.1	-0.070 0.059 -0.056	μ_{10} μ_{13} μ_{7}	0.149 -0.149 0.113 0.110	$\partial\mu_{12}/\partial q_{18}$ $\partial\mu_{12}/\partial q_{29}$ $\partial\mu_{8}/\partial q_{20}$ $\partial\mu_{12}/\partial q_{19}$ $\partial\mu_{8}/\partial q_{23}$
461	4.98	5.5	-0.146	μ_{7} μ_{13} μ_{14}, μ_{15}, μ_{16}	0.201 0.128 0.118 -0.163	$\partial\mu_{12}/\partial q_{19}$ $\partial\mu_{11}/\partial q_{19}$ $\partial\mu_{8}/\partial q_{20}$ $\partial\mu_{7}/\partial q_{30}$
430	0.082	1.2	0.232 0.105 0.080	μ_{8}, μ_{9}, μ_{11} μ_{14}, μ_{1}, μ_{16} μ_{12}	0.097 0.097	$\partial\mu_{7}/\partial q_{44}$ $\partial\mu_{13}/\partial q_{44}$
401	4.77	4.0	-0.110 0.102	μ_{7} μ_{13}	0.166 -0.111 0.111 -0.135 -0.135	$\partial\mu_{8}/\partial q_{20}$ $\partial\mu_{2}/\partial q_{18}$ $\partial\mu_{12}/\partial q_{19}$ $\partial\mu_{7}/\partial q_{19}$ $\partial\mu_{13}/\partial q_{19}$
342	4.98	3.0	-0.261 0.146 0.124	μ_{13} μ_{7} μ_{10}	-0.443 -0.443	$\partial\mu_{14}/\partial q_{51}$ $\partial\mu_{14}/\partial q_{52}$

Bands with frequencies 2233, 3057, 3063 and 3069 cm^{-1} are observed in the high-frequency region. It is the fourth group of absorption bands. The absorption bands intensity of this spectrum region does not depend on dipole moments of polar bonds. The observed absorption bands intensity of this region mainly depends on derivatives of dipole moments on oscillatory coordinates of the polar bond of the C_2H_8 type. The intensity of the absorption band 2233 cm^{-1} is determined by the derivative of the dipole moment of the C-C=N group on oscillatory coordinates. It has been established by means of the theoretical study, that bands 566, 756, 871, 962, 1006, 1455, 1919, 1920 and 3057cm^{-1} are completely polarized. Bands 756, 871, 962 and 1006 cm^{-1} display from these absorption bands at the expense of the vibration of bond exit type from the plane.

The theoretical IR-spectrum, which has been visually compared with the experimental spectrum of this molecule, has been built by us with calculated values of electrooptic parameters after solving of the reverse electrooptic task of the *o*-tolunitrile molecule. The comparison of these spectral curves shows, that the received theoretical curve of the spectral distribution of the absorption coefficient describes quite satisfactory the experimental spectrum of the o-tolunitrile molecule, that proves the reliability of determined by us electrooptic parameters of this molecule.

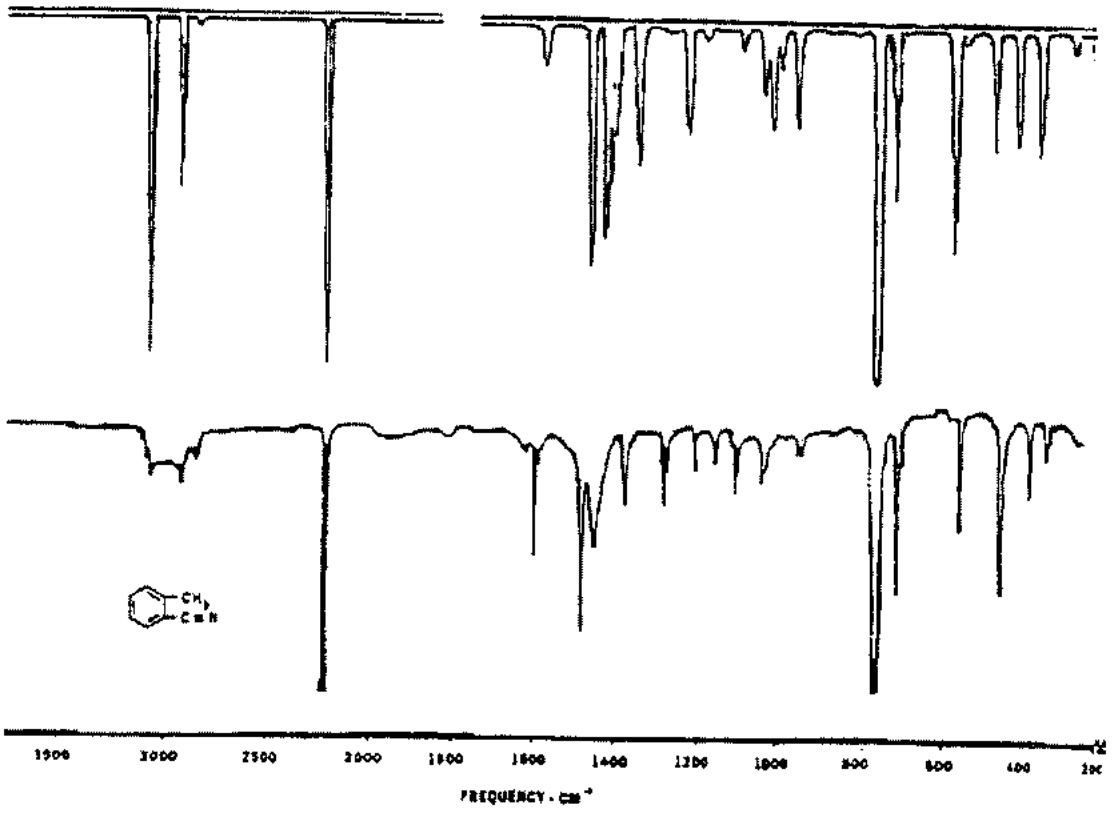

Fig. 2 The theoretical (upper) and experimental spectrum of the *o*-tolunitrile molecule.

[1] *M.B. Volkenshtein, L.A. Gribov, M.A. Elyashevich, B.I.Stepanov* «Vibrations of molecules»: M., Science, 1972.

[2] *L.A. Gribov* «Light elucidation of vibrations. The description of the program and instruction to the user». OOO «INLAN», 1995.

[3] *S.D. Demukhamedova, Z.I.Gadjiev* Fizika, 7, 2001, №2, p. 5-10.

[4] The Saddler standard spectra infrared grating spectra Philadelphia: Saddler research laboratories, 1978.

S.D. Demühəmmədova, Z.İ. Hacıyev

o-TOLUNİTRİL MOLEKULUNUN İQ SPEKTRİNİN UDMA ZOLAQLARININ İNTENSİVLİYİNİN HESABLANMASI

Nəzəri rəqs spectroskopiyası metodu ilə *o*-tolunitril molekulunun İQ spektrinin udma zolaqlarının intensivliyi tədqiq olunmuşdur. Molekulunun İQ-spektrinin udma zolaqlarının intensivliyinin nəzəri qiymətləri təyin olunmuşdur. Elektrooptik parametrlər toplusu tapılmış və udma zolaqlarının təbiəti təhlil edilmişdir. Udma əmsalının spektrdə paylanması əyrisi qurulmuşdur.

С. Д. Демухамедова, З.И. Гаджиева

РАСЧЕТ ИНТЕНСИВНОСТЕЙ ПОЛОС ПОГЛОЩЕНИЯ ИК-СПЕКТРА МОЛЕКУЛЫ *o*-ТОЛУНИТРИЛ

Методом теоретической колебательной спектроскопии произведено теоретическое исследование интенсивностей полос поглощения ИК спектра молекулы *o*-толунитрил. Получены теоретические значения интенсивностей полос поглощения ИК-спектра молекулы, найден набор электрических параметров, проведен анализ природы появления каждой полосы поглощения и построена теоретическая кривая спектрального распределения коэффициента поглощения молекулы *o*-толунитрил.

Received:11.10.01

ISOPERIODIC HETEROJUNCTIONS BASED ON $Pb_{1-x}Sn_xSe$, $PbSe_{1-x}S_x$ EPITAXIAL FILMS

I.R. NURIYEV, Kh.D. JALILOVA, N.V. FARADJEV, A.M. NAZAROV
Institute of Photoelectronics of Azerbaijan National Academy of Sciences
370141, F.Agayev str., 555quarter, Baku

p-$Pb_{1-x}Sn_xSe$/n-$PbSe_{1-x}S_x$/BaF_2 isoperiodic epitaxial heterostructures have been obtained and peculiarities of growth and their electrical and photoelectrical properties have been investigated. Epitaxial films have been grown by molecular beams condensation method at 10^{-4} Pa of vacuum. The data on structure of films were obtained by electronographic, X-ray diffractometric and electron-microscopic methods. The heterojunctions are photosensitive in the spectral range 8÷12 μm. Maximum of the photosensitivity is observed at the wave length λ=11,8 μm. The observed displacement of the photosensitivity maximum in the short-wave length of the region of the spectrum is interpreted by the increase of the condensation temperature of the upper layer.

Persisting interest in $Pb_{1-x}Sn_xSe$ narrow gap solid solution and their use in different fields of optoeletronics stimulates all round research of their physical properties, playing a decisive role in development of the infrared photoreceiver in the atmospheric window from 8 to 14 μm based this material [1,2]. It is informed in [3] about photodiodes with the Shottky barrier based on $Pb_{1-x}Sn_xSe$ ($0.06<x<0.07$) layers, obtained on BaF_2 spallings, and the delectability is on one order higher than for photodiodes based on $Pb_{1-x}Sn_xSe$ monocrystals. In these layers the concentration of charge carriers is $(2\div6)\cdot10^{17}$ cm^{-3} at 77 K. Peculiarities of the growth and electrophysical properties of $Pb_{1-x}Sn_xSe$ (x=0.03÷0.07) epitaxial layers doped by indium (N_{In}=0.3÷0.05 weight.%) with various degrees of compensation, grown on BaF_2 spallings, were investigated in [4,5]. The optical absorption edge on the indium-doped ($N_{In}\leq0.08$ weight.%) $Pb_{1-x}Sn_xSe$ (x=0.07) epitaxial layers have been investigated in [6]. It is necessary to note that, until recently, there were not experimental works on the receipt and investigation of photovoltaic srtuctures on the base of $Pb_{1-x}Sn_xSe$ thin films of monocrystals or epitaxial films of $Pb_{1-x}Sn_xSe$ solid solutions. It is connected, apparently, with the absence of materials with the lowered concentration ($\leq10^{16}$ cm^{-3}). However theoretical analysis of $A^{IV}B^{VI}$ solid solutions demonstrates a number of advantages of $Pb_{1-x}Sn_xSe$ solid solutions for making of such structures. The same experimental work on making of $Pb_{0,93}Sn_{0,07}Se$/PbSe heterojunctions, and investigation of their electrical and photoelectrical properties for the first time was published in 1997 [8]. Heterojunctions were produced by the vacuum epitaxy method of PbSe films on the $Pb_{1-x}Sn_xSe$ monocrystals. However, for creation of monolithic matrix photoreceivers, producing isoperiodic heterojunctions based on epitaxial layers on the dielectrical substrates are very interesting. Such substrates allow to realize the electrical decoupling of separate functional elements at the creation of multi-elements devices. In this work we present results of investigation of electrophysical and photoelectric properties of p-$Pb_{0,93}Sn_{0,07}Se$/n-PbSe heterojunctions obtained on the basis of epitaxial films of above-mentioned solid solutions.

The films were grown by the molecular beams condensation method on the newly chiped off and polished sides of BaF_2 {111,100} substrate, under a vacuum of about 10^{-4} torr. Lattices constants of contacting pairs have the identical value ($a_{PbSnSe}=a_{PbSeS}$=6,19Å). Synthesized samples, doped by indium (In), were used for receipt of p-$Pb_{1-x}Sn_xSe$ films with low concentration of charge carriers ($p\leq10^{17}cm^{-3}$). Perfection of films structure was controlled by electronographic, X-ray diffractometric and electronmicroscopic methods. The spectral and volt-current characteristics have been investigated.

Fig. 1a. Electronogram and the electron microscopic photograph of $Pb_{0,93}Sn_{0,07}Se$ a) electronogram of the reflection,

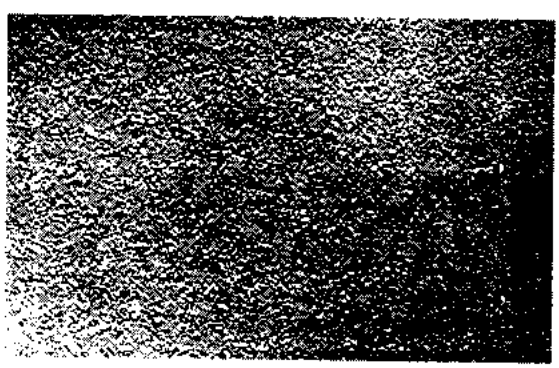

Fig. 1b. Electronogram and the electron microscopic photograph of $Pb_{0,93}Sn_{0,07}Se$ b) electron microscopic photograph of the surface.

For the making of heterojunctions, at first, the thin p-$Pb_{1-x}Sn_xSe$ films with the thickness about 1÷1.5 μm ($\upsilon_{cond.}$=7÷8 Å/s) were

ploted on BaF_2 {111,100} substrate at the temperature (400÷450)±0.5°C by the method [4]. Measurements of the half-width of X-ray diffraction swinging curves showed, that the structural perfection of films is on the level of best samples obtained by the method condensation of molecular beams ($W_{1/2}$=100÷150 angl.s.) and films grow in the plane parallel to the base according to [4-6]. Electronograms and electromicroscopic photographs also confirm this fact. Electronograms on reflection are characterized by reflexes stretched from the shade to the sample. It testifies on relative large dimensions of the blocks and on high crystalline perfection, respectively (fig.1.a). The smooth surface without second inclusions have been observed (fig.1.b) on the electron-microscopic photographs. p-$Pb_{1-x}Sn_xSe$ epitaxial films with the mobility $\mu=(2\div3)\cdot10^4 cm^2/V\cdot s$ and charge carriers concentration $p=2\cdot10^{16}\div3\cdot10^{18} cm^{-3}$ on the BaF_2 substrates, have been received with application of the additional compensating Se steam source at the growth process. The method with the additional source of selenium allowed to lower the concentration of charge carriers and to receive single phase films without second inclusions. Then $Pb_{1-x}Sn_xSe$ (x=0.12) epitaxial films of the n-type conductivity were grown without breakdown of the vacuum. Additional compensating selenium source was used during this growth. $Pb_{1-x}Sn_xSe$ films had the charge carriers concentration $n=3\cdot10^{17}\div4\cdot10^{18} cm^{-3}$ which was estimated on measurements of Hall effect and photomagnetic effect. The n-type $PbSe_{1-x}S_x$ films were received at temperatures of condensation T=(250; 300; 350)°C. Mask with the size of gaps about 0.3 mm was used for making of heterojunctions conducted in the united technological cycle in the process of films growth.

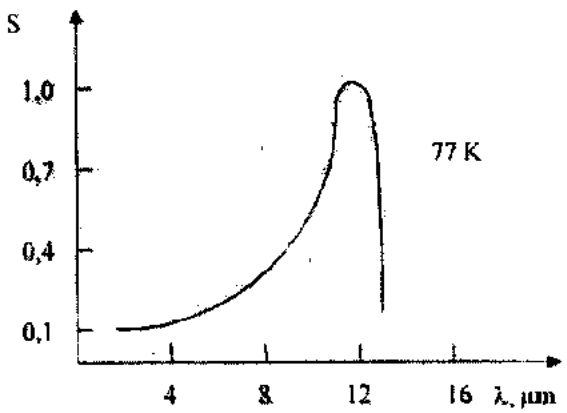

Fig.2. Volt-ampere characteristics of the p-$Pb_{0,93}Sn_{0,07}Se$/n-$PbSe_{0,88}S_{0,12}$ heterojunctions.

The obtained heterojunctions with charge carriers concentrations ($p=2\cdot10^{16}\div3\cdot10^{17} cm^{-3}$; $n=3\cdot10^{17}\div4\cdot10^{18} cm^{-3}$) have rectifying properties (fig.2). The volt-ampere characteristics of the heterojunctions show that the insulation current strongly depends on the degree of structural perfection of the p-layer. The straight branch of the volt-ampere characteristic at small displacements (U=30÷100 mV) is submited to the exponential law $J=J_o\cdot\exp(eU/\beta kT)$. The coefficient β changes in the range from 2.0 to 2.5 at T=77 K, that is characteristic for the generation-recombination process of the current leaking through the region of the space charge [10]. In the region of high straight displacements (U=100÷130 mV) the current leaking is determined by the tunnelling (β=9÷10). The spectral dependence of p-$Pb_{1-x}Sn_xSe$/n-$PbSe_{1-x}S_x$ photosensitivity at T=80 K is shown on fig.3. The reduction of the charge carriers concentration in $PbSe_{1-x}S_x$ thin film leads to the decrease of nonequilibrium defects in the n-type layer and, at the same, time stimulates appearance of the photosensitivity peak in the short-wave range of the spectrum with the maximum at λ=7,8 μm in the spectral characteristics of heterojunction photo reply.

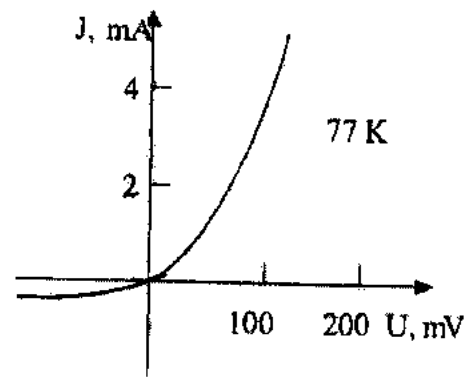

Fig.3. Spectral dependence of the p-$Pb_{0,93}Sn_{0,07}Se$/n-$PbSe_{0,88}S_{0,12}$ heterojunction photosensitivity.

The shift of the photosensitivity maximum to the short-wave region is observed with the increase of the condensation temperature (T_k) on the spectral characteristics of heterojunctions produced at T_k=(250; 300; 350)°C. Indeed, such increase of T_k leads to decrease of the concentration of nonequilibrium defects in the n-layers and, at the same time, stimulates processes of atomic diffusion in the contact region of heterojunction components. Apparently, in accordance with work [8], the diffusion of tin become noticeable from the base to the growing layer of $PbSe_{1-x}S_x$ at temperatures of condensation more than 300°C. As a result, the blurring of the metallurgical border occurs. In this case geometrical dimensions of blurring regions are comparable with the extent of regions of the spatial charge and the heterojunction acquires characteristics of the varizon structure that leads to the shift of the photosensitivity maximum of heterojunctions at the temperature growth of their making. Thus, for practical applications, heterojunctions are interesting, manufactured at the condensation temperature T_k<300°C with the spectral distribution of the photosensitivity determined by characteristics of heterojunction components in basic regions.

[1] Foreign electronic technique, Russia, 1977, 13, p. 3-60.
[2] Photoreceivers of visible and IR diapason. *R.G. Kiesa*, M., 1985.
[3] *D.K. Hohke, H. Holloway, K.F. Yeung and M. Hurley.* Appl. Phys. let., 1979, 29, p.2.
[4] *E. Yu.Salaev, I.R. Nuriyev, Ch.J. Jalilova, N.V. Faradjev.* Scientific Center of the Russia Federation Rd&p. Center ORION. 1998. p. 164.
[5] *Kh.D. Jalilova, H.R. Nuriev, N.V. Faradjev, M.I. Abdullyaev and E.K. Guseynov.* Fizika, Azerbaijan, 1999, 1, p. 22-24.

[6] *E. Yu.Salaev, I.R. Nuriyev, Ch.J. Jalilova, N.V. Faradjev.* Scientific Center of the Russia Federation Rd&p. Center ORION. 2000. p. 213.
[7] *H. Preier.* Jnfr. Phys., 1978, 18, 1.
[8] *T.A. Gavrikova, V.A. Zikov.* Phys. and Tech. of Semiconductors, 1997, 31, 11.
[9] *I.R. Nuriyev.* Doctor disser. Azerbaijan, Baku ,1987.
[10] *A. Milns, D. Foyxt.* Heterojunction and metal-semiconductor junctions. Russia, Moscow, 1975.

İ.R. Nuriyev, X.D. Cəlilova, N.V. Fərəcov, A.M. Nəzərov

$Pb_{1-x}Sn_xSe$, $PbSe_{1-x}S_x$ EPİTAKSİAL TƏBƏQƏLƏRİ ƏSASINDA İZOPERİODİK HETEROKEÇİDLƏR

BaF_2 altlıqları uzərində p-$Pb_{1-x}Sn_xSe$/n-$PbSe_{1-x}S_x$ izoperiodik epitaksial heterokeçidlər alınmış, onların elektrik və fotoelektrik xassələri tədqiq edilmişdir. Epitaksial təbəqələr molekulyar dəstənin kondensasiyası metodu ilə 10^{-4}Pa vakuumda yetişdirilmişdir. Təbəqələrin struktur mükəmməlliyi elektronoqrafik, rentgendifraktometrik və elektronmikroskopik metodlar vasitəsi ilə öyrənilmişdir. Alınmış heterokeçidlər spektrin 8÷12 mkm dalğa oblastında fotohəssadırlar. Fotohəssalığın maksimumu dalğa uzunluğunun λ=11,8 mkm qiymətinə uyğun gəlir. Göstərilmiş dir ki, yuxarı *n*-tip təbəqənin kondensasiya temperaturu artdıqca, fotohəssaslığın maksimumu qısa dalğalar oblastına tərəf sürüşür.

И.Р. Нуриев, Х.Д. Джалилова, Н.В. Фараджев, А.М. Назаров

ИЗОПЕРИОДИЧЕСКИЕ ГЕТЕРОПЕРЕХОДЫ НА ОСНОВЕ ЭПИТАКСИАЛЬНЫХ ПЛЕНОК $Pb_{1-x}Sn_xSe$, $PbSe_{1-x}S_x$

Получены изопериодические эпитаксиальные гетероструктуры *p*-$Pb_{1-x}Sn_xSe$/*n*-$PbSe_{1-x}S_x$/BaF_2, исследованы их электрофизические и фотоэлектрические свойства. Эпитаксиальные пленки выращены методом конденсации молекулярных пучков в вакууме 10^{-4} Па.

Структурное совершенство пленок контролировалось электронографическим, рентгенодифрактометрическим и электронномикроскопическим методами. Изготовленные гетеропереходы оказались фоточувствительными в области спектра 8÷14 мкм. Максимальное значение фоточувствительности наблюдается при длине вольны λ=11,8 мкм. Показано, что с увеличением температуры конденсации верхнего слоя максимум фоточувствительности смещается в коротковолновую область.

Received: 20.11.01

THERMOMAGNETIC EFFECTS OF NONDEGENERATE KANE SEMICONDUCTORS UNDER THE CONDITIONS OF MUTUAL ELECTRON-PHONON DRAG IN A STRONG ELECTRIC FIELD

M.M. BABAYEV, T.M. GASSYM
Institute of Physics of Azerbaijan National Academy of Sciences
370143, H. Javid av., 33, Baku

The thermoelectric power and Nernst - Ettingshausen effects of nondegenerate Kane semiconductors with due regard of the electron and phonon heating and their mutual drag are investigated. It is shown that the nonparabolicity of electron spectrum significantly influences on values of thermoelectric power and Nernst - Ettingshausen coefficients, leads to the change of their dependence upon the electron temperature T_e, as well as upon the heated electric field E. Under the conditions of strong mutual electron-phonon drag for the semiconductors with parabolic spectrum of electrons the phonon part of Nernst - Ettingshausen coefficient Q_p=0, but in the nonparabolic case $Q_p \neq 0$ and Q_p is larger than the electron part of Nernst - Ettingshausen coefficient Q_e, i.e. Nernst - Ettingshauzen field mainly consists of the phonon part.

The interest to the studies of thermoelectric power and thermomagnetic effects in different systems under the conditions of carrier heating at the strong external electric field has recently been intensified [1-3]. Lei [1], Xing, Liu, Dong and Wang [2] discussed the thermoelectric power under the conditions of carrier heating at the external high electric field neglecting the contribution of the phonon drag, which is very important at low temperatures of the lattice [4]. The role of the phonon drag in thermoelectric power of hot carriers was studied by Wu, Horing and Cui [3], by taking into account only the drag of electrons by phonons (thermal drag), but the mutual drag of electrons and phonons was neglected. The thermoelectric power and thermomagnetic effects of hot carriers with regard of both the electron drag by phonons and their mutual drag were studied in [5]. In all papers [1-3,5] the electron dispersion law was assumed to be parabolic. In the publication [6] the thermoelectric power and thermomagnetic effects of hot electrons in strongly degenerated semiconductors for two-band Kane spectrum of electrons was discussed.

In this paper the thermoelectric power and transverse Nernst - Ettingshausen effect of nondegenerate Kane semiconductors placed in high electric $(\vec{E})$ and nonquantized magnetic $(\vec{H})$ fields are investigated with regard of both the drag of heated electrons by phonons and their mutual drag. The electron temperature gradient ∇T_e can be produced by the gradient of $(\vec{E})$ or by the lattice temperature gradient ∇T. The phonons were assumed to be heated or non-heated. Two-band Kane spectrum of electrons is assumed [4] as follows:

$$p(\varepsilon) = (2m_n\varepsilon)^{\frac{1}{2}}\left(1 + \frac{\varepsilon}{\varepsilon_g}\right)^{\frac{1}{2}}, \qquad (1)$$

where m_n is the electron effective mass at the bottom of the conduction band, ε_g is the band gap, p and ε are the electron momentum and energy, respectively.

The basic equations of the problem are the coupled Boltzmann transport equations for electrons and phonons. The case of quasi-elastic electron scattering by acoustic phonons is considered. For the considered case the distribution functions of electrons $f(\vec{p}, \vec{r})$ and phonons $N(\vec{q}, \vec{r})$ may be presented in the form:

$$f(\vec{p}, \vec{r}) = f_0(\varepsilon, \vec{r}) + \vec{f}_1(\varepsilon, \vec{r})\frac{\vec{p}}{p}, \quad |\vec{f}_1| \ll f_0, \qquad (2)$$

$$N(\vec{q}, \vec{r}) = N_0(q, \vec{r}) + \vec{N}_1(q, \vec{r})\frac{\vec{q}}{q}, \quad |\vec{N}_1| \ll N_0. \qquad (3)$$

Here f_0 and $\vec{f}_1$, N_0 and $\vec{N}_1$ are the isotropic and anisotropic parts of the electron and phonon distribution functions, respectively.

If the inter-electronic collision frequency ν_{ee} is much larger than the collision frequency of the electrons for the energy transfer to of lattice ν_ε, then $f_0(\varepsilon, \vec{r})$ is the Fermi distribution function with an electron temperature T_e. We consider the case when for long-wavelength (LW) phonons there is a "thermal reservoir" of short-wavelength (SW) phonons: $q_{max} \approx 2\bar{p} \ll \frac{T}{S_0}$, where S_0 is the sound velocity in the crystal, q_{max} is the maximum quasi-momentum of LW phonons. In this case $N_0(q, \vec{r})$ has the form [7]

$$N_0(q, \vec{r}) \approx \frac{T_p(\vec{r})}{s_0 q}, \qquad (4)$$

where T_p is the effective temperature of the LW phonons.

Starting from the Boltzmann transport equations we obtain the following equations for $\vec{f}_1$ and $\vec{N}_1$ in the steady state :

$$\frac{p}{m(\varepsilon)}\nabla f_0 - e\overline{E_c}\,\frac{p}{m(\varepsilon)}\frac{\partial f_0}{\partial \varepsilon} - \Omega(\varepsilon)\left[\vec{h}\vec{f}_1\right] + \nu(\varepsilon)\vec{f}_1 + \frac{2\pi m(\varepsilon)}{(2\pi\hbar)^3 p^2}\frac{\partial f_0}{\partial \varepsilon}\int_0^{2p}\overline{N}_1(q)W(q)\hbar\omega_q q^2 dq = 0, \tag{5}$$

$$S_0\nabla N_0 + \beta(q)\vec{N}_1 - \frac{4\pi m(\varepsilon)}{(2\pi\hbar)^3}W(q)N_0(q)\int_{q/2}^{\infty}\vec{f}_1 dp = 0. \tag{6}$$

Here e is the absolute value of the electron's charge, $\vec{E}_c = \vec{E} + \vec{E}_T$, $\vec{E}_T$ is the thermoelectric field, $m(\varepsilon)$ is the electron's effective mass, $\Omega = eH/m(\varepsilon)c$ is the electron cyclotron frequency, $\vec{h} = \vec{H}/H$, $\hbar\omega_q = s_0 q$ is the phonon energy, $W(q) = W_0 q^t$ is the square matrix element of the electron-phonon interaction (t=1 for deformation, and t=-1 for piezoelectric interaction), $\beta(q)$ and $\nu(\varepsilon)$ are the total phonon and electron momentum scattering rates, respectively.

For the Kane semiconductors with the electron spectrum (1) the expressions of $m(\varepsilon)$ and $\nu(\varepsilon)$ have the form [4]:

$$m(\varepsilon) = m_n\left(1 + \frac{2\varepsilon}{\varepsilon_g}\right) \tag{7}$$

$$\nu(\varepsilon) = \nu_0(T)\left(\frac{T_p}{T}\right)^l\left(1 + \frac{2\varepsilon}{\varepsilon_g}\right)\left(1 + \frac{\varepsilon}{\varepsilon_g}\right)^{-r}\left(\frac{\varepsilon}{T}\right)^{-r} \tag{8}$$

where r=3/2, l=0 for the scattering of elektrons by impurity ions and r=-t/2, l=1 for the scattering of elektreons by acoustic phonons. When LW phonons are scattered by SW phonons or by crustal boundaries, $\beta(q)$ doesn't depend on the spectrum of elektrons and has the form [7]:

$$\beta_p(q) = \frac{T^4}{4\pi\rho\hbar^4 s_0^4}q,\ \beta_b(q) = \frac{S_0}{L} \tag{9}$$

where the indices p and b denote the scattering by SW phonons and crystal boundaries, ρ and L are the density and the minimum size of a specimen, respectively. When LW phonons are scattered by electrons, $\beta(q)$ depends on the spectrum of electrons and for the spectrum (1) we obtain:

$$\beta_e(q) = \left(\frac{m_n s_0^2}{8\pi T_e}\right)^{1/2}\frac{NW_0}{T_e}\left(1 + \frac{2T_e}{\varepsilon_g}\right)^2\left(1 + \frac{3T_e}{2\varepsilon_g}\right)^{-3/2}q^t, \tag{10}$$

where N is the concentration of electrons.Solving the coupled equations (5) - (6) by the same way as in [5] and using the conditions $j_x = j_z = 0\left(\vec{E}\|\vec{H}\|oy,\ \nabla T_{e,p}\|oz\right)$ we obtain the following expressions for the thermoelectric field E_{Tz} and the transverse Nernst - Ettingshausen (NE) field E_{Tx}:

$$E_{Tz} + \frac{1}{e}\nabla_z\zeta(T_e) = \alpha_e\nabla_z T_e + \alpha_p\nabla_z T_p;\ \alpha_{e,p} = -\frac{\sigma_{11}\beta_{11}^{(e,p)} + \sigma_{12}\beta_{12}^{(e,p)}}{\sigma_{11}^2 + \sigma_{12}^2}, \tag{11}$$

$$E_{Tx} = -H(Q_e\nabla_z T_e + Q_p\nabla_z T_p);\ Q_{e,p} = \frac{1}{H}\frac{\sigma_{11}\beta_{12}^{(e,p)} - \sigma_{12}\beta_{11}^{(e,p)}}{\sigma_{11}^2 + \sigma_{12}^2}, \tag{12}$$

where $\alpha_{e,p}$ are the electron (e) and phonon (p) parts of the thermoelectric power and $Q_{e,p}$ are the respective parts of NE coefficient,

$$\sigma_{1l} = \int_0^{\infty}\alpha(x)\left(\frac{\Omega(x)}{\nu(x)}\right)^{l-1}\left[1 + b_l(x)\right]dx,\ x = \frac{\varepsilon}{T_e}, \tag{13}$$

$$\beta_{1l}^{(e)} = \frac{1}{e}\int_0^{\infty}\alpha(x)\left(\frac{\Omega(x)}{\nu(x)}\right)^{l-1}\left\{x - \frac{\zeta(T_e)}{T_e} + \left[1 - \frac{\zeta(T_e)}{T_e}\right]b_l(x)\right\}dx, \tag{14}$$

$$\beta_{1l}^{(p)} = \frac{1}{e}\int_0^{\infty}\alpha(x)\left(\frac{\Omega(x)}{\nu(x)}\right)^{l-1}\left[\lambda(x) + \lambda(1)b_l(x)\right]dx\ ,\ \vartheta_e = \frac{T_e}{T},\ \vartheta_p = \frac{T_p}{T}. \tag{15}$$

Here $\zeta(T_e)$ is the chemical potential of hot electrons,

$$\alpha(x) = \frac{e^2}{3\pi^2\hbar^3}\frac{p^3(x)\nu(x)}{m(x)\left[\Omega^2(x) + \nu^2(x)\right]} \times exp\left[\frac{\zeta(T_e)}{T_e} - x\right], \tag{16}$$

$$b_1(x) = \frac{\gamma(x)\nu(x)}{\Omega^2(1) + \nu^2(1)(1-\gamma_0)^2}\frac{m(x)}{m(1)}\left[\nu(1)(1-\gamma_0) - \frac{\Omega(x)\Omega(1)}{\nu(x)}\right], \quad (17)$$

$$b_2(x) = \frac{\gamma(x)\nu(x)}{\Omega^2(1) + \nu^2(1)(1-\gamma_0)^2}\frac{m(x)}{m(1)}\left[\nu(1)(1-\gamma_0) + \nu(x)\frac{m(x)}{m(1)}\right], \quad (18)$$

$$\gamma(x) = \frac{3+t}{(2p)^{3+t}}\frac{\nu_p(x)}{\nu(x)}\int_0^{2p}\frac{\beta_e(q)}{\beta(q)}q^{2+t}dq, \quad (19)$$

$$\lambda(x) = \frac{3+t}{(2p)^{3+t}}\frac{m(x)s_0^2}{T_p}\nu_p(x)\int_0^{2p}\frac{1}{\beta(q)}q^{2+t}dq, \quad (20)$$

$\nu_p(x)$ is the electron scattering frequency by phonons. The coefficient $\lambda(x)$ characterizes the efficiency of the thermal drag, whereas $\gamma(x)$ describes the same for the mutual drag.

Because of the complexity of general analysis of expressions (11) - (15), later we examine the dependence of electron momentum upon its energy in the form

$$p(\varepsilon) = (2m_n\varepsilon_g)^{1/2}\left(\frac{\varepsilon}{\varepsilon_g}\right)^s, \quad (21)$$

which for the spectrum (1) corresponds to the parabolic ($T_e << \varepsilon_g$, $s=1/2$) and strongly nonparabolic ($Te >> \varepsilon_g$, $s=1$)) cases, $m(\varepsilon)$, $\nu(\varepsilon)$ and $\beta(q)$ respectively. In these cases, and may be presented in the form:

$$m(\varepsilon) = 2sm_n\left(\frac{\varepsilon}{\varepsilon_g}\right)^s, \quad (22)$$

$$\nu(\varepsilon) = 2s\nu_0(T)\vartheta_p^{1}\left(\frac{\varepsilon}{\varepsilon_g}\right)^{(2s-1)(1-r)}\left(\frac{\varepsilon}{T}\right)^{-r} \quad (23)$$

$$\beta(q) = \beta(T)\vartheta_e^{n(s-2)}\left(\frac{T}{\varepsilon_g}\right)^{n\left(s-\frac{1}{2}\right)}\left(\frac{s_0 q}{T}\right)^k, \quad (24)$$

where $n=1$, $k=t$ for scattering of LW phonons by electrons, $n=0$, $k=0$ for the scattering by crystal boundaries and when $n=0$, $k=1$ LW phonons are scattered by SW phonons. For the spectrum (21) the chemical potential of hot nondegenerate electrons with concentration N takes the form:

$$\zeta(T_e) = T_e\ ln\frac{3\pi^2\hbar^3 N}{\Gamma(1+3s)(2m_nT)^{3/2}}\left(\frac{T}{\varepsilon_g}\right)^{-3\left(s-\frac{1}{2}\right)}\vartheta_e^{-3s}. \quad (25)$$

Let us study and in weak and strong magnetic fields. In weak magnetic fields in a first approximation on we obtain

$$\alpha_e = -\frac{1}{e}\left(1 + C_1\frac{\gamma_0}{1-\gamma_0}\right)^{-1}\left\{3 - s + 2sr - \frac{\zeta(T_e)}{T_e} + \left[1 - \frac{\zeta(T_e)}{T_e}\right]C_1\frac{\gamma_0}{1-\gamma_0}\right\}, \quad (26)$$

$$\alpha_p = -\frac{1}{e}\frac{C_2 + (C_1 - C_2)\gamma_0}{1 + (C_1 - 1)\gamma_0}\lambda(1), \quad (27)$$

$$Q_e = \frac{1}{ec}C_6\left(1 + C_1\frac{\gamma_0}{1-\gamma_0}\right)^{-2}\left\{(4-4s+2sr)C_3 + \left[(4-5s+4sr)C_1C_3 - (2-s+2sr)C_4\right]\frac{\gamma_0}{1-\gamma_0} - (2 - s + 2sr)C_1\frac{\gamma_0}{(1-\gamma_0)^2}\right\}\mu_s(T_e), \quad (28)$$

$$Q_p = \frac{1}{ec}C_6\left(1 + C_1\frac{\gamma_0}{1-\gamma_0}\right)^{-2}\left\{C_5 - C_2C_3 + (C_4 + C_1C_5 - C_1C_3 - C_2C_4)\frac{\gamma_0}{1-\gamma_0} + C_1(1 - C_2)\frac{\gamma_0}{(1-\gamma_0)^2}\right\}\lambda(1)\mu_s(T_e), \quad (29)$$

where is the mobility of hot electrons with spectrum (21) in the nondegenerate case:

$$\mu_s(T_e) = \frac{\Gamma(3 - s + 2sr)}{4s^2\Gamma(1 + 3s)} \frac{e}{m_n \nu_0(T)} \left(\frac{T}{\varepsilon_g}\right)^{(1-2s)(2-r)} \vartheta_e^{2-4s+2sr} \vartheta_p^{-1}. \tag{30}$$

From (26)-(29) it appears that in weak magnetic fields the mutual drag essentially influences on electron and phonon parts of thermoelectric power and NE coefficients.

In strong magnetic fields from (11) and (12) we obtain

$$\alpha_e = -\frac{1}{e}\left[1 + 3s - \frac{\zeta(T_e)}{T_e}\right], \tag{31}$$

$$\alpha_p = -\frac{1}{e} C_7 \lambda(1), \tag{32}$$

$$Q_e = \frac{c}{eH^2} \frac{1}{C_6^2} \left[(2 - 4s + 2sr)C_8 - 3s\gamma_0 C_9\right] \frac{1}{\mu_s(T_e)} \tag{33}$$

$$Q_p = \frac{c}{eH^2} \frac{1}{C_6^3} \left[C_7 C_8 - C_6 C_{10} + C_9(C_6 - C_7)\gamma_0\right] \frac{1}{\mu_s(T_e)} \lambda(1). \tag{34}$$

As it seen from (31) - (34), in strong magnetic fields thermoelectric power explicitly does not depend on mutual drag coefficient γ_0, but Q_e and Q_p linearly depend on γ_0.

Here

$$C_1 = \frac{\Gamma(1 + 3s + 2sr + 2st - sk)}{\Gamma(3 - s + 2sr)},$$

$$C_2 = \frac{\Gamma(1 + 3s + 2sr + st - sk)}{\Gamma(3 - s + 2sr)},$$

$$C_3 = \frac{\Gamma(5 - 5s + 4sr)}{\Gamma(3 - s + 2sr)},$$

$$C_4 = \frac{\Gamma(3 - s + 4sr + 2st - sk)}{\Gamma(3 - s + 2sr)},$$

$$C_5 = \frac{\Gamma(3 - s + 4sr + st - sk)}{\Gamma(3 - s + 2sr)},$$

$$C_6 = \frac{\Gamma(1 + 3s)}{\Gamma(3 - s + 2sr)},$$

$$C_7 = \frac{\Gamma(7s - 1 + st - sk)}{\Gamma(3 - s + 2sr)},$$

$$C_8 = \frac{\Gamma(7s - 1 - 2sr)}{\Gamma(3 - s + 2sr)},$$

$$C_9 = \frac{\Gamma(7s - 1 + 2st - sk)}{\Gamma(3 - s + 2sr)},$$

$$C_{10} = \frac{\Gamma(11s - 3 - 2sr + st - sk)}{\Gamma(3 - s + 2sr)}. \tag{35}$$

$$\gamma_0 = \frac{(3 + t)2^{\frac{3(t+k)}{2}}}{3 + 2t - k} \left(\frac{m_n s_0^2}{T}\right)^{\frac{t-k}{2}} \left(\frac{T\vartheta_e}{\varepsilon_g}\right)^{\left(s-\frac{1}{2}\right)(2r+2t-k-n+1)} \vartheta_e^{r+t+\frac{3n-3-k}{2}} \vartheta_p^{1-l} \frac{\beta_e(T)}{\beta(T)} \frac{\nu_{f0}(T)}{\nu_0(T)}, \tag{36}$$

$$\lambda(1) = \frac{(3 + t)2^{2-\frac{3k}{2}}}{3 + t - k} \left(\frac{m_n s_0^2}{T}\right)^{1-\frac{k}{2}} \left(\frac{T\vartheta_e}{\varepsilon_g}\right)^{\left(s-\frac{1}{2}\right)(4+t-k-n)} \vartheta_e^{\frac{3n+t-k}{2}} \frac{\nu_{f0}(T)}{\beta(T)}, \tag{37}$$

The expressions (26) - (34) are valid for any values of the mutual drag coefficient ($0 \le \gamma_0 < 1$). The thermoelectric power and thermomagnetic effects of hot carriers in absence of mutual drag ($\gamma_0 = 0$) were studied in papers [8,9]. Thus we consider here just the strong mutual drag regime. This regime takes place when the electrons and phonons are scattered mainly by each other, i.e. $k=t$, $n=1$, $r=-t/2$, $l=1$, $\vartheta_p = \vartheta_e$, $\gamma_0 = \frac{\beta_e(T)}{\beta(T)} \frac{\nu_{f0}(T)}{\nu_0(T)} \to 1$. Under these conditions the expressions (26) - (29) and (31) - (34) can be transformed to the following forms.

In weak magnetic fields electron part of thermoelectric power both in parabolic and non- parabolic cases has the

identical form and depends on degree of nonparabolisity only through the chemical potential of elektrons:

$$\alpha_e = -\frac{1}{e}\left[1 - \frac{\zeta(T_e)}{T_e}\right], \qquad (38)$$

but phonon part of thermoelectric power strongly depends on degree of nonparabolicity:

$$\alpha_p = -\frac{1}{e}\cdot\frac{4\sqrt{2}(2s)^2}{3\pi^{\frac{3}{2}}}\left(\frac{T}{\varepsilon_g}\right)^{3\left(s-\frac{1}{2}\right)}\frac{(m_nT)^{\frac{3}{2}}}{\hbar^3N}\vartheta_e^{3s}. \qquad (39)$$

As it follows from (25), (38) and (39) α_e weakly (logarithmic manner) depends upon T_e, whereas α_P strongly increases with increasing of electron temperature: $\alpha_P \sim T_e^{3/2}$ for the parabolic, and $\alpha_P \sim T_e^3$ for the strong nonparabolic cases.

The electron and phonon parts of NE coefficient in weak magnetic fields:

$$Q_e = -(2 - s - st)\frac{\mu_s(T)}{ec}\vartheta_e^{1-4s-st}, \qquad (40)$$

$$Q_p = \frac{4\sqrt{2}(2s)^2}{3\pi^{\frac{3}{2}}}\left[1 - \frac{\Gamma(1+3s-st)}{\Gamma(3-s-st)}\right]\frac{\mu_s(T)}{ec}\left(\frac{T}{\varepsilon_g}\right)^{3\left(s-\frac{1}{2}\right)}\frac{(m_nT)^{\frac{3}{2}}}{\hbar^3N}\vartheta_e^{1-s-st}, \qquad (41)$$

where $\mu_s(T)$ is the mobility of cold $(T_e=T)$ electrons.

Since $1-4s-st<0$ for the both electron - phonon scattering mechanisms $(t\neq1)$ and for each spectrum of electrons with $s\geq1/2$, from (40) we obtain that Q_e decreases with increasing of T_e. From (41) it is seen that in the parabolic case $(s=1/2)$ $Q_p=0$. In the strong nonparabolic case $(s=1)$ $Q_p\neq0$ and $Q_p \sim \vartheta_e^{-t}$, i.e. Q_p increases with increasing of T_e at piezoelectric electron-phonon interaction, and Q_p decreases with increasing of T_e at deformation interaction.

In the strong magnetic fields:

$$\alpha_e = -\frac{1}{e}\left[1 + 3s - \frac{\zeta(T_e)}{T_e}\right], \qquad (42)$$

$$\alpha_p = -\frac{1}{e}\frac{4\sqrt{2}(2s)^2}{3\pi^{\frac{3}{2}}}\frac{\Gamma(7s-1)}{\Gamma(3-s-st)}\left(\frac{T}{\varepsilon_g}\right)^{3\left(s-\frac{1}{2}\right)}\frac{(m_nT)^{\frac{3}{2}}}{\hbar^3N}\vartheta_e^{3s}. \qquad (43)$$

From (38) and (42) it follows that electron part of thermoelectric power increases in magnetic field:

$$\Delta\alpha_e \equiv |\alpha_e(H)| - |\alpha_e(0)| = \frac{1}{e}3s, \qquad (44)$$

and the increase in the non-parabolic case is bigger than in the parabolic case. The dependence of α_P upon T_e in strong magnetic field is the same as in weak magnetic field.

In the strong magnetic fields for Q_e and Q_p we obtain:

$$Q_e = -(7s-2+st)\frac{\Gamma(7s-1+st)}{\Gamma^2(1+3s)}\frac{c}{eH^2}\frac{1}{\mu_s(T)}\vartheta_e^{4s+st-1}, \qquad (45)$$

$$Q_p = \frac{4\sqrt{2}(2s)^2}{3\pi^{\frac{3}{2}}}\frac{\Gamma(3-s-st)}{\Gamma^2(1+3s)}\left[\Gamma(7s-1+st) - \Gamma(11s-3+st)\right]\frac{c}{eH^2}\frac{1}{\mu_s(T)}\times$$
$$\times\left(\frac{T}{\varepsilon_g}\right)^{3\left(s-\frac{1}{2}\right)}\frac{(m_nT)^{\frac{3}{2}}}{\hbar^3N}\vartheta_e^{7s+st-1}. \qquad (46)$$

As follows from expression (45), in contrast to the weak magnetic fields, in the strong magnetic fields Q_e increases with increase of T_e (for the all real cases $(4s+st-1>0)$). Expression (46) shows that for the parabolic case $Q_p=0$ whereas for the strong nonparabolic spectrum of electrons $(s=1)$ Q_p strongly increases with increase of T_e: $Q_p \sim \vartheta_e^{6+t}$ i.e. $Q_p \sim \vartheta_e^7$ at deformation interaction and $Q_p \sim \vartheta_e^5$ at piezoelectric interaction of electrons with phonons.

As it follows from (25) for the nondegenerate electrons

$$\left(\frac{T}{\varepsilon_g}\right)^{3\left(s-\frac{1}{2}\right)}\frac{(m_nT)^{\frac{3}{2}}}{\hbar^3N} \approx \exp\left[-\frac{\zeta(T)}{T}\right] >> 1, \qquad (47)$$

and from the comparison (38) with (39) and (42) with (43) it is seen that under the conditions of strong mutual drag $|\alpha_p| >> |\alpha_e|$, both in weak and in strong magnetic fields, i.e. the thermoelectric power mainly consists of the phonon part.

Since in the case of a parabolic spectrum $Q_p=0$, the NE field consists only of the electron part. But in the case of the strong nonparabolic spectrum from (40), (41), (45) and (46) it follows that $|Q_p| >> |Q_e|$, i.e. NE field mainly consists of the phonon part.

Under the conditions of the strong mutual drag ($\vartheta_e=\vartheta_p, \gamma\to 1$) the electron temperature is determined from the energy balance equation

$$\sigma_{11}(\vartheta_e)E^2 = W_{pp}(\vartheta_e), \qquad (48)$$

where $W_{pp}(\vartheta_e)$ is the power transferred by the LW phonons to the thermal reservoir of the SW phonons. The calculation of the expression $\vartheta_e(E)$ from (48) at ($\vartheta_p = \vartheta_e >> 1$ in following limiting cases gives:

Case 1) $\dfrac{\beta_p + \beta_b}{\beta_e} << \dfrac{\nu_i}{\nu_p}$: $\vartheta_e \sim E^{\frac{2}{5s-1}}$, (49)

Case 2) $\beta_p >> \beta_b$, $\dfrac{\beta_p}{\beta_e} >> \dfrac{\nu_i}{\nu_p}$: $\vartheta_e \sim E^{\frac{1}{4s+1}}$, (50)

Case 3) $\beta_p << \beta_b$, $\dfrac{\beta_p}{\beta_e} >> \dfrac{\nu_i}{\nu_p}$: $\vartheta_e \sim E^{\frac{2}{7s+2}}$, (51)

As it seen from (49) - (51) the nonparabolicity of electron spectrum strongly changes the E -dependence of electron temperature. Using these expressions one can easily obtain the dependence of thermoelectric power and NE coefficient upon the heated electric field in the considered cases. From (25), (38) and (42) it follows that α_e weakly (logarithmic manner) depends upon E for the all cases (49) - (51). The dependence of α_p, Q_e and Q_p upon E in these cases are shown in the table.

Table

The dependence of α_p, Q_e and Q_p upon E under the conditions of strong mutual drag

	Case 1	Case 2	Case 3
α_p	$\sim E^{\frac{6s}{5s-1}}$	$\sim E^{\frac{3s}{4s+1}}$	$\sim E^{\frac{6s}{7s+2}}$
$Q_e\left(\bar{\Omega} << \bar{\nu}\right)$	$\sim E^{\frac{2(1-4s-st)}{5s-1}}$	$\sim E^{\frac{1-4s-st}{4s+1}}$	$\sim E^{\frac{2(1-4s-st)}{7s+2}}$
$Q_e\left(\bar{\Omega} >> \bar{\nu}\right)$	$\sim E^{\frac{2(4s+st-1)}{5s-1}}$	$\sim E^{\frac{4s+st-1}{4s+1}}$	$\sim E^{\frac{2(4s+st-1)}{7s+2}}$
$Q_p\left(\bar{\Omega} << \bar{\nu}\right)$	$\sim E^{\frac{2(1-s-st)}{5s-1}}$	$\sim E^{\frac{1-s-st}{4s+1}}$	$\sim E^{\frac{2(1-s-st)}{7s+2}}$
$Q_p\left(\bar{\Omega} >> \bar{\nu}\right)$	$\sim E^{\frac{2(7s+st-1)}{5s-1}}$	$\sim E^{\frac{7s+st-1}{4s+1}}$	$\sim E^{\frac{2(7s+st-1)}{7s+2}}$

When one uses this table, he must take into account that in parabolic case $Q_p=0$, and the total NE coefficient $Q=Q_e+Q_p=Q_e$, but in strong nonparabolic case $|Q_p| >> |Q_e|$, and $Q\approx Q_p$. For instance, if d-interaction and inequality (49) are satisfied in the semiconductors, pased in the strong magnetic fields $Q\sim E^{7/2}$ for the parabolic, and for the strong nonparabolic spectra.

Under the conditions of strong mutual drag $|\alpha_p| >> |\alpha_e|$, and the total thermoelectric power $\alpha=\alpha_e+\alpha_p\approx\alpha_p$, both in parabolic and nonparabolic cases.

For instance, if inequality (49) is satisfied then $\alpha\sim E^2$, in the parabolic, and $\alpha\sim E^{3/2}$ in the strong nonparabolic cases. From the Table it is seen that for the all cases nonparabolicity of spectrum essentially changes the dependence of α and Q upon E.

[1] *X.L.Lei. J.Phys.*: Condensed Matter, 1994, 6, L305.

[2] *D.Y.Xing, M.Liu, J.M.Dong and Z.D.Wang.* Phys, Rev. B, 1995, 51, 2193.

[3] *M.W.Wu, N.J.M.Horing and H.L.Cui.* Phys,Rev. B, 1996, 54, 5438.

[4] *B.M.Askerov.* Electron Transport Phenomena in Semiconductors (Singapore: World Scientific), 1994.

[5] *M.M.Babaev, T.M.Gasymov and A.A.Katanov.* Phys. Status Solidi (b), 1984, 125, 421.

[6] *T.M.Gasymov,A.A.Katanov and M.M.Babaev.* Phys. Status Solidi (b), 1983, 119, 391.

[7] *L.E.Gurevich and T.M.Gasymov.* Fizika Tverdogo Tela, 1967, 9, 105.

[8] *T.M.Gasymov, A.A.Katanov, M.M.Babaev.* Fizika i Texnika Poluprovodnikov, 1977, 11, 1985.

[9] *M.M.Babaev, T.M.Gasymov.* Fizika i Texnika Poluprovodnikov, 1980, 14, 1227.

M.M. Babayev, T.M. Qasım

QARŞILIQLI ELEKTRON-FONON SÖVQÜ ŞƏRAİTİNDƏ GÜCLÜ ELEKTRİK SAHƏSİNDƏ YERLƏŞDİRİLMİŞ CIRLAŞMAMIŞ KEYN YARIMKEÇİRİCİLƏRİNDƏ TERMOMAQNİT EFFEKTLƏR

Elektron və fononların qızması və qarşılıqlı sövqü şəraitində cırlaşmamış Keyn yarımkeçiricilərində termoelektrik hərəkət qüvvəsi və Nernst–Ettingshausen effektləri tədqiq edilmişdir. Göstərilmişdir ki, elektron spektrinin qeyri-parabolikliyi termoelektrik hərəkət qüvvəsinin və Nernst–Ettingshausen əmsalının qiymətlərinə güclü təsir edir və onların elektron temperaturundan, eləcə də qızdırıcı elektrik sahəsinin intensivliyindən asılılıqlarını dəyişdirir. Güclü elektron-fonon qarşılıqlı sövqü şəraitində, elektronlarının spektri parabolik olan yarımkeçiricilərdə Nernst–Ettingshausen əmsalının fonon hissəsi $Q_p=0$ olur, amma qeyri parabolik halda

$Q_p \neq 0$ və Q_p Nernst–Ettingshausen əmsalının elektron hissəsindən (Q_e) xeyli böyük olur, yəni Nernst–Ettingshausen sahəsi, əsasən, fonon hissədən təşkil olunur.

М.М. Бабаев, Т.М. Гасым

ТЕРМОМАГНИТНЫЕ ЭФФЕКТЫ В НЕВЫРОЖДЕННЫХ КЕЙНОВСКИХ ПОЛУПРОВОДНИКАХ, НАХОДЯЩИХСЯ В СИЛЬНОМ ЭЛЕКТРИЧЕСКОМ ПОЛЕ В УСЛОВИЯХ ВЗАИМНОГО УВЛЕЧЕНИЯ ЭЛЕКТРОНОВ И ФОНОНОВ

Исследованы термоэдс и эффекты Нернста-Эттингсгаузена в невырожденных Кейновских полупроводниках, с учетом разогрева электронов и фононов, а также их взаимного увлечения. Показано, что непараболичность спектра электронов значительно влияет на величины термоэдс и коэффициента Нернста-Эттингсгаузена, изменяет их зависимости от электронной температуры, а также от греющего электрического поля. В условиях сильного взаимного увлечения в полупроводниках с параболическим спектром электронов фононная часть коэффициента Нернста-Эттингсгаузена $Q_p \neq 0$, а в непараболическом случае $Q_p \neq 0$ и Q_p значительно больше, чем электронная часть коэффициента Нернста-Эттингсгаузена Q_e, т.е. поле Нернста-Эттингсгаузена, в основном, состоит из фононной части.

Received: 05.12.01

ON THE SUDDEN DECREASES IN THE BRIGHTNESS OF NOVA HR DEL AT THE MINIMUM.

M.B. BABAYEV and A.M. BABAYEVA
Shamakha Astrophysical Observatory named after N. Tusi,
Azerbaijan National Academy of Sciences,
373243, Shemakha, Pirgulu, Azerbaijan

Extensive photometric observations of Novae HR Del 1967 at the brightness minimum showed that in addition to the orbital minima [3,5], 82 second ultrashort periodic changes in the brightness [10] and secondary minima in the light curve for the first time there are sudden decreases of the brightness.

New Delphina 1967=HR Del for the first time was observed as Nova on June 15, 1967. According to the form of its brightness change it was determined as ultra-slow Nova [1]. Stefanson observed this star seven months before the flare. At that time it had magnitude m_V=11^m.8±0^m.5 and its spectral class was determined as late *O* or early *B*. In 1981 it had magnitude of 12^m.5 [3]. Regular observations showed that all the phases of the flare were proceeding very slowly: just after 4 weeks after the discovery the magnitude reached the value of 5^m.0 after which during 5 months its brightness remained constant and just December 6-13, 1967 the brightness suddenly increased up to the value of m_V=3^m.5. As it can be seen, the evolution of the flare of HR Del proceeded very slowly, which made possible to observe this Nova by many astronomers. Systematic observations of HR Del showed a number of phenomena never observed in other Nova. After the first maximum, after which usually the decrease of the brightness is expected, in the case of HR Del another two flares with intensities comparable with the intensity of main flare were detected [4]. These events took place after fluctuations of the brightness of HR Del 1967 about some level. The reason of such brightness fluctuations of the typical Novae still remains unclear [5].

The results of investigations of line and continuous spectra and the change of the brightness of HR Del 1967 have been published in many works. The light curve of HR Del 1967 which is built up by using enduring photometric observations (June, 1967 - December, 1971) is presented in [4]. By using this light curve we have found periodical changes which are in a good agreement with the epoch calculated by us [5].

So, HR Del is a cataclysmic variable with some peculiarities, which justifies future intensive investigations.

With the aim to detect sudden decreases of the brightness of the Nova HR Del 1967 we have observed them photometrically for one night 2-3.08.1994. Photoelectrical observations of HR Del were carried out with the telescope ZEIS - 600 at Shamakha Astrophysical observatory with the help of photometer AFM - 6 by the method of photon counting. Fast photometric observations were carried out in the UBVR filters with diaphragm of 43". FEA-79 has been used as light receiver. The observations were carried out by a differential method using very close stars for comparison. The results of observations were received in a digital form by using EUM-23. The accumulation time for each point of measurement was taken 10 sec. As the standard star was taken star N1 (m_V=13^m.83) from the list of [6].

Using the data of the star of comparison the root mean square errors of one measurement, making on the average ±0^m.002, and sometimes not exceeding ±0^m.005, were determined. To construct the light-curve average values of the difference $\Delta m=m_{st}-m_*$, made on 3 or 4 measurements of Δm, consisting each of them of 15 measurements with accumulation time of 10 sec were used.

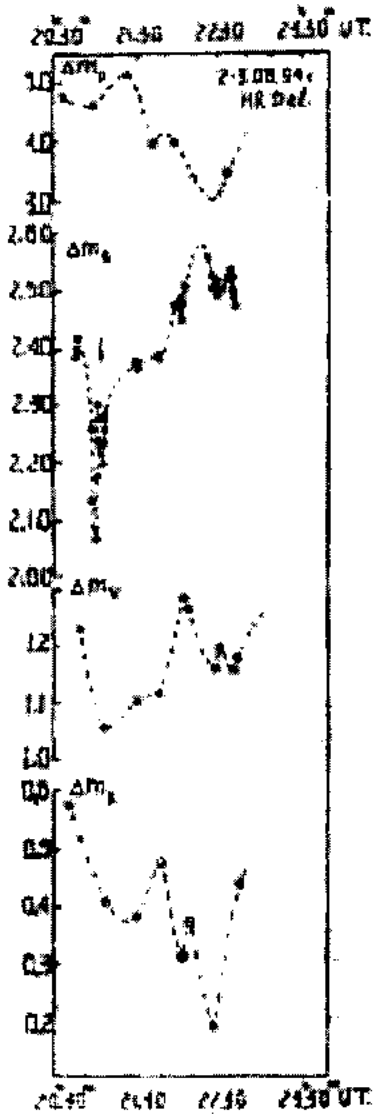

Fig.1. Part of the differential light curve of Nova HR Del 1967 in UBVR-filters

Fig.1 shows the part of the light curve of HR Del measured relative to the standard star, on observations on August 2-3, 1994. These observations gave us an opportunity to find for the first time a complete picture of sudden falls of

the brightness of HR Del 1967 in filter *B*, identical for Polars - flare Nova-like stars such as TT Ari and other [7].

2.1 hour parts of orbital period is covered by measurements and in each filter it is found narrow -4-5 minute sudden falls of the brightness, which have different depth depending on the wave length.

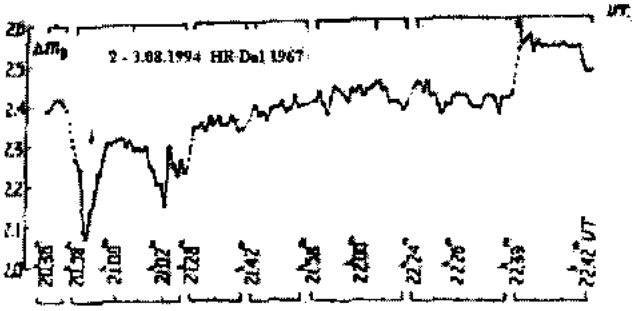

Fig.2. Light curve of HR Del 1967 in B-filter with sudden falls of the brightness.

Such sudden decreases of the brightness are well visible in the filter B (fig. 2). In this filter plenty of measurements was carried out. In fig. 2 bifurcation, amplitude of changes and duration of sudden falls of the brightness of HR Del 1967 are well appreciable.

For the time for an explanation of such effect being it is supposed, that the sudden falls of the brightness is the result of absorption of emission of the source, being near to the white dwarf, by falling flow of matter. Such simple eclipse of the emitting source cannot explain the observing falls of the brightness. The picture is more complex. Probably it is necessary to attract for this purpose short-term amplifications of intensity of the gas flow, the change of the structure of the flow, the change of its density and direction or different combinations of these phenomena. It seems more likely, that such sudden falls of the brightness, especially in the filter *B*, are caused by eclipse in the field of radiation by non-stationary clouds in equator ring around binary system and by the jet of accreting matter.

Thus, observations carried out in 1994 showed that except some peculiarities in the brightness change of the Nova HR Del, revealed earlier, sudden falls of the brightness characteristic for Polars - flaring nova-like stars as TT Ari are took place. These phenomena do not depend on the phase. The purpose of present paper is to attract the attention of observers to short-term sudden falls in the brightness in the minimum of Nova. Extensive observations could confirm similarity of characteristic changes of the brightness of Polars and typical Novae and could confirm the presence of patchy formations in the disk environments and jets of accreting matter.

Summarizing all photometric data we can conclude that for Nova HR Del 1967 6 basic types of small amplitude changes of the brightness are typical:

1) 32-day quasi-periodic changes observed during a maximum and further [3,5,6]

2) $0^d.17$ - $0^d.21$ periodic changes ($\Delta m=0^m.15$) connected, apparently, with the orbital motion of the star [3,8,9].

3) $0^d.13$ - $0^d.14$ periodic changes ($\Delta m=0^m.06$) connected, apparently, with the non-uniform brightness distribution in circumstellar disk [3,8].

4) 82 second ultra-short periodical changes ($\Delta m=0^m.05$), precisely observed in an orbital light maximum, where the fluctuations of brightness are very small [10]

5) Quasi-periodical changes of the brightness as secondary minima, not depending on orbital motions, which have variable form and amplitude. Apparently, these minima are due to the presence of circumstellar disk and clots of matter, which form common envelope around the Nova.

6) Finally, in observations carried out in 1994 in different filters, especially in the filter *B*, in Nova HR Del 1967 sudden falls of the brightness, characteristic for Polars - flaring nova-like stars are revealed.

Thus, our photometric observations, carried out on different telescopes at the Shamkha Astrophysical observatory showed that slow Nova HR Del 1967 is a binary system, which has 6 types of small amplitude fluctuations of the brightness.

[1] *J. Malakpur.* Astronomie. 1974, v. 88, p. 251-254.
[2] *C.B. Stepenson.* PASP , 1967 , v. 88, p. 584-588
[3] *M.B. Babaev.* Tsirkulyar ShAO 1983, №71, p.16-21
[4] *J.E. Isles.* JBAA, 1974, v. 85.№1, p. 58-62
[5] *M.B. Babaev and M.S. Gadzhiev.* Peremenie zvezdi, 1994,v.23,№5, p.305-318 (in Russian).
[6] *T.G. Barnes and N.R. Evans.* PASP, 1970, v.82, №488, p.889-893
[7] *J. Tremko, A. Anton, M.B. Babaev, et al.* Contrib.astron. observ. Scalnate Pleso. 1990, v.232, p.69-75
[8] *J.B. Hutchings.* Ap. J. 1979. v. 232. p. 176.
[9] *H.M. Steinbach, L. Kohoutek.* IBVS, 1983, №2367, p.1-3
[10] *M.B. Babaev, M.S. Gadzhiev* Astronomoch.Tzirkulyar., 1990. №1546. p. 17-18.
[11] *M.B. Babaev.* Astron. Tsirkulyar. 1990, №1546, p.17-18.

M.B. Babayev, A.M. Babayeva

YENİ HR DEL ULDUZUNUN MİNİMUM AFZALINDA PARLAQLIĞININ QƏFLƏTƏN DÜŞMƏSİ

Ardıcıl fotometrik müşahidələrin tədqiqi göstərdi ki, Yeni HR Delfin ulduzunun parlaqlığının dəyişmə orbital, əlavə udulma minimumları və 82 saniyəlik qısa periodik dəyişkənliyi ilə yanaşı, onun parlaqlığının qəfil düşməsi ilk dəfə müşahidə edilmişdir.

М.Б. Бабаев и А.М. Бабаева

ВНЕЗАПНЫЕ ПАДЕНИЯ БЛЕСКА НОВОЙ HR DEL В МИНИМУМЕ

Продолжительные фотометрические наблюдения Новой HR Del 1967 г в минимуме блеска показали, что помимо орбитальных минимумов, 82-секундных ультракоротко периодических изменений побочных минимумов, в орбитальных кривых блеска впервые обнаружены внезапные кратковременные падения блеска Новой.

Received: 16.11.01

MAGNETIC PROPERTIES OF $TlMnS_2$ AND $TlMnSe_2$ COMPOUNDS.

R.Z. SADIKHOV, E.M. KERIMOVA, Y.G. ASADOV, R.K. VELIEV
Institute of Physics, Azerbaijan National Academy of Sciences
H. Javid av. 33, Baku, 370143

$TlMnS_2$ and $TlMnSe_2$ compounds have been synthesized and X-ray analysis was carried out. Magnetization and paramagnetic susceptibility of these compounds have been investigated in the temperature interval 77÷300K. It is shown that $TlMnS_2$ and $TlMnSe_2$ are low-dimensional magnetics and the antiferromagnetic exchange interaction takes place in them. Experimental values of the effective magnetic moment are ~4.5 μ_B for $TlMnS_2$ and 4.7 μ_B $TlMnSe_2$, that is in agreement with theoretical values for the three-valence Mn ion.

Roentgenographic, thermal and magnetic investigations of compounds with the general crystallochemical formula $TlMeX_2$ (Me=Cr, Fe, Co; X=S, Se, Te) allowed paper's authors [1 - 7] to conclude about the low-dimension of these compounds.

For determination of influence of the 3-d configuration of Me ions on magnetic properties, in given work we have investigated the magnetization and paramagnetic sensibility of $TlMnS_2$ and $TlMnSe_2$ belonging to this class of compounds.

$TlMnS_2$ and $TlMnSe_2$ samples were synthesized in vacuum quartz ampoules by the solid state method of caking of binary compounds TlS (Se) and MnS (Se) which beforehand were put into the powdered state and weighed in the equimolecular relation. Synthesis was carried out in the following sequence. Ampoule with initial components was placed into the furnace where the temperature rises from room one up to 1000K with the rate 100deg/hour. At this temperature the ampoule was held for 30 hours, then it is cooled up to the room temperature with the same rate. For prevention of interaction of initial components with the internal wall of the quartz ampoule the last one was in the rotation during the synthesis process. Obtained samples were rubbed to the powder, pressed under the high pressure and undergone to the homogenizing annealing for 240 hours at 700K.

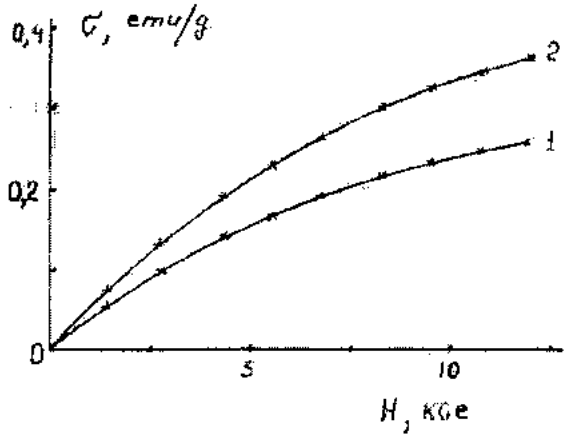

Fig. 1. Dependence of the specific magnetization of $TlMnS_2$ (1) and $TlMnSe_2$ (2) on the magnetic field at 77K.

X-ray analysis of samples was carried out on the diffractometer DRON-3M (CuK_α-radiation Ni- filter). Angle resolution of the photographing was ~0,1°. Continuous scanning regime was used. Diffraction angles were determined by the method of measurements on the intensity maximum. At experiments the determination error of reflection angles did not excess $\Delta\theta$ ± 0,02°.

Diffractograms of synthesized samples written down in the angle interval $10° \le 2\theta \le 70°$ at the room temperature, are definitely induced in tetragonal ($TlMnS_2$) and hexagonal syngonies with parameters of the crystalline lattice a=7.74; c=30.60Å, roentgen density ρ_x=6.40g/cm^3, atom number in the unit cell z=20 and a= 6.53, c=23.96Å, z=8, ρ_x=6.71g/cm^3, respectively.

Magnetization (σ) was measured on the pendular magnetometer Domenicalli, and the paramagnetic susceptibility (χ) was measured -by the Faraday method on the magnetoelectric balance.

Fig.1 presents the dependence of the specific magnetization of $TlMnS_2$ and $TlMnSe_2$ compounds on the magnetic field at 77K. As it is seen, the dependence $\sigma(H)$ at given temperature for both compounds has the form characteristic for the paramagnetic state. However the temperature dependence of the reverse paramagnetic susceptibility of these compounds (fig.2) follows to the Curie-Weice law with the extrapolation to the range of negative temperatures which testifys on existence of the antiferromagnetic exchange interaction. According to fig.2, the temperature of the magnetic transformation of both compounds is below 77K.

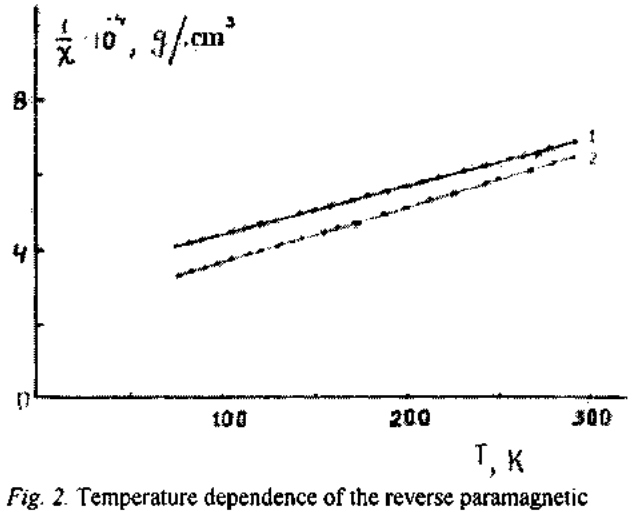

Fig. 2. Temperature dependence of the reverse paramagnetic susceptibility of $TlMnS_2$ (1) and $TlMnSe_2$ (2).

From the temperature dependence of the reverse paramagnetic susceptibility we have calculated experimental values of the effective magnetic moment of compounds under investigation which are equal to 4.5 ($TlMnS_2$) and 4.7μ_B ($TlMnSe_2$). Calculation of the theoretical value of the effective magnetic moment (4.9μ_B) was carried out with account of the purely spin value of the magnetic moment of the three- valent Mn ion. Comparison shows good agreement

of experimental and theoretical results that is the indirect confirmation of the accepted ionic configuration of given compounds.

Interpretation of obtained experimental results, testifying on the antiferromagnetic interaction in $TlMnS_2$ and $TlMnSe_2$, can be done on the basis of the crystalline structure of these compounds. As it is known, this structure determines the periodicity of arrangement of spin magnetic moments where the exchange interaction is responsible for their mutual orientation. Taking into account this fact, we, apparently can imagine the crystalline structure of $TlMnS_2$ and $TlMnSe_2$ as sequentially alternating two-dimensional layers of ions Mn^{3+}, Tl^{+} and S^{2-}(or Se^{2-}) parallel to the basal plane. Sufficiently large ratio c/a ~4 testifys on the laminated structure of these compounds. Ferromagnetic ordering have been carried out in the plane, including ions Mn^{3+}. Therefore layers of ions Mn^{3+} are two- dimensional ferromagnetic. Layers Tl^{+} and S^{2-}(or Se^{2-}) have been arranged between the nearest layers of ions Mn^{3+}. Therefore ferromagnetic layers are connected with each other by weaker forces of the antiferromagnetic type. Co - existence of ferromagnetic (within layers) and antiferromagnetic (between layers) interactions leads to the resulting antiferromagnetic interaction in $TlMnS_2$ and $TlMnSe_2$.

We note that authors [6], following from the abovementioned model consider that the ferrimagnetic ordering in compounds $TlCoS_2$ and $TlCoSe_2$ is the result of a noncomplete compensation of spin magnetic moments of ferromagnetic layers formed by Co ions.

Thus results of X-ray and magnetic investigations testify on the low - dimension of compounds $TlMnS_2$ and $TlMnSe_2$ and existence of the antiferromagnetic exchange interaction in them.

[1] *M.Rosenberg, A.Knulle, H.Sabrowsky, C.Platte.* J. Phys. Chem. Solids, 1982, 43, 2, 87.

[2] *G.I. Makovetski, E.I. Kasinski.* Non-organic materials. 1984, v. 20, №10, p. 1752.

[3] *M.A.Aljanov, N.G.Guseinov, G.D.Sultanov, M.D. Nadjafzade.* J. Phys. Stat. Sol. (b), 1990, 159, k107.

[4] *M. Aljanov, M. Nadjafzade, Z. Seidov, M. Gasumov.* Turkish Journal of Physics, 1996, 20, 9, 1071.

[5] *E.M. Kerimova, F.M. Seidov, S.N. Mustafaeva, S.S. Abdinbekov.*. Non-organic materials, 1999, v.35, №2, p.157.

[6] *R.Z. Sadikov, E.M. Kerimova, Y.G. Asadov, R.K.* Veliev. FTT, 2000, v. 42, 8, p.1449.

[7] *S.N. Mustafaeva, E.M. Kerimova, A.I. Dzabbarli.* FTT, 2000, v. 42, №12, p. 2132.

R.Z. Sadıxov, E.M. Kərimova, Y.Q. Əsədov, R.K. Vəliyev

$TlMnS_2$ VƏ $TlMnSe_2$ BİRLƏŞMƏLƏRİNİN MAQNİT XASSƏLƏRİ

$TlMnS_2$ və $TlMnSe_2$ birləşmələri sintez olunmuş, onların rentgenoqrafik analizləri aparılmışdır. 77÷300 K temperatur intervalında maqnitlənmə və paramaqnit qavrayıcılığı tədqiq edilmişdir. Göstərilmişdir ki, $TlMnS_2$ və $TlMnSe_2$ kiçik ölçülü maqnetikdirlər və onlarda qarşılıqlı antiferromaqnit mübadiləsi mövcuddur. Effektiv maqnit momentinin –4.5 ($TlMnS_2$) və 4.7μ_B ($TlMnSe_2$) təcrübi qiymətləri Mn–in üçvalentli ionunun nəzəri qiymətləri ilə uyğun gəlir.

Р.З. Садыхов, Э.М. Керимова, Ю.Г. Асадов, Р.К. Велиев

МАГНИТНЫЕ СВОЙСТВА СОЕДИНЕНИЙ $TlMnS_2$ и $TlMnSe_2$

Синтезированы соединения $TlMnS_2$ и $TlMnSe_2$, проведен их рентгенографический анализ. В интервале температур 77÷300 К исследована намагниченность и парамагнитная восприимчивость. Показано, что $TlMnS_2$ и $TlMnSe_2$ являются низкоразмерными магнетиками и в них осуществляется антиферромагнитное обменное взаимодействие. Экспериментальные значения эффективного магнитного момента –4.5 ($TlMnS_2$) и 4.7μ_B ($TlMnSe_2$) - согласуются с теоретическим значением для трехвалентного иона Mn.

Received: 08.10.01

THE ELECTROMAGNETIC HYDROCYCLONE FILTER FORCES ANALYSES

ERKAN IMAL, PARVIZ ALI-ZADA, FETHI GÖKTEPE, FERHAT KARACA
FATIH University, Istanbul, Turkey;

FEYZULLAH VARDARLI
Textile Painting Factory, Istanbul, Turkey

HIKMET KULIEV, EMIN GUSSEYNOV
The Azerbaijan State Oil Academy
370010, Baku, pr. Azadliq, 20

There are a great number of different kind organic and natural admixtures (sand, ferrous, nuclear particles, phenols, oil, etc.) in technological liquids and gases, which can drop production quality for the worse. That is why improved universal treatment devices (filters, separators, etc) for these liquids and gases are in great need. From the other hand the waste liquids and gases should be filtered before disposal because they damage environment. The importance of the environmental pollution control and treatment is undoubtedly the key factor in the human future. This paper deals with design of fine treatment technique for the technological and waste liquids and gases (separation of microscopic suspended water, sand, oil and other organic and not organic components). The paper briefly reviews existing processes and technique for liquids and gases treatment and is focused on construction of electromagnetic hydrocyclone. The effect of main forces (centrifugal, electrical and magnetic) on the separation of very small-size admixtures (smaller than 10 microns) is analyzed and compared. Some delicate technologies are shown where even a very small amount of even micro admixtures can bring misfortune or accident.

INTRODUCTION

Technological and waste liquids and gases usually have a great number of different kind admixtures (ferrous, phenol, oil, organic, nuclear particles, etc.) which can change production quality for the worse. That is why improved cleaning devices (filters, separators etc) for these liquids and gases are in immense need. Waste liquids and gases should be filtered before disposal because they damage environment. Otherwise, the producers have to pay a heavy emission fees. There are a lot of methods and filter constructions to separate the above mentioned particles from technological and waste liquids and gases and main of them are hydro or gas cyclones, magnetic or electrostatic traps etc. In most cases they meat the all demands of the industries if very small (less then 10 microns) impurities do not disturb their main processes. The efficiencies of the above mentioned filters and traps are high and very well known for different types of admixture in liquids and gases [1-4]. But there are some delicate technologies where even a very small amount of even micro admixtures can bring misfortune or accident. To empathize this more clearly, some matter-of-fact examples are given below:

1. There is a very little amount of microscopic water bolls in plane fuel (less than 0.01% or 100gr in a ton) that can cause sometimes accident. The water may freeze at any valve or at narrow pipe and fuel will not be pumped into engine. The filtration process of these micron size water particles is possible by the help of some chemical methods or centrifugal machine, but difficult and expensive.
2. There is a tiny quantity of some phenols and other light organic particles (up to molecule size) in the distil water of thermal plant boilers. These particles separation by the help of mechanical or chemical methods is extremely difficult and expensive. Nevertheless that those particles are too small, but they are very dangerous. They make thousands small bursts on the inner surface of high temperature and pressure boiler pipes, pluck out micro particles of the metal, slowly damage (erode) the pipes and increase risk of the boiler steam leakage or even explosion.
3. One of the method of different liquids (in particular sea water) desalination or demineralization is mixing them with another active sprayed liquid (or a subtle powder), that is able to entrap the appropriate mineral salts, and then separate the liquid or the powder from the main one. The smaller micro particles of the entrapping liquid or the powder the more effective the entrapping process. One of these active and rather cheap liquids is kerosene. But to separate these salty micro particles from main liquid by ordinary hydrocyclone is very difficult and more expensive. Electric and magnetic forces here are more effective than only centrifugal force.
4. Finding and filtering out different nuclear particles from liquids and gases, especially after Chernobyl Nuclear Station accident, became a very important issue. It is used in UKRAINE to reveal and to filter the electrically charged nuclear particles in milk by the help of electric and magnetic forces.
5. Textile manufacturing is a very important branch of Turkish industry. Multi-cycle painting processes in textile industry use huge amount water: the higher quality water, the higher quality textile. There are more than twelve different operations during panting process of a textile tela (fabric, cloth) and every one of them demands new portion good quality water or recycled waste water. It is very ease to take out rather big specific textile particles (rubbish) from waste water, but taking out small admixtures less than 50 microns and especially less than 10 microns (dust, pant particles etc) is extremely difficult. Here is reasonable to apply more effective electrical or magnetic forces for separation and to recycle waste water or, as a minimum, bring it to the required waste limit norm.

Thus, there are some cases where separation (filtration) liquids from all admixtures up to even micro particles is very important and it demands application of more effective forces for micro particles. Here is important to stress that electromagnetic forces can help to rise the total coefficient of

filtration efficiency, but a bit - not more than 1%, even less. The main effect is coming from higher quality of the concrete technology, from higher reliability and safety reserve for humanity, ecology and so on.

DISCUSSIONS

Electromagnetic hydro (gas) cyclone (EMH) is a combined apparatus for the technological and waste liquids and gases treatment. A special construction joints collinear influences of electric, magnetic, and centrifugal forces. Similarly to traditional hydrocyclones, there are several different types of EMH construction [4,5,7-10]: cylindrical and conic EMH for two products, EMH for three products etc. First and especially second type of EMH are most useful ones and will be mainly discussed in this paper (fig. 1 and 2). EMH consists of cylindrical diamagnetic metal (or plastic) main body 1, conic or flat ferromagnetic metal inferior body 2, entrance 3 and output 4 nipple pipes (tangential to cylindrical main body), central light product pore out nipple pipe 5 (central electrode), flat ferromagnetic metal cover 6, bobbin around main body 7 and the pipes electrical isolations 8.

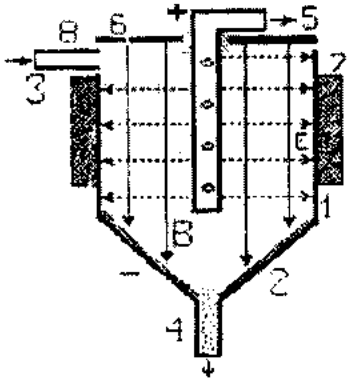

Fig. 1. Conic EMH

As it is illustrated by fig 1 and 2, an electric field force is produced by applied DC voltage between main body and central pour out nipple (electrode). A bobbin around the main body produces a magnetic field force between flat ferromagnetic cover and magnetic conical (or flat) bottom part of the EMH. There is inertial centrifugal force due to liquid (gas) high-speed rotation in cylindrical main body, because of the entrance nipple is tangential to the latter and high incoming flow velocity is equal to liquid (gas) tangential rotation velocity. For some special cases ozone (O_3) can be produced around the central electrode to kill microbes, to fire poisonous natural or organic admixtures in outgoing pipe (central electrode). In such a case an additional high frequency voltage can be applied throw a capacitor to this electrode.

Thus, in two words, technological or waste liquid (gas) enters throw input nozzle and heavy particles, such as sand, metals, silt, etc are displaced by centrifugal force to main body inner cylinder surface, then down and quit from conic exit. While light particles, such as oil and organic traces, gas bubbles etc, are ousting to the central electrode-pipe and pour out of the EMH. In this system quality filtration rises very high (especially for micron size impurities) due to electric and magnetic field application in addition and collinear to the centrifugal force: the three forces act in the same direction.

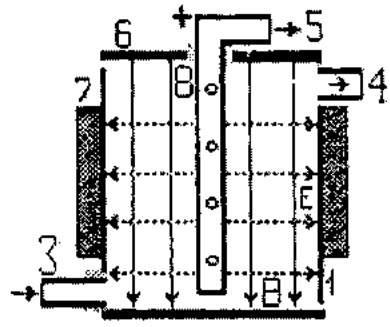

Fig. 1. Cylindrical EMH

There are several vector forces that affect a particle in EMH in a common case:

$$F_m+F_e+F_s+F_i+F_a+F_w+F_c = 0, \qquad (1)$$

where: F_m -magnetic forces, F_e-electric force, F_s - Stokes' force (resistive), F_i -inertia force, F_a – Archimede's force, F_w -weight force, F_c -centrifugal force.

Comparative analyses [1] have shown that influences of F_a, F_i and F_w on a very small (less than 50 micron) dispersed particles are negligible small and they can be omitted. The main influences belongs to forces F_m, F_e, F_c and resistive force F_s (depends on viscosity of a liquid).

The effect of centrifugal force on particle filtration is determined as:

$$F_C = \frac{\pi * d^3(\rho_1 - \rho_2) * v_t^2}{6r}, \qquad (2)$$

where: d - diameter of particle [m],
ρ_1 - density of technological liquids. [kg/m^3],
ρ_2 - density of particles [kg/m^3],
r - average revolving radius [m],
v_t - velocity of particles, m/sec.

In the case of $\rho_1<\rho_2$ (water - ferrous, sand etc admixtures) cleaned liquid exits trough the central pour out tube and mechanical particles are removed from bottom conical product pipe. In the case of $\rho_1>\rho_2$ (water - oil, phenols etc), cleaned liquid is extracted trough bottom conical product tube and oil is removed from central pour out nipple pipe. But most micro particles cannot be removed just by cyclone application due to floatation effects, which presents in liquids and gases: for $d<d_{critical}$ the smaller weight of a micro particle (proportional to d^3 of a particle) the higher floating force (proportional to d^2 of a particle) as compared with weight.

Generally, 70-80% of particles in technologic liquids are charged by negative electric charge [1,2,3]. Electric and magnetic forces effect on the negatively charged particles. They can be pushed or pulled to the electrodes. Due to this fact central pour out tube is often used as a positive electrode and cylindrical body as a negative one. There are some holes on this central tube for collecting light and charged particles such as oil, gas babbles, acetone, phenols, etc. The electric force effect on a charged particle can be found as:

$$F_e = E * q_m \ , \qquad (3)$$

where: E –electric field strength (V/m), q - average electric charge of a particle (C). EMH radial electric field E (similar to electric field of cylindrical capacitor) can be found as:

$$E = \frac{V}{r \ln \frac{R}{r_{CE}}} \ , \qquad (4)$$

where: R -diameter of outer electrode, r_{CE} -diameter of central electrode-pipe, r - diameter of any cross-section.

Electric field reaches its maximum around the central electrode when $r=r_{CE}$ and its minimum around the outer (cylindrical) electrode when $r=R$.

The average electric charge of a particle can be calculated as:

$$q = \frac{\varepsilon_0 \varepsilon S \xi}{\delta} \qquad \text{Coulomb (C)}, \qquad (5)$$

where: ε -relative permittivity $\varepsilon_m/\varepsilon_0=81$, $\varepsilon_0=8.86\text{x}10^{-12}$ Farad/m,

S -surface area of $d=10\mu m$ particle $\pi d^2=3{,}14*10^{-10}m^2$,

ξ - electrokinetic potentials $\xi=0.1$-0.5Volt (for some organic matter higher),

δ - doubled electric areas thickness $\delta=10^{-6}$m.

Thus, it can be obtained for different matter and $d=10\mu m$ $q=(2-6)*10^{-14}$C, for $d=5\mu m$ $q=(0.5-1.5)*10^{-14}$ C and for $d=1\mu m$ $q=(0.125-0.375)*10^{-14}$ C.

There are two main magnetic forces that suppose to be taken into account [3,4,6].

The first one is for magnetic particles only:

$$F_{qm}=H*q_m \ , \qquad (6)$$

where: H -magnetic field strength (intensity), q_m -magnetic charge of a particle.

When oil, phenol, etc particles separation from water is concerns, q_m is too small [4,6], magnetic field is homogeneous and this magnetic force can be neglected. On the contrary, the second magnetic force - the Lorenz one, - in some cases can be taken into account: any movement of electrically charged particle in magnetic field creates the Lorenz force that helps filtration process:

$$F_L=q*B*v \ , \qquad (7)$$

where: B - magnetic field induction, v - charged particle velocity.

In the designed construction of EMH tree of the above mentioned forces (centrifugal, electric and magnetic) effect along the same direction and help the filtration process especially in the case of micro particles. For comparison of the centrifugal and electric forces effects on a particle all calculations were made for this type of EMH: particles diameter $d=1$; 5 and $10\mu m$, average revolving radius $r=0.1$m, velocity of input water and charged particle $v=0.5$–1.0m/sec, particle charge $q=(6$–$0.375)*10^{-14}$ coulomb, applied voltage $V=600$V, volume capacity $V_v=5$ liters, $r_{CE}=25$mm, $r_{in}=25$mm. An emulsion of water with small amount phenol was taken as a liquid under treatment. The calculations for several variants of particle diameter d and its charging ability ξ (electrokinetic potential) influence of electrical field force 5–15 times more efficient than centrifugal force (the smaller diameter, the higher efficiency: for $d=1$ μm and $\xi=0.3$ V $F_C=0.026*10^{-8}$ Newton (N), while $F_E=0.225*10^{-8}$N. The special particles pre-charging technique can rise these figure two-three times and even more. The electric field also helps particles to coagulate (get bigger size) and simplify the separation process. It needs only 400-600V electrical voltage on main electrode. The Lorenz force influence for this particular emulsion is very small and can be neglected ($F_L=4.1*10^{-10}$N).

CONCLUSION

The special construction of EMH was designed for filtration and separation processes of different liquids and gases, which have micro admixtures along with rather big particles. Similarly, special constructions can be designed for many kinds of technological and waist liquids and gases taking into account their parameters, demands and performance attributes. Some advantages of the EMH are the following:

1. It is a combined system designed to use the main three forces in the same direction.
2. There is no any active rotating mechanical part in EMH. Because of that this type EMH can be used in high-pressure technological systems without any risk.
3. Simple process control by electric and magnetic fields (applied voltage and current).
4. Available for many separating matters (liquid/liquid, liquid/gas, liquid/solid particles, liquid/ferromagnetic particles, etc.)
5. Possibility of ozone formation (by high frequency AC) in terms to burn left as a residue poisonous organic admixtures, microbes and microorganisms at the end of filtration.
6. EMH is an ecology improving system.

[1] *C. Sozov.* Electro-hydro-dynamics of Liquid Drop, The Time Dependent Problem, Progress pub. h., Moscow, 1987, vol. A, 331pp.

[2] *V.I. Klassen. Magnetization of water systems*, Chemistry pub, Moscow, 1982, 296 pp.

[3] *R.R. Oder, and L.A. Taylor.* Magnetic beneficiation of highland and hi-Ti mare soils: Magnet requirements. Proc. Space 90, 1982, Amer. Soc. Civil Engr., 133-142 pp.

[4] *O.S. Habarov.* Wastewater treatment in Metallurgy, Metallurgy pub. h., 1976, Moscow 223 pp.

[5] *A.M. Mustafayev, B.M. Gutman.* Theory of hydrocyclone and its calculation, Maarif pub. h., Baku, 1969, 172pp.

[6] *P. Ali-Zade, T. Abbasov, A. Nayir*, "Akışkan Ortamların Elektromanyrtik Filtrelerle Temizlenmesi, Ekoloji, cilt:7, Sayı 25, 1997, pp17-18. Turkey.

[7] *P.G. Ali-Zade, H.M. Kuliev, T.A. Abbasov, G.K. Gladkov.* Electromagnetic cyclone separator, AC SU 1692652, USSR, 1989/1991.

[8] *P.G. Ali-Zade, T.A. Abbasov, G.K. Gladkov.* Electromagnetic filter-precipitator, PATENT RU 1788915, RUSSIA, 1990/1992.

[9] *P.G. Ali-Zade, H.M. Kuliev, T.A. Abbasov, Z.A. Radjabov.* Electromagnetic filter for viscous fluids (liquids), RUSSIAN PATENT RU 2014149, 1991/1994.

[10] *P.G. Ali-Zade, H.M. Kuliev, T.A. Abbasov, Z.A. Radjabov.* Magnetic device for gas cleaning, RUSSIAN PATENT RU 2023476, 1991/1994.

[11] *E. Imal, P. Ali-zada, F. Karaca, F.Vardarli, H. Kuliev, E. Gusseynov.* 'Electromagnetic hydro (gas) cyclone filters (main forces analysis)' Green Engineering Conference, July 29-July 31 2001 in Roanoke, Virginia,USA.

Erkan İmal, Pərviz Əlizadə,Fəthi Göytəpə, Fərhad Qaraca, FeyzullaVardarlı, Hikmət Quliyev, Emin Hüseynov

ELEKTROMAQNİT HİDROSİKLON SÜZGƏCLƏRDƏ TƏSİR GÖSTƏRƏN QÜVVƏLƏRİN ANALİZİ

Məqalə, tullantı mayelərin və qazların aşqarlardan təmizlənməsinin müasir üsullarının işlənməsinə həsr olunmuşdur. Məqalədə, maye və qazların təmizlənməsi qurğularının və üsullarının qısa icmalı verilmişdir. Elektromaqnit hidrosiklon süzgəcin konstruksiyası və iş prinsipi geniş şərh olunur. Kiçik ölçülü (10 mikrona qədər) aşqarların separasiya prosesinə təsir edən (mərkəzdənqaçma, elektrik və maqnit) quvvələrin, müqayisəli səkildə, analizi verilmişdir. Qeyd olunur ki, bəzi incə proseslərdə, çox kiçik ölçülü, az miqdarda aşqarların mövcudluğunu arzuolunmaz halların əmələ gəlməsinə səbəb ola bilər.

Эркан Имал, Парвиз Али-заде, Фетхи Гектепе, Фархад Караджа, Фейзулла Вардарлы, Хикмет Кулиев, Эмин Гусейнов

АНАЛИЗ СИЛ, ДЕЙСТВУЮЩИХ В ЭЛЕКТРОМАГНИТНОМ ГИДРОЦИКЛОННОМ ФИЛЬТРЕ

Настоящая статья посвящена разработке оборудования для тонкой очистки сточных жидкостей и газов (сепарация микропримесей воды, песка, нефти и др. органических и неорганических компонентов). В статье содержится краткий обзор методов и устройств, для очистки жидкостей и газов и подробное описание конструкции электромагнитного гидроциклонного фильтра. Анализируется и сравнивается влияние основных сил (центробежных, электрических и магнитных) на сепарацию примесей очень малых размеров (менее 10 микрон). Отмечены некоторые тонкие процессы, в которых даже очень малое количество очень мелких примесей может привести к нежелательному эффекту.

Received: 14.12.01

OPTICAL AND MAGNETOOPTICAL PROPERTIES OF $Ni_3Fe_{1-x}Ti_x$ ALLOYS

T.M. PANAHOV, Z.S. MUSAYEV, I.A. ISKENDEROV, N.T. PANAHOV

"Physics of Metals and Alloys" Scientific Research Laboratory,
Department of Physics, Azerbaijan *University of Architecture and Civil Engineering*
370073, Baku, Azerbaijan

The dispersion dependences of $\sigma(h\nu)$ optical conductivity and Kerr $\delta(h\nu)$ equatorial effect for $Ni_3Fe_{1-x}Ti_x$ are learnt. Under the measured optical and magnetooptical characteristics have evaluated values of nondiagonal ε' components of the dielectric constant tensor. The obtained theoretical results satisfactory are compounded with experiment.

Iron-nickel alloys doped with a transition group of metals characterized by high initial and maximal dielectric constants are widely used in industry. Increasing their quality is closely connected with the study of their electronic structure. For a solution of the problems, connected with electronic structure of ferromagnetic alloys the knowledge of the complete electronic spectra of the external energetic bands is necessary. This problem is successfully solved by using optical and magnetooptical methods. Optical methods are used for revealing additional ultrastructural gaps in the electronic spectrum under ordering as well as for the investigation of the influence of doping elements on different physical properties of alloys. The determination of the positions of energetic bands with differently oriented spins by this methods gives information for a evaluation of different physical characteristics of metals and metal alloys such as an exchange spin-orbital splitting, degree of electron polarization, etc.

By observation of the changes on the optical and magnetooptical spectra under doping and ordering, one can study the influence of doping on ordering and trace electronic structure changes under order-disorder transition [1-3].

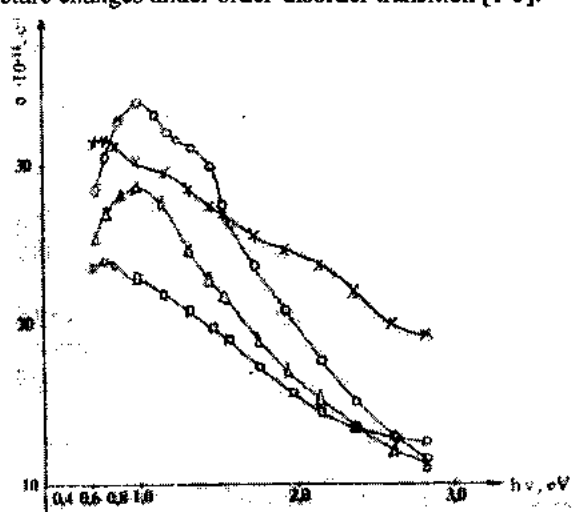

Fig.1 Optical conductivity $\sigma(h\nu)^2$ for $Ni_3Fe_{1-x}Ti_x$ alloys. o-Ni_3Fe, x-Ni_3Fe, Δ-$Ni_3Fe_{1-x}Ti_x$ (x=0,04), □- $Ni_3Fe_{1-x}Ti_x$ (x=0,06)

The processes of ordering exert strong influence on magnetic state of alloys, and thus on magnetooptical properties. From this point of view Ni_3Fe alloy remains as ferromagnetic under order-disorder transition, but its magnetooptical spectrum exhibits strong anomalies [4-6].

In this paper results of the study of optical and magnetooptical properties in 0.7-3.0eV region for Ni_3Fe ordering alloy systems, doped by titanium are presented. Ni-Fe-Ti alloy was alloyed in vacuum high-frequency furnace. Purity of source alloy compounds was higher than 99.9 %. After the melting alloys were annealed in hydrogen furnace at 1100°C during 10 hours. The ingots obtained were forged and rolled up to 1.5mm thickness. From rolled material specimens of rectangular shape with 5x10 mm dimension were cut out which further were refined to 0.5-0.7 mm thickness and mechanically polished for obtaining a mirror surface. Specimens obtained were placed into quartz tubes (vacuum in the tube was ~10^{-4}Pa) and exposed to long time ordering annealing with slow cooling in accordance with regime offered elsewhere [6]. Non-ordered state of Ni_3Fe alloy was obtained under cooling tube in water at 1100°C.

For the measurements of the optical and magnetooptical characteristics and Kerr equatorial effect the universal automated plant, developed at "Physics of Metals and Alloys" Scientific Research Laboratory [7] on the basis of polarimetric Bytti-Cone method was used. An accuracy of our measurements was about 2-3%.

In fig.1 curves of optical conductivity $\sigma(h\nu)$ for ordered and non-ordered Ni_3Fe alloy and $Ni_3Fe_{1-x}Ti_x$ (where $0.01<x<0.08$) alloy systems are presented.

It is seen that total shape of frequency dependence $\sigma(h\nu)$ for non-ordered Ni_3Fe alloys doped with titanium (x<0.1) coincides with the shape of $\sigma(h\nu)$ for pure nickel [6]. Fine electronic structure manifests itself on the $\sigma(h\nu)$ curves; that is double anomaly at 0.7-0.9 eV and bending at 1.1-1.3eV is observed.

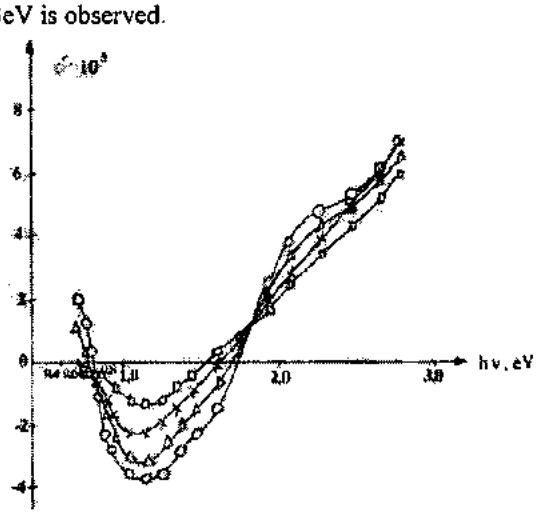

Fig.2. Kerr equatorial effect $\delta(h\nu)$ for $Ni_3Fe_{1-x}Ti_x$ alloys. o-Ni_3Fe, x - Ni_3Fe, Δ - x=0,04, □-x=0,06

It must be noted that total increasing occurs on the optical properties of alloys.

Ordering of Ni_3Fe alloys leads to change of characteristic

behaviour of the optical conductivity $\sigma(h\nu)$ curves. In near infrared region decreasing in $\sigma(h\nu)$ values is observed, which is accompanied by decreasing in energy in contrast to increasing of conductivity for non-ordered alloys. In 0.7-1.4eV energy region pronounced maximum in $\sigma(h\nu)$ is observed. Small additions of titanium leads to total increasing of $\sigma(h\nu)$. Further increase of titanium concentration results in decreasing $\sigma(h\nu)$ values as elsewhere [6].

Frequency dependences of Kerr equatorial effect (KEE) for $Ni_3Fe_{1-x}Ti_x$ alloys is shown in fig.2.

From the data of frequency dependence of the KEE and optical constants with using well-known formulas [8] we have evaluated values of non-diagonal ε'_1 and ε'_2 components of the dielectric constant tensor. $\varepsilon'_1(h\nu)^2$ and $\varepsilon'_2(h\nu)^2$ dependences for $Ni_3Fe_{1-x}Ti_x$ alloys are presented in fig.3(a, b). The obtained optical and magnetooptical spectra can be qualitatively understood on the basis of existing representations on electron structure changes of Ni_3Fe alloy under ordering. The main peculiarity in the behaviour of density of states $n(E)$ of Ni_3Fe ultra-structure is the appearance of the region with low values of $n(E)$ in Fermi level region [9]. Such a condition in density of states arises under the formation of ultra-structure at the expense of dividing of $d\downarrow$-bands on two groups and formation of the energy gap. The density of states far from the gap and in other spin sub-band, which as in the case of Ni is assumed fully to be fully filled, changes slightly. Carrying out the comparison of $\varepsilon'_2(h\nu)^2$ curves proportional to interband density of states [8] for NisFe in ordered and disordered states one can see that the main peculiarity of considered curves is sharply decreasing ε'_1 $\sigma(h\nu)$ value in 0.7-1.2 eV region under ordering. Assuming that in alloys main peculiarities of optical spectra can be explained on the basis of non-direct interband transition model [3, 10] one can to modelling the shape of occurred energetic gap in $\downarrow$ spin sub-band starting from the peculiarities of experimental cures in 0.7-1.5 eV region. Optical curve $\sigma(h\nu)$ is proportional to the sum of $\uparrow$ and $\downarrow$ sub-bands contributions and must have maximum at the energy equal to a distance between peaks in $n(E)$ $h\nu_{max}=E_{12}$ and magnetooptical curve ε'_2 $(h\nu)^2$ is proportional to the difference of this contributions and must have maximum at $h\nu_{min}=E_{12}-2\Delta E$ and maximum at $h\nu_{max}=E_{12}$. From the Berglund-Spicer formula [11] intra-band density of states $N(h\nu)$ is estimated for each of spin sub-band which are in a good agreement with the shape of experimental $\varepsilon'_2(h\nu)^2$ and $\sigma(h\nu)^2$ curves. Thus one can say that experimental results on optical and magnetooptical properties of ordered and non-ordered $Ni_3Fe_{1-x}Ti_x$ alloys are in qualitative agreement with energetic structure in the Fermi level region.

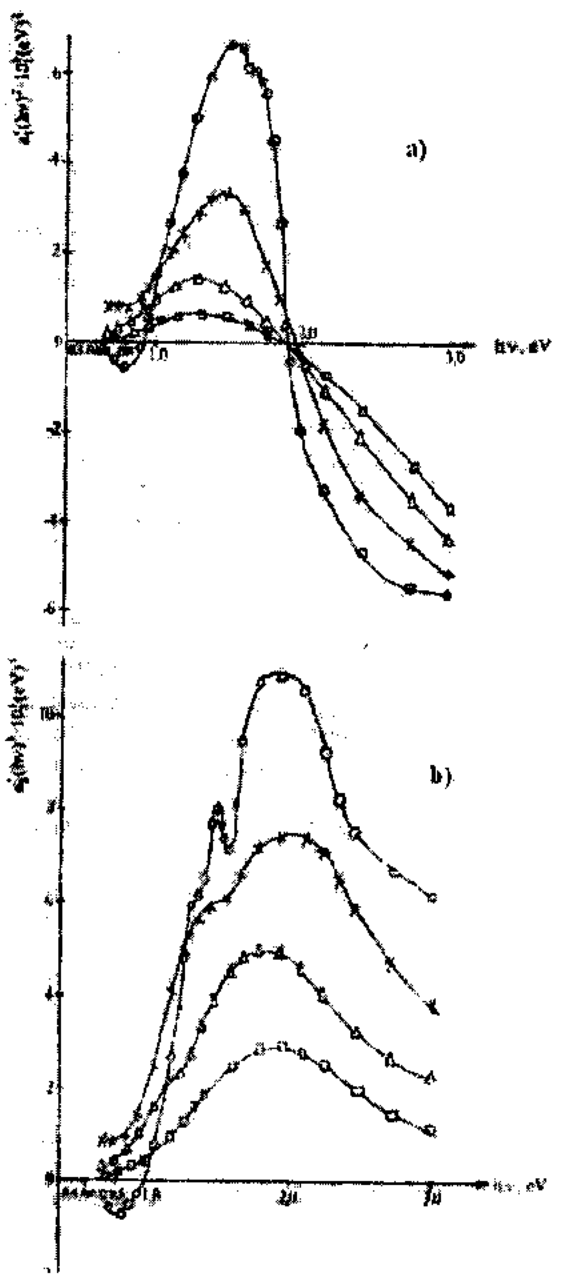

Fig.3 (a,b). Non-diagonal components of dielectric constant tensor $\varepsilon'_1(h\nu)^2$ and $\varepsilon'_2(h\nu)^2$ for $Ni_3Fe_{1-x}Ti_x$ alloys. o -Ni_3Fe, x - Ni_3Fe, Δ - x=0,04, □ - x=0,06

For complete quantitative estimation of the experimental data and the theory for the whole of spectra, detailed calculations of energetic structure of this alloys are needed.

[1] *W.R.Scott, I.Muldawer.* Phys.Rev., B, 1974, 9, p.1115-1125.

[2] *H.L.Scriver, H.P.Lengkuck.* Phys.rev., b, 1979,19,p.900-910.

[3] *S.E.Kulkova, V.E.Egorushkin, I.N.Anokhina, V.P.Fadin.* Phys. Stat. Sol. (b), 1981, 103, p.653-658.

[4] *I.M. Sasovskaya, Y.V. Knyazev.* FMM, 1982, v.53, 2, p.285-289.

[5] *G.S. Krinchik, R.D.Nuraliyeva.* JETF, 1962, v.42, i 6, p. 1442-1450.

[6] *E.A.Ganishina, G.S.Krinchik, Z.S.Musayev, T.M.Panahov.* FMM, 1984, v.58, i 2, p. 298-305.

[7] *Z.S.Musayev, I.A.Iskenderov etc.* 1993, Preprint, 23 p.

[8] *G.S.Krinchik* Physics of the magnetic phenomens. M., MGU, 1986, p. 324-325.

[9] *J.Jamaschita, S.Asano.* J.Phys. Soc.Japan. 1986, 21, №7, p. 1323-1331.

[10] *M.Tokumoto.* Phys.Rev., B, 1980, 22, №2, p. 638-64.

[11] *C.N. Berglung, W.E.Spicer.* Phys.Rev., 1964, 136, p.1030-1044.

OPTICAL AND MAGNETOOPTICAL PROPERTIES OF $Ni_3Fe_{1-x}Ti_x$ ALLOYS

T.M. Pənahov, Z.S. Musayev, İ.A. İskəndərov, N.T. Pənahov

$Ni_3Fe_{1-x}Ti_x$ ƏRİNTİLƏRİN OPTİK VƏ MAGNİTOOPTİK XASSƏLƏRİ

$Ni_3Fe_{1-x}Ti_x$ ərintiləri üçün optik keçiricinin və ekvatorial Kerr effektinin dispersiya asılılıqları öyrənilmişdir. Ölçülmüş optik və maqnitooptik xarakteristikalarına görə dielektrik nüfuzluğu tenzorunun qeyri-diaqonal komponentlərin qiymətləri hesablanmışdır. Alınan təcrübi nəticələrin mövcud nəzəriyyə ilə uyğunluğu qənaətbəxşdir.

Т.М. Панахов, З.С. Мусаев, И.А. Искендеров, Н.Т. Панахов

ОПТИЧЕСКИЕ И МАГНИТООПТИЧЕСКИЕ СВОЙСТВА СПЛАВОВ $Ni_3Fe_{1-x}Ti_x$

Изучены дисперсионные зависимости оптической проводимости $\sigma(h\nu)$ и экваториального эффекта Керра $\delta(h\nu)$ для сплавов $Ni_3Fe_{1-x}Ti_x$. По измеренным оптическим и магнитооптическим характеристикам рассчитаны значения недиагональных компонент тензора диэлектрической проницаемости ε'. Полученные теоретические результаты удовлетворительно согласуются с экспериментом.

Received: 13.12.01

TEMPERATURE DEPENDENCES OF SECONDARY ELECTRON EMISSION FACTORS OF THE TUNGSTEN AND MOLYBDENUM MONOCRYSTALS

N.M. TABATABAEI
Tabriz Tarbiyat University, P.O. Box 51745-406, Islamic Republic of Iran

B.Z. ALIYEV
.Azerbaijan Technological University, Gandja, 28 May st.,103

A.Z. PANAKHOV
Baku State University, 370148, Baku, Z. Khalilov st., 23

The parameters describing process of secondary electron emission (SEE) of tungsten (W) and molybdenum (Mo) monocrystals are investigated at liquid nitrogen temperatures. It is established that obtained effects of crystal's temperature influence on structure of the basic (SEE) characteristics are caused by interactions of electrons with phonons.

At study of temperature influence on monocrystals W and Mo (SEE) the basic attention was concentrated on measurements at low temperatures corresponding approximately to the liquid nitrogen boiling temperature (≅80K). It is caused by what at low temperatures was possible to expect the strongest display of (SEE) anisotropy effects of the monocrystals different sides. The measurements of electron reflection factors (ERF) were partially carried out at the increased temperatures of crystals up to (1200 - 1300) K. The reception of data about the true secondary electron emission factors (SEEF) at the used device construction was complicated, due to possible influence of parasitic thermal currents from the heater.

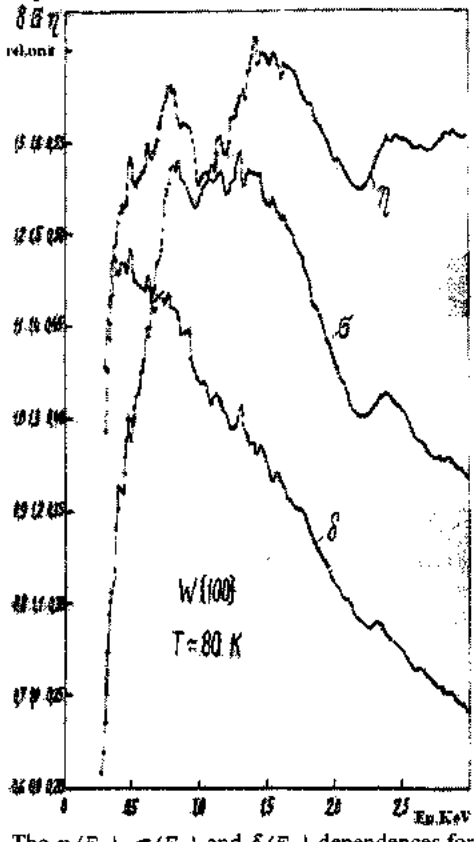

Fig.1. The $\eta(E_p)$, $\sigma(E_p)$ and $\delta(E_p)$ dependences for tungsten {100} side at T=80 K.

The measurement of monocrystals secondary-emission characteristics at T≅80K began in (1,5-2) hours after filling of the liquid nitrogen in vacuum bottle, in which the experimental device was placed. On fig.1 and fig 2 the dependences $\eta(E_p)$, $\sigma(E_p)$ and $\delta(E_p)$ for W two sides {100} and {111} are given as illustration of primary experimental material received in these experiences.

Here:

$\eta(E_p)$ is primary electrons inelastic reflection factor;

$\sigma(E_p)$ is complete secondary electron emission factor;

$\delta(E_p)$ is true - secondary electron emission factor;

E_p is primary electrons (falling on a target) energy.

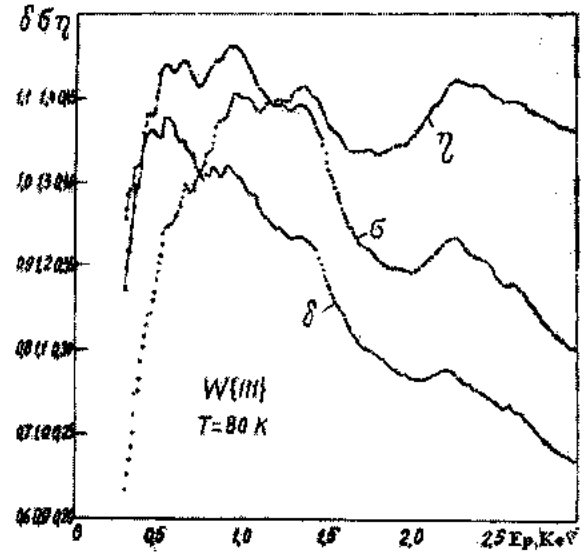

Fig.2. The $\eta(E_p)$, $\sigma(E_p)$ and $\delta(E_p)$ dependences for tungsten {111} side at T=80 K.

From fig.1 and fig.2 follows, that decrease of crystal's temperature is causes to strengthening of their structure. Much more evident and more precisely it can be seen, if the appropriate curves concerning the different temperatures to put on one diagram. It is made in a fig. 3 and fig.4 for a side of the investigated W crystals.

It is visible from the fig.3 and fig.4 data that decrease of temperature practically does not influence on absolute values of tungsten (SEEF).

Also it does not change appreciably the 1-st order structure. The influence of a crystal cooling is obtained, firstly, in the essential increase of amplitudes of structure nonmonotonities of the 2-nd order at T=300 K, and secondly, in occurrence of new (not observable at T=300 K) maximum and minimum of structures of the 2-nd order.

The differently the Mo crystals have another behaviour at cooling. For them, alongside with the above mentioned strengthening of the 2-nd order structure, as a rule, in most cases the common shift of curves in the part of factors reduction was observed.

The research of monocrystals (SEE) at low temperatures is carried out in the present work for the first time. In a number of cases the (ERF) was measured at the increased temperatures of samples (≅1000÷1300K).

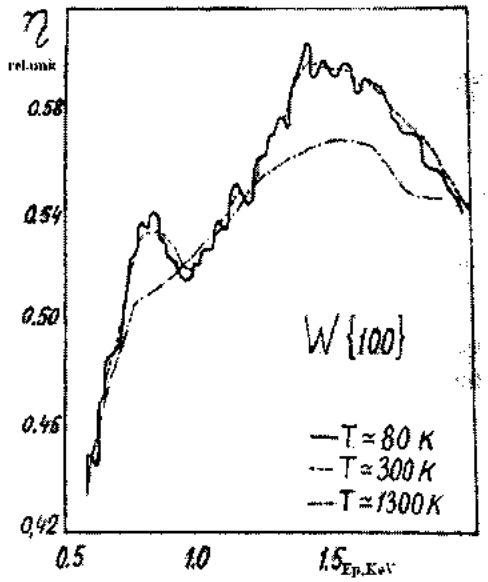

Fig.3. The $\eta(E_p)$ dependence for tungsten {100} side at T=80 K, T=300 K and T=1300 K.

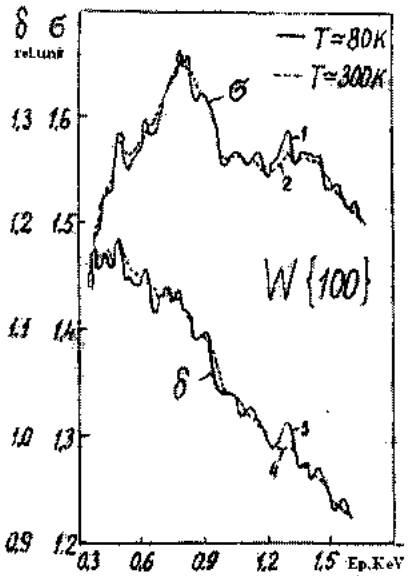

Fig.4. The $\sigma(E_p)$ and $\delta(E_p)$ dependences for tungsten (100) side at T=80 K and T=300 K.

Let address to consideration of the data received at T>300K. For the W's {100} and {110} sides the $\eta(E_p)$ dependences, measured at T=1300K, are shown on fig.3 and fig.4. It is visible, that the increase of crystal temperature results, on the contrary, to smoothing of curves structure: disappear completely the nonmonotonities of the 2-nd order structure and the 1-st order structure is less expressed. Especially distinctly it is appreciable at the W {100} side (fig.3), for which, as was specified above, the 1-st order structure is shown most strongly.

The smoothing of $\eta(E_p)$ curves structure at increase of the crystal temperature was observed for Mo samples.

The basic attention, according to specified above, in this part of work was inverted on measurements of (SEEF) at liquid nitrogen boiling temperature (≅80K).

It shown, that the downturn of crystal temperature appreciable strengthens the 2-nd order structure on $\eta(E_p)$, $\sigma(E_p)$ and $\delta(E_p)$ dependences and even reveals its additional features. Much more poorly the downturn of temperature has an effect on the 1-st order structure. For molybdenum the cases were observed, when the cooling of a crystal was accompanied by common small shift of secondary–emission characteristics in the party of smaller values.

Apparently, it is connected with the adsorption phenomena. At the crystal temperature increase, on the contrary, there is a smoothing of structure nonmonotonities of the investigated $\eta(E_p)$ dependence.

It is specified that the influence of a crystal temperature on structure of basic secondary - emission characteristics, obtained on experience, is caused by the electron-phonon interactions.

[1] *L.N. Dobretsov, M.V. Gomoyunova.* Emissionnaya electronica, Izd."Nauka", M., 1966. (Russian).

[2] *A.R. Shulman, V.V. Korablev, Y.A. Morozov.* Izd. AN SSSR, ser. fiz.,33, 1218, 1971. (Russian).

N.M. Tabatabaei, B.Z. Əliyev, A.Z. Pənahov

VOLFRAM VƏ MOLİBDEN MONOKRİSTALLARININ İKİNCİ NÖV ELEKTRON EMİSSİYASINI XARAKTERİZƏ EDƏN ƏMSALLARIN TEMPERATUR ASILILIQLARI

Volfram və molibden monokristallarında ikinci növ elektron emissiyası prosesini xarakterizə edən parametrlərin temperatur asılılıqları tədqiq edilmişdir. Müəyyən edilmişdir ki, kristalın temperaturunun ikinci növ emissiyasının xarakteristikalarına təsir effekti, elektronlarla fononların qarşılıqlı təsiri ilə müəyyənləşir.

Н.М. Табатабаеи, Б.З. Алиев, А.З. Панахов

ТЕМПЕРАТУРНЫЕ ЗАВИСИМОСТИ КОЭФФИЦИЕНТОВ ВТОРИЧНОЙ ЭЛЕКТРОННОЙ ЭМИССИИ МОНОКРИСТАЛЛОВ ВОЛЬФРАМА И МОЛИБДЕНА

Исследованы параметры, характеризующие процесс вторичной электронной эмиссии монокристаллов вольфрама и молибдена при температурах жидкого азота. Установлено, что обнаруженные эффекты влияния температуры кристалла на структуру основных характеристик ВЭЭ обусловлены взаимодействиями электронов с фононами.

Received:10.12.01

THE INVESTIGATION OF STRUCTURAL, ELECTRIC AND PHOTOELECTRIC PROPERTIES OF *n*-CdS-*p*-CdTe HETEROJUNCTION, OBTAINED BY THE DIFFUSION ANNEALING

L. A. ALIEVA
Institute of Physics of Azerbaijan National Academy of Sciences
370143, H. Javid av., 33, Baku

In the present work the original experimental results on properties of *n*-CdS-*p*-CdTe heterostructures, obtained by the diffusion annealing of two-layer CdS-Te structures are presented. It has been established that the CdTe layer is created in the vacuum or the inert atmosphere on the CdS and Te boundary by annealing of the CdS-Te structures. Electric and photoelectric properties of CdS-CdTe-Te structures have been investigated. The CdS-CdTe-Te structures band energy diagram explaining the photoelectric properties of these structures has been constructed.

INTRODUCTION

The A^2B^6-CdS, CdTe compounds are of the special interest for their use as components of the cheap and effective thin-film solar converters [1,2].

Works, devoted to the creation of the heterojunction in the CdS-Te system are few [3,4]. The creation of the *n*-CdS-*p*-CdTe by means of the diffusion annealing in the CdS and Te system is of the great interest because of the opportunity to create the two-phase wurtzite-sphalerite systems in an one crystal. The choice of the method for the production of the given heterojunction has been dictated by the simplicity and technological availability.

THE METHODS OF THE EXPERIMENT

The *n*-CdS-*p*-CdTe heterojunction has been created by the following methods:

1. The tellurium film of 1-2 μm thickness has been produced by the vacuum evaporation on a substrait of the monocrystal CdS of the specific resistance ρ =0.01 Ωcm. Then these structures have been placed in the ampoule and have been annealed in the inert atmosphere at temperatures 380-500°C during 10-30 minutes with the following sharp cooling.

Ohmic contacts have been produced on the CdS and Te by the vacuum evaporation of the indium. The air has been evacuated from the ampoule and this ampoule has been connected with the special system, which was providing the inert medium.

2. The Te film has been produced on the glass substrate by the vacuum evaporation at the room temperature. Then the CdS film has been put on this film by the vacuum evaporation of the monocrystal CdS of the specific resistance 15 Ohm. cm; moreover the mask configuration has been chosen so, that the CdS film would partially cover the Te film. The substrate temperature has been 170-190°C at the covering. Later the annealing of the obtained structure in the vacuum has been carried out at the temperature 330°C during 30 minutes with the following cooling in an hour. Ohmic contacts were prepared by means of the vacuum evaporation of the In (indium) on the CdS film and the deposition of the In-Ga alloy on the Te layer.

3. The piece of the monocrystal Te has been melted into the monocrystal CdS at the temperature 450°C. The melting has been carried out in the vacuum camera of VUD-4 device in the inert atmosphere 10^{-1} mm mercury column during 10 min. with the following slow cooling (at the rate of 14,2 grade/min.). The temperature was controlled by the chromel-aluminium (C-A) thermocouple attached to the sample Indium to *n* CdS and In-Ga alloy to the tellurium have been used as ohmic contacts.

EXPERIMENTAL RESULTS AND THEIR DISCUSSION

The investigation of the *X*-ray diffraction and also electric and photoelectric characteristics shows, that the CdTe layer is created between the tellurium and cadmium sulphide in all three types of CdS-Te structures, described above. *X*-ray diffractograms of the CdTe structure of the type 2 are shown on the fig. 1. Diffractograms have been registered both at the presence of the CdS layer (fig. 1a, the Cu K_α radiation was used), and after the selective etching of the CdS layer in the HCl solution (the Co K_α radiation was used on the fig.1b). Three lines of $2\theta \approx 23{,}80°$, 26, 45°, 27, 20° are given on the fig. 1.a. Lines of $2\theta \approx 26{,}45°, 27{,}20°$ correspond to the reflection from (002) and (101) planes of the hexagonal CdS with the principal orientation of grains in the direction of *c*; and to the perpendicular plane of the bulk. The weak line of $2\theta \approx 23{,}80°$ is identified with the (111) plane of the cubic granecentred CdTe.

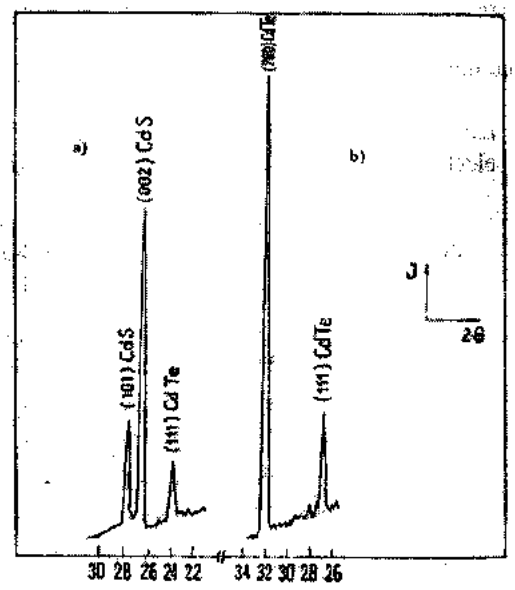

Fig. 1. *X*-ray diffractograms of the CdS-Te structures of the type 2 before (a; Cu K_α=1,5418 Å radiation) and after (b; Co K_α λ =1,7002 Å radiation).

Two intensive lines of $2\theta \approx 23{,}80°$ and $32{,}05°$ are given on the fig. 1.b. Calculations of interplanar distances show, that these lines are identified with (111) and (200) planes of the cubic CdTe.

Therefore, the analysis of X-ray diffractional figures of CdTe structures of the type 2 points to the presence of the CdTe layer between CdS and Te films.

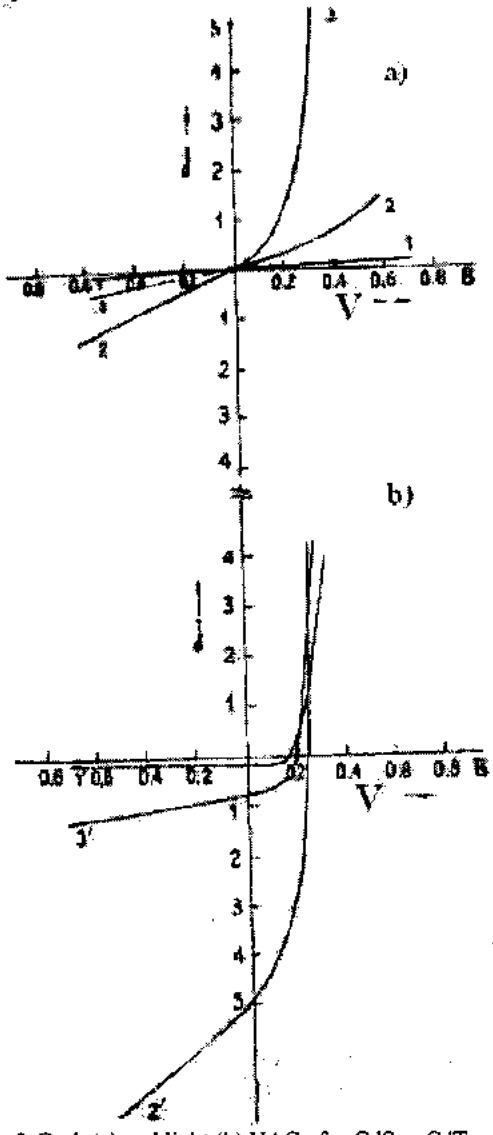

Fig. 2. Dark (a) and light (b) VAC of p-CdS-n-CdTe structures of the type 1,2,3. The lighting by the sun simulation of W=100 mW/cm².

As it is known the mechanicm of the CdTe creation is connected to the exothemicity of the creation of Cd and Te atoms [3]. The temperature gradient, directed from the boundary to the volume of the tellurium film, arises at the expense of the local heat release on the boundary. The distribution of the vacancies concentration in the tellurium has the identical nature. At the first moment atoms of Cd diffuse in Te with the creation of the CdTe combination. The vacancies concentration in the growing layer, directed to the opposite direction, stimulates the diffusion of cadmium atoms through the growing layer of the CdTe in the tellurium and leads to the growth of the layer thickness of the cadmium telluride in consequence of the reactive diffusion. By this the boundary between the cadmium telluride and tellurium moves in the direction of the Te [3]. As the excess of Cd atoms always exists in the CdS, then the creation of the CdTe layer between Te and CdS may be also explained by the previous mechanism. Dark (fig.2a) and light (fig. 2b) volt-ampere characteristics of three types of n-CdS-p-CdTe samples are shown on the fig.2. As it is seen from the figure, volt-ampere characteristics of three types of samples are asymmetric and manifest the sufficient photosensitivity (fig.2b).

Photoelectric parameters of samples of types 1,2,3 have the value j_{sc}≈0,14 mA/cm²; V_{oc}≈0,18V; j_{sc}≈5mA/cm²; V_{oc}≈0,24 V and j_{sc}≈0,8 mA/ cm²; V_{oc}≈0,21 V, respectively.

Let us note, that all three types of the CdS-Te sample had not manifested the rectifiable properties before the realization of the thermal treatment and were non-photosensitive. It is the confirmation of the fact, that the new CdTe combination is created between CdS and Te.

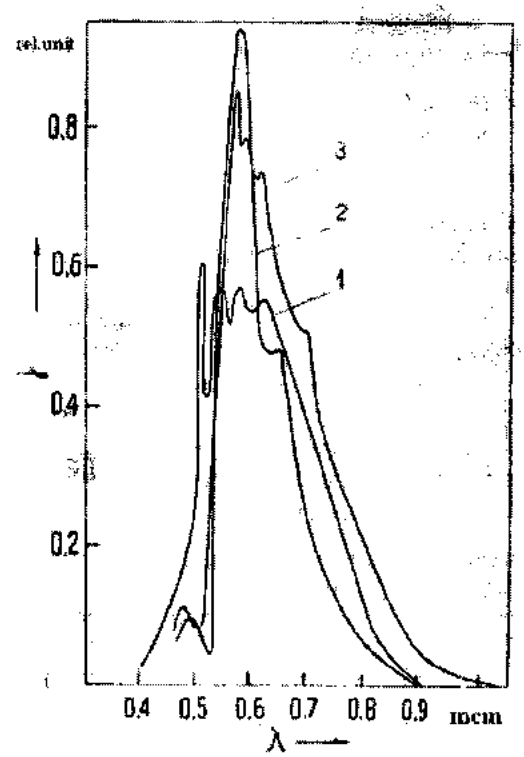

Fig. 3 The spectral distribution of the density of the photocurrent of the short circuit of j_{sc} structures of the type 1, 2, 3.

The spectral distribution of the density of the photoelectric current of the short circuits, j_{sc} of the CdS-CdTe structure is shown on the fig.3. It is seen, that the form of the j_{sc} spectra is identical for all types of samples, the short-wave maximum is caused by the absorption in CdS at $< 0{,}5\mu m$ and the long-wave boundary of the photosensitivity corresponds to the width of the forbidden band of the CdTe layer; E≈1.44eV (λ=0.86μm), which is created between CdS and Te. As it is seen from the fig.3, this layer is enough photoactive and the photosensitivity is caused by the light absorption in CdTe in the interval of the length of waves 0,5-0,9μm. As it is concern the oscillation j_{sc} in this region, then it is obviously connected with the interference of the incident light in the CdTe layer. The thickness of the CdTe layer, determined from the interference patterns (for example, for sample of type 2) makes ≈1μm.

The type of the conductivity and the specific resistance of the rest of the CdTe layer have been measured for samples of the type 2 after the selective etching in the HCl solution of

the CdS film. Measurements showed, that the CdTe layer has the *p*-type of the conductivity of the specific resistance ≈0,1Ωcm. The specific resistance of the CdS film has made 10^2Ωcm. The estimation of the carriers concentration in CdS and CdTe gives the value $n \approx 2 \cdot 10^{16}$cm^{-3} and $\rho \approx 7 \cdot 10^{17}$cm^{-3}.

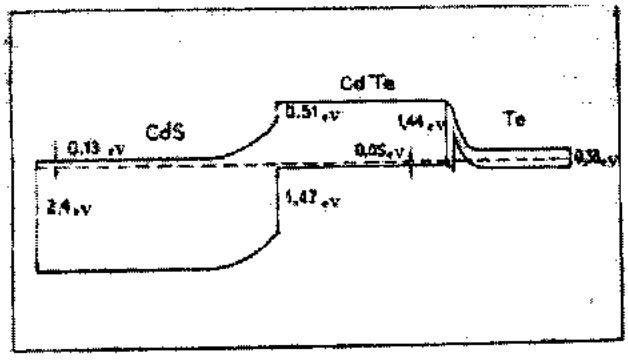

Fig.4. The supposed band energy diagram of CdS-CdTe-Te structures.

Using these data, we show the supposed band energy diagram of *n*-CdS-*p*-CdTe-Te structure on the fig.4. As it is seen from the diagram, the band bends have identical signs to the right and left of the CdTe layer, in other words, fields signs are opposite on boundaries of CdS-CdTe and CdTe-Te. Obviously, low values of photoelectric parameters of the obtained CdS-CdTe heterostructure are explained by this.

CONCLUSION

1. It has been established, that the CdTe layer is created on the boundary of CdS and Te at the annealing of the CdS-Te structure in the vacuum or the inert atmosphere.
2. Electric and photoelectric properties of the CdS-CdTe-Te structure have been investigated, the band energy diagram of the CdS-CdTe-Te structure has been constructed, explaining photoelectric properties of these structures.

[1] *L.A. Alieva, T.D. Jafarov, A.I. Bairamov and V.D. Novruzov.* Fizika Cild 6. 2000, №2, pp. 46-48.
[2] *E.N. Zamanova, M.A. Jafarov and N.M. Mamedov* Semiconductor Science and Technology 12 SST/ABC, 1999, pp. 1234-1239.
[3] *R.W. Dutton and R.S. Muller.* Solid. State Electronics. Pergamon Press, 1968, vol. 11, pp. 749-756.
[4] *G.A. Anner.* Proc. IEEE, 1969, 57, №6, pp.1219-1220.
[5] *G.B. Abdullaev and T.D. Jafarov* The atomic diffusion in semiconductive structures. M: " Atomizdat", 1980, p. 280.

L.Ə. Əliyeva

DİFFUZİON İŞLƏNMƏ YOLU İLƏ ALINMIŞ *n* CdS - *p* CdTe HETEROKEÇİDLƏRİNİN STRUKTUR, ELEKTRİK VƏ FOTOELEKTRİK XASSƏLƏRİNİN TƏDQİQİ

Məqalədə ikiqat Te-CdS strukturunun termik işlənməsi nəticəsində alınmış CdS-CdTe heterokeçidinin xassələri üzrə orijinal eksperimental nəticələr alınmışdır.
Müəyyən olunmuşdur ki, CdS-Te strukturunun vakuumda və ya təsirsiz qaz mühitində işlənməsi zamanı CdS ilə Te təbəqəsinin sərhəddində CdTe təbəqəsi yaranır. CdS-CdTe-Te strukturunun elektrik və fotoelektrik xassələri tədqiq olunmuşdur. Alınan nəticələr əsasında bu strukturun fotoelektrik xassələrini izah eden zona diaqramı qurulmuşdur.

Л.А. Алиева

ИССЛЕДОВАНИЕ СТРУКТУРНЫХ, ЭЛЕКТРИЧЕСКИХ И ФОТОЭЛЕКТРИЧЕСКИХ СВОЙСТВ ГЕТЕРОПЕРЕХОДОВ *n*- CdS-*p*-CdTe, ПОЛУЧЕННЫХ ДИФФУЗИОННЫМ ОТЖИГОМ

В настоящей работе приведены оригинальные экспериментальные результаты по свойствам *n*-CdS-*p*-CdTe гетероструктур, полученных диффузионным отжигом двухслойных CdS-Te- структур. Установлено, что при отжиге CdS-Te структуры в вакууме или инертной атмосфере на границе CdS и Te образуется слой CdTe. Исследованы электрические и фотоэлектрические свойства CdS-CdTe-Te структуры. Построена энергетическая зонная диаграмма CdS-CdTe-Te структуры, объясняющая фотоэлектрические свойства этих структур.

Received: 15.12.01

THE CALCULATION OF THE GETTERING EFFICIENCY OF THE CHARGE-COUPLED DEVICES

F. D. KASIMOV, E. S. MAMEDOV
Azerbaijan National Aerocosmic Agency
Azerbaijan Technical University

The calculation of the gettering efficiency of silicon CCD-structure (charge-coupled devices) has been carried out by means of the microscopic model of the gettering layer capacity, taking into account processes of the capture and the ejection of impurity atoms to runoffs. It has been shown, that the temperature of the process, parameters of the gettering layer and also the initial impurity concentration have the essential influence on the gettering efficiency.

In spite of variety of devices with the charge transfer, where capacities of both the p–n junction and the Shottki barrier are used [1-3], base of their majority is the MOS-condenser. Therefore the great attention is paid to research of electrophysical properties of Si-SiO_2 structure and the growth of their stability [4]. Problems of the growth of the charge transfer efficiency in CCD-structures and their quick-action essentially depend on the quality of the surface of the monocrystal silicon film, which is determined essentially by the gettering operation [5]. The specific charge capacity of the volumetric channel of the CCD-structure is reduced in comparison with the surface channel and demands the decrease of the density of the generation-recombination centers, the suppression of different types of heterogeneities in the silicon and on the boundary surface. On this reason the gettering has to be intensified, satisfying the technology of CCD-structures with the surface channel and the internal getter has to be created in the initial plates of the silicon [6].

Existing methods of the gettering have essential defects [7], concluding, firstly, in the large duration and the high temperature of the treatment, the instability of gettering centers, usually introduced in the plane at the first stage of the microscheme preparation and capable to the decay in the process of the prolonged high-temperature operations. Therefore it is necessary to create new efficient methods of the formation of the gettering centers.

By means of C-V-characteristics measurement of MOS-structures, formed on the base of silicon plates, the gettering efficiency of their volume at the introduction of gettering centers by means of the rapid thermal treatment (RTT) has been shown in [8]. The RTT operation has been produced on the ITT-18M device by samples irradiation by the incoherent IR radiation [9]. The gettering efficiency is determined by the value of the product of part of the substrate volume, occupied by the gettering layer, on the segregation coefficient of quick-diffused impurities (QDI) on the boundary surface of the gettering layer-substrate. Such approach allows to explain experimental results of the impurity redistribution in the substrate-gettering layer system at known empirical values of the segregation coefficient of the QDI for concrete conditions of gettering operations. However, the experimental determination of the segregation coefficient for different gettering conditions and levels of the substrate soiling is the sufficiently laborious task. The microscopic model of the gettering layer capacity, taking into account processes of the capture on runoffs and ejection of impurity atoms in the gettering layer [10], allows to avoid these difficulties.

Structural defects of gettering layers provide the reduction of the free energy of atoms of QDI in the gettering layer in comparison with the substrate. In the gettering process atoms of QDI diffuse on the interstices of the crystal lattice of the substrate, reach the gettering layer; are captured by structural defects in it and become low-mobile.

Any structural defects of the gettering layer may be presented in the form of one or several centers of the impurity capture. The dependence of the energy E of the impurity atom on the x coordinate near the capture center is shown on fig.1,a.

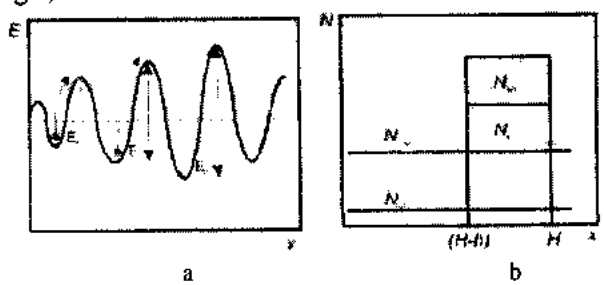

Fig.1. The energy diagram of the capture center of impurity atom (a) and the scheme of the distribution of gettering impurities in the substrate with the gettering layer (b).

The given energy diagram includes energetic barriers for interstitial diffusion of quick-diffusing impurities E_1, for the atom transfer of these impurities from the interstice to the center of capture E_1 and for the reverse transition E_2.

Let us assume, that the monocrystal substrate of the H thickness, homogeneously alloyed by the monotype QDI with the concentration $N=N_{sio}$, exists in the initial state. The concentration of structural defects is low in substrates and therefore atoms of quick-diffusing impurities are placed mainly in interstices [11]. The gettering layer of the H thickness is created on the reverse side of the substrate, containing monotypical capture centers with the concentration N_{co}. The gettering layer may be characterized by the surface density of capture centers because of its small thickness with respect to the substrate. Later the substrate is exposed to the thermal treatment for the redistribution of QDI from the substrate to the gettering layer. The new equilibrium concentrations of quick-diffusing impurities (N_{cnf}, N_{cf}) are established in the substrate and in the gettering layer. The concentration of structural defects is high in the gettering layer and only the part of centers is filled by atoms of quick-diffusing impurities:

$$N_{co} = N_{cnf} + N_{cf} \qquad (1)$$

where N_{cnf} and N_{cf} are concentrations of free and filled by impurity atoms of capture centers respectively. The following expression was obtained in [10] for the segregation coefficient:

$$k_C = 1 + \frac{H}{2h}\left\{\left[1 + 2(k_{max} - 1)(N_{SiO}/N_{CO} - h/H) + (k_{max} - 1)^2 (N_{SiO}/N_{CO} - h/H)^2\right]^{\frac{1}{2}} - (k_{max} - 1)(N_{SiO}/N_{CO} - h/H) - 1\right\} \quad (2)$$

$$k_{max} = 1 - \frac{N_{SiO}}{N_{1Si}} \exp\left[(E_2 - E_1)/kT\right] \quad (3)$$

where k_{max} is the limiting value of the segregation coefficient, obtained at low concentrations of quick-diffusing impurities in initial substrates, N_{1Si} is the limiting solubility of interstitial atoms of QDI.

The conception of the cleaning degree is used for the estimation of the gettering efficiency, $\delta_N = N_{SiO}/N_{Si}$ is the value, showing in how many times the concentration of QDI has reduced near the working surface of the substrate in consequence of the gettering, N_{Si} is the concentration of interstitial atoms of QDI in the substrate and in the gettering layer after the gettering completion,. It is easy to obtain the expression for the cleaning degree from the equation of the impurities balance [12]:

$$\delta_N = 1 + (k_C - 1)\ h/H \quad (4)$$

It follows from relationships (2)-(4), that the cleaning degree is determined by the concentration N_{Cd} and by the nature of capture centers ($\Delta E = E_2 - E_1$), by the temperature of the gettering process, by the part of the substrate volume, occupied by the gettering layer h/H and by the type of the QDI (N_{1Si}). Results of calculations of the cleaning degree, according to formulas (2)-(4), are shown on fig. 2 for the basic set of gettering conditions and parameters of the structure: T=1273K; ΔE=0.5eV; $N_{Co}=10^{23}m^{-3}$, $N_{SiO}=10^{19}m^{-3}$; $h=10^{-5}$m; $H=4\cdot10^{-4}$m. The known quantitative characteristics [12] of temperature dependences of the limiting solubility of atoms of copper, gold and iron in the silicon have been used at calculations. The following conclusions may be done in the result of the carried out calculations.

The gettering efficiency reduces with the growth of the temperature (fig.2,a). The gettering layer capacity grows according to the exponential law at the temperature reduction. It is necessary to remember, that calculated values of the cleaning degree are limiting for the given temperature. The gettering efficiency will be determined also by the gettering coefficient at low temperatures and the limited time of the process.

The gettering effect becomes essential only at the presence of the sufficient number of capture centers in the gettering layer (fig.2,b). The minimum necessary concentration of capture centers, determined by the level δ_N=10, essentially depends on the type of the gettering impurity.

Since practically all QDI are contained in real silicon plates, then, according to the fig. 2,b, the density of capture centers should exceed 10 cm² in the gettering layer.

Such situation is realized, if the gettering layer is saturated by vacancies, is in the stressed compression state and is alloyed by the slowly diffusing impurity on interstices. One and the same gettering layer possesses by the different gettering capacity with respect to different QDI exactly in connection with the different limiting solubility of impurities.

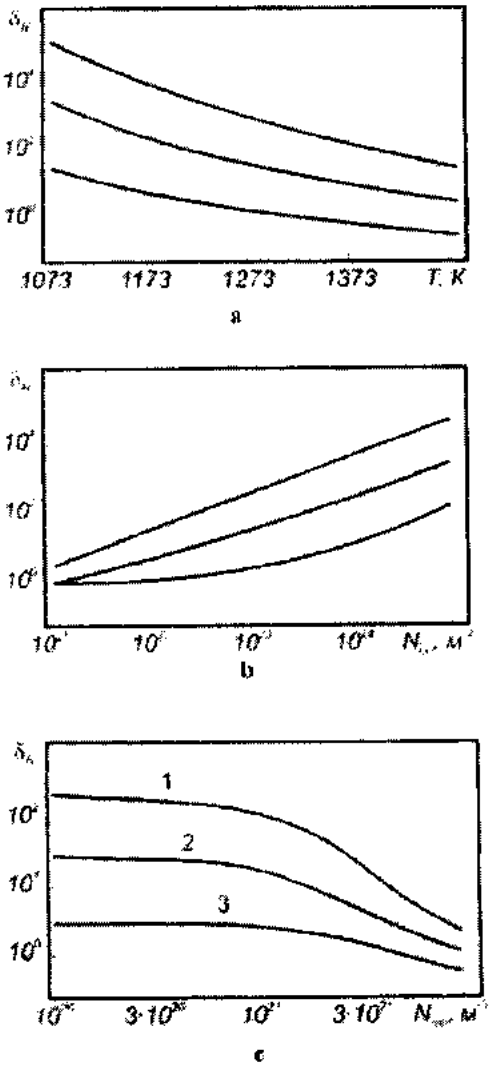

Fig.2. The dependence of the limiting cleaning degree of the working surface of siliceous plates on the temperature of the gettering process (a), on the concentration of capture centers in the gettering layer (b), concentrations of atoms of iron (1), gold (2), copper (3) – in the initial substrates (c).

The most high values of the cleaning degree occur for atoms of iron, possessing by the low limiting solubility in the silicon (fig.2). The figure 2 illustrates the essential dependence of the gettering efficiency on the initial impurity concentration in the plate. The sharp fall of the geterring efficiency at high levels of the pollution of initial plates is caused by the fact, that the impurity concentration in the gettering layer grows quickly in the gettering process and reaches summary limiting solubility: ($N_{1Si}+N_{CO}$). Then capture centers in the gettering layer are practically completely filled and this layer loses the gettering capacity with respect to the rest in the QDI substrate. The loss of the gettering capacity of the gettering layer begins on the identical levels of the pollution of initial substrates independently of the impurity type. The use of

more effective capture centers with the higher value of the energy barrier $\Delta E=E_2-E_1$ does not allow to increase the cleaning degree of the substrate. In given case the cleaning degree may be increased only by means of the growth of the number of capture centers in the gettering layer.

Therefore, it has been established, that the initial concentration of QDI has essential influence on the gettering layers efficiency side by side with the temperature of the gettering process and parameters of the gettering layer.

The given model of the gettering efficiency takes into account both parameters of initial substrates and characteristics of gettering layers, and may be used at the choice of methods and conditions of the gettering layer creation on defined substrates.

[1] *F.P. Press.* M:"Radio i svyaz", 1991, p.264. (in Russian)

[2] *Y.A. Kuznetsov, A.V. Veto, Y I. Zavadskii et al.* Elektronnaya promishlennost, 1993, №6-7, pp. 30-34. (in Russian).

[3] *V.I. Khainovskii, V.V. Uzdovskii, N.M. Gordo.* Izv. Vuzov. Electronika, 1999, №3, pp. 45-51. (in Russian)

[4] *A.P. Baraban, V.V. Bulavinov, A.G. Troshikhin.* Pisma JTF, 1993, v.19, issue 1, pp. 27-30. (in Russian)

[5] *V.A. Labunov.* "Zarubejnaya elektronnaya tekhnika", 1983, №11, pp. 3-66. (in Russian)

[6] *V.K. Prokophyeva, E.B. Sokolov, J.M. Sergeev* "Elektronnaya tekhnika", ser.6, Materials, 1991, Issue 6(260), pp.26-29. (in Russian)

[7] *Z.A. Jastrzebski.* J. Electrochem. Soc. 1987, v. 134, №4, pp.1018-1025

[8] *Z.A. Iskender-zade, M.G. Abbasov, F.D. Kasimov* Uchoniye Zapiski, Az TU, 1998, №3, pp. 239-242. (in Russian)

[9] *M. Svetlichnii, D.A. Sechenov, I.M. Burshtein et al.* Elektronnaya promishlennost, 1991, №3, pp.6-7.(in Russian)

[10] *V.A. Gusev, N.V. Bogach.* Mikroelektronika, 1990, v.19, issue 4, pp. 374-379. (in Russian)

[11] *B.I. Boltax, M.K. Badirkhanov, S.M. Goretskii.* The compensated silicon", L: "Nauka", 1973, p. 124.

[12] *V.V. Yemtsev, T.V. Mashovets.* " Impurities and point defects in semiconductors", M: " Radio i svyaz", 1981, p. 248. (in Russian)

F.C. Qasımov, E.S. Məmmədov

YÜK ƏLAQƏLİ CİHAZ STRUKTURLARIN HETTERİRLƏMƏ EFFEKTİVLİYİNİN HESABATI

Müxtəlif metallar üçün aşqar atomlarının axına zəbt etmə və tullanma proseslərini nəzərə alan hetterirləmə təbəqəsinin tutumunun mikroskopik modelinin köməyi ilə silisium YƏC-strukturların (yük əlaqəli cihaz–struktur) hetterirləmə effektliliyinin hesabatı aparılmışdır. Göstərilmişdir ki, hetterirləmə effektliliyinə prosesin temperaturu, hetterirləmə parametrləri, həmçinin aşqarların ilkin konsentrasiyası kifayət qədər təsir göstərir.

Ф.Д. Касимов, Э.С. Мамедов

РАСЧЕТ ЭФФЕКТИВНОСТИ ГЕТТЕРИРОВАНИЯ ПЗС-СТРУКТУР

Проведен расчет эффективности геттерирования кремниевых ПЗС-структур при помощи микроскопической модели емкости геттеростоя, учитывающей процессы захвата и выброса примесных атомов на стоки. Показано, что на эффективность геттерирования оказывает существенное влияние температура процесса, параметры геттеослоя, а также исходная концентрация примесей.

Received:15.12.01

INFLUENCE OF A SURFACE CONDITION ON THRESHOLD CHARACTERISTICS OF FERROELECTRIC LIQUID CRYSTALS

A.R. IMAMALIYEV, S.Z. TEMIRNIYAZOVA
Baku State University
Baku 370148, Z.Khalilov str.23

In this paper the dependence of ferroelectric liquid crystal threshold voltage on surface treatment (orientant covering and rubbing) has been experimentally studied and the simple theoretical model explaining this results has been proposed.

1. INTRODUCTION

Ferroelectric liquid crystals (FLC) attract the attention of researchers because of their high sensitivity to external electric field. As a result of strong interaction of spontaneous polarization with electric field the submicrosecond electrooptic effect occurs in thin planar sample of FLC [1]. In practice the threshold voltage of this effect that depends on material parameters of FLC and surface conditions [2] plays an important role. In this paper the dependence of threshold voltage on surface treatment (orientant covering and rubbing) has been experimentally studied and the simple theoretical model explaining this results has been proposed.

2. EXPERIMENT

An object of investigation was the induced ferroelectric liquid crystal that was obtained by doping of smectic C matrix

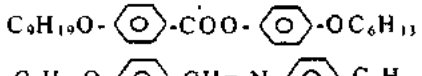

(38)%

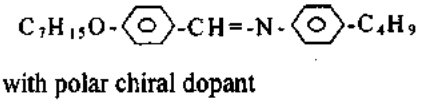

(57)%

with polar chiral dopant

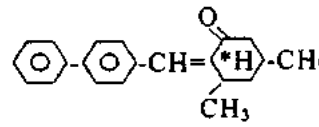

5%

The spontaneous polarization per unit tilt angle for this FLC is equal to $16nC \cdot cm^{-2}deg^{-1}$. .

The FLC-cell consist of thin film (about 5μm) of FLC between two plane-parallel glass plates separated by thin teflon spacer. The internal surfaces of plates are covered by thin transparent film of In_2O_3 and undergo further treatment. The later includes the covering by polyimide lacquer in order to obtain a planar orientation and the rubbing to achieve the monodominization of the sample.

The measurement was carried out in the device on the basis of polarizing microscope. The threshold voltage was obtained from transmittance-voltage dependence, when applying triangular wave to the cell. As a threshold voltage we take a value of voltage for which a transition to final uniform state starts.

The results of the measurement are presented in the following table.

Table

№№	Surface conditions		Cell thickness d, μm	Tilt angle θ, deg	Threshold voltage U_{th}, V	$\frac{U_{th}}{d\theta}$
	Presence of orientant	rubbing				
1	-	-	6	8	1,7	0,16
2	-	+	6	11,5	2,3	0,13
3	+	-	5,6	7	1,8	0,25
4	+	+	6	11	2,5	0,18

3. DISCUSSION

We propose a simple model qualitatively explaining these experimental data. The surface free energy density for ($\theta \ll 1$) can be presented in the form [4].

$$F = \int_{-d/2}^{d/2} \left[\frac{1}{2} G_\phi \theta^2 \left(\frac{\partial \phi}{\partial x} \right)^2 - P_s E \sin \phi \right] dx + (\mp W_1 \theta^2 \sin \phi + W_2 \theta \cos^2 \phi + W_3 \theta^2 \sin^2 \phi) \quad (1)$$

The first term in the integrand is the elastic energy, G_ϕ is the elastic constant corresponding to azimuthal angle change along the cell thickness, i.e. X axis (fig.1). The second term is interaction energy of the spontaneous polarization Ps and external electric field $\bar{E}$.

The first term in the surface energy is its polar part. Depending on the orientant nature the spontaneous polarization is directed towards the surface or from it: for instance, the condition $\left(\phi\left(\frac{d}{2}\right)=-\phi\left(-\frac{d}{2}\right)=\frac{\pi}{2}\right)$ corresponds to the minimum of polar part of the surface energy. The second contribution is the surface energy due to dispersion interaction of liquid crystal molecules with surface, which tends constrain molecules parallel to surface $\phi\left(\frac{d}{2}\right)=\phi\left(-\frac{d}{2}\right)=\pm\frac{\pi}{2}$. The surface profiling (rubbing) that is necessary to obtain the monodomain sample generates an opposite effect: it tends to align molecules paralel to Z axis ($\phi\left(\frac{d}{2}\right)=\phi\left(-\frac{d}{2}\right)=0$ or π) which was taken into account by

the third part of the surface energy. Coefficients W_1, W_2 and W_3 are corresponding coupling energies.

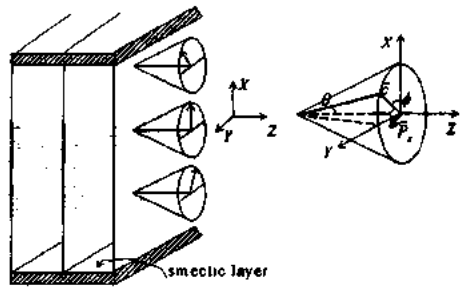

The minimization of the free energy (1) with respect to azimuthal angle leads to balance torque equation

$$G_\phi \theta^2 \frac{\partial^2 \phi}{\partial x^2} + P_s E \cos\phi = 0 \qquad (2)$$

with boundary conditions

$$G_\phi \frac{d\phi}{dx}\Big|_{\pm d/2} = [W_1 \cos\phi \pm (W_2 - W_3)\sin 2\phi]\Big|_{\pm d/2} \quad (3)$$

in order to define the equilibrium director distribution.

In all considered cases in the absence of electric field the equilibrium configuration corresponds to the twist state ($\phi(x) = -\frac{\pi}{2} + \frac{x}{d}\pi$), that takes place for strong polar cohesive $W_1 \geq \frac{G}{d}$ and $W_1 >> \Delta W$. Then we appl a weak electric field, the azimuthal angle ϕ takes a value $\frac{\pi}{2}$ everywhere, except of the range of size $\xi = \sqrt{\frac{G_\phi \theta^2}{P_s E}}$. Then the azimuthal angle dependent part of the free energy takes the form

$$F' = \frac{1}{2} G_\phi \theta^2 \left(\frac{\partial \phi}{\partial x}\right)^2\Big|_{-d/2} \xi + W \sin\phi\left(-\frac{d}{2}\right) - (W_2 - W_3)\cos^2\phi\left(-\frac{d}{2}\right) \qquad (4)$$

The first integral of equation (2) gives

$$\left(\frac{d\phi}{dx}\right)^2 = \frac{2}{\xi^2}(1 - \sin\phi)$$

After a substitution of this expression into the equation (4) it is not difficult too see that the value $\phi(-d/2) = -\pi/2$ corresponds to the minimum of energy (4) for small fields. When the condition $P_s E \xi \geq [W + 2(W_2 - W_3)]\theta^2$ takes place this minimum loses its stability. From the later inequality we obtain an expression for threshold voltage

$$U_{th} = \frac{[W_1 + 2(W_2 - W_3)]^2 \theta^2 d}{G_\phi P_s} \approx \frac{(W_1^2 + 4\Delta W)\theta^2 d}{G_\phi P_s} \qquad (5)$$

Since $P_s \sim \theta$, the ratio $U_{th}/\theta d$ does not depend on a tilt angle for given substance and depends only on surface conditions.

The formula (5) allows us to interpret the obtained data. The greater values of $U_{th}/\theta d$ for last two cases show that the covering of substrates by orientant (polymid) strongly increases the value of the polar part of cohesive energy. This fact has been confirmed by independent experiments: in the case of polymide covering the stability of twist states increases essentially in comparison with a non-covered substrate.

[1] *N.A.Clark, S.T.Lagerwall.* Apple.Phys.Let, 1980, v.36, p.899.
[2] *N.A. Clark, M.A. Handshy, S.T. Lagerwall.* Mol. Cryst.Liq. Cryst., 1983, v.23, p.213
[3] *Y. Ouchi, H.Takezoe, A. Fukuda.* Jap. J.Apple.Phys., 1987, v.26, p.1
[4] *Y. Yamada, T. Tsuge et al.* Ferroelectrics, 1988, v.85, p.123

A.R. İmaməliyev, S.Z. Temirniyazova

SƏTH ŞƏRAİTİNİN SEQNETOELEKTRİK MAYE KRİSTALIN ASTANA XARAKTERİSTİKALARINA TƏSİRİ

İşdə səthin işlənməsinin (oriyentant çəkilməsi və silinmə) seqnetolektrik maye kristalın astana xarakteristikalarına təsiri təcrübi öyrənilmiş və təcrübi verilənləri izah edən sadə nəzəri model təklif edilmişdir.

A.P. Имамалиев, С.З. Темирниязова

ВЛИЯНИЕ ПОВЕРХНОСТНЫХ УСЛОВИЙ НА ПОРОГОВЫЕ ХАРАКТЕРИСТИКИ СЕГНЕТОЭЛЕКТРИЧЕСКОГО ЖИДКОГО КРИСТАЛЛА

В работе экспериментально изучено влияние поверхностной обработки (нанесение ориентанта и натирание) на значение порогового напряжения сегнетоэлектрического жидкого кристалла и приведена простая модель, объясняющая эти данные.

Received:21.12.01